FFI-RAPPORT

16/01477

MODITIC

Reynolds-averaged Navier-Stokes simulations of dense gas dispersion in urban environments

–

Stéphane Burkhart
Jan Burman
Daniel Eriksson
Emma M. M. Wingstedt

MODITIC

Reynolds-averaged Navier-Stokes simulations of dense gas dispersion in urban environments

Stéphane Burkhart
Jan Burman
Daniel Eriksson
Emma M. M. Wingstedt

Norwegian Defence Research Establishment (FFI) 13 October 2016

Keywords

EDA
Computational Fluid Dynamics (CFD)
Gassutslipp
Spredning
Vindtunnel
Turbulent spredning
Atmosfærisk turbulens

FFI-rapport
FFI-RAPPORT 16/01477

Prosjektnummer
1392

ISBN
P: ISBN 978-82-464-2814-7
E: ISBN 978-82-464-2815-4

Approved by
Hanne Breivik, *Research Manager*
Janet Martha Blatny, *Director*

Summary

The European Defence Agency (EDA) project B-1097-ESM4-GP “MOdelling the DIspersion of Toxic Industrial Chemicals in urban environments” (MODITIC) (2012 – 2016) has studied the release and transport of neutral and non-neutral chemicals in complex urban environments, in order to enhance the understanding of the dominating physical processes involved, and to support improvements in modelling techniques.

This report describes the work conducted using the unsteady Reynolds-averaged Navier-Stokes (URANS) approach to simulate release and dispersion of neutral and dense gas in geometries with increasing complexity. The main purpose of the study is to assess the used software’s ability to handle realistic atmospheric conditions and release of dense gas for urban environments by validating the results against wind tunnel data. The simulations reported in WE5200 have been performed by the Direction Générale de l’Armement (DGA) and the Swedish Defence Research Agency (FOI) using two different solvers: Code Saturne and PHOENICS.

The results show that the models used capture the flow: simulated turbulence levels and flow directions are mainly in line with the findings from the experiment. The comparison of the neutral release shows for both models that they can capture the mean flow and turbulence. However, the result for the dense gas release indicates that the buoyant effects are only partially captured. A possible improvement would consist in using low-Reynolds models and more refined meshes in stratified regions to better capture the boundary layer and the dense plume edge gradients.

Sammendrag

European Defence Agency-prosjektet B-1097-ESM4-GP MODITIC (MOdelling the DIspersion of Toxic Industrial Chemicals in urban environments) (2012 – 2016) har studert utslipp og spredning av nøytrale og ikke-nøytrale industrikjemikalier i urbane miljø. Målene er både å øke kunnskapen om de dominerende fysikalske prosessene som er involvert, og å støtte opp om forbedring av modelleringsteknikker.

Denne rapporten beskriver arbeidet som er utført ved hjelp av metoden unsteady Reynolds-averaged Navier-Stokes (URANS) for å simulere utslipp og spredning av nøytral og tung gass i geometrier med økende kompleksitet. Hovedformålet med studien er å vurdere de brukte programvarenes kapasitet til å håndtere realistiske atmosfæriske forhold og utslipp av tung gass for urbane miljøer ved å validere resultatene mot vindtunnel data. Simuleringene rapportert i WE5200 har blitt utført av det franske Direction Générale de l'Armement (DGA) og det svenske Totalförsvarets forskningsinstitut (FOI) ved hjelp av to forskjellige løsere: Code Saturne og PHOENICS.

Resultatene viser at modellene som brukes lykkes i å predikere strømmen: turbulensnivå og strømningsretninger er i hovedsak i tråd med funnene fra eksperimentene. Sammenligningen av det nøytrale utslippet viser at begge modellene kan fange middelstrømmen og middelturbulensen. Utslippet av tung gass tyder imidlertid på at oppdriftseffekter bare delvis fanges opp. En mulig forbedring ville bestå i å bruke lave Reynolds modeller og et finere oppløst beregningsnett i de stratifiserte regionene for å fange opp grensesjiktet og gradientene i kanten av den tunge gassen på en bedre måte.

Contents

Preface

This work is part of the European Defence Agency (EDA) project B-1097-ESM4-GP “Modelling the dispersion of toxic industrial chemicals in urban environments” (MODITIC) (2012–2016). The scientific objective of this project is the systematic study of the release and transport of neutral and non-neutral chemicals in complex urban environments, to enhance understanding of the dominating physical processes involved, and to support improvements in modelling techniques. The participating organisations are:

- Direction Générale de l’Armement (DGA), DGA CBRN Defence, France
- Institut National de l’Environnement Industriel et des Risques (INERIS), France
- Norwegian Defence Research Establishment (FFI), Norway
- Swedish Defence Research Agency (FOI), Sweden
- University of Surrey (UoS), United Kingdom

FFI is the lead organisation. The project was initiated September 1, 2012, with duration of three-and-a-half years. The project is funded by the Norwegian Ministry of Defence, the Swedish Ministry of Defence, the French Ministry of Defence, and the French Ministry of Ecology, Sustainability and Energy.

This report describes the work and results for WE5200 “RANS computations, analysis, and reporting”. Chapters 1–3 are authored by FFI and Chapter 4 is authored by DGA. Each institute has conducted a validation of the quality of their own contribution.

1 Introduction

In recent years attention has been focused on release and aerial dispersion of toxic industrial chemicals (TIC), whether it is due to industrial accidents or terrorist activities, since this may threaten the lives and health of an urban population. In order to estimate the consequences and to identify most effective countermeasures to limit the impact, responsible authorities need to have reliable predictions of the spatial patterns as well as the time variations of the TIC concentrations. When considering non-neutral TIC, i.e. a denser-than-air or lighter-than-air gas, the dispersion process poses severe challenges especially in complex urban environments and is an important area of research.

The transport and dispersion of pollutants in the atmosphere are governed by the conservation laws of mass, momentum, and energy. Non-neutral gases will predominantly be transported with the wind field, but the transport may also be significantly affected by e.g. the density differences, heat exchange, and gravitational force. The density difference may severely alter the turbulence field due to the resulting stably or unstably stratified background. The impact of the stratification primarily modifies the vertical mixing process of the plume, and therefore also the overall transport process. A neutral gas, i.e. a gas with the same density as air, on the other hand will be transported with the wind field without affecting its dynamics. In both cases it is the wind field that is the most important dynamical process, and in order to model the dispersion successfully, it is crucial to accurately model the wind field.

In urban environments the dominating effects on the flow field are kinematic blocking of velocity components normal to solid surfaces and non-local pressure effects caused by reflections (cf. e.g. [1]). The kinematic blocking dominates the local flow conditions in built up areas, where buildings cause street canyon effects, flow separation and generation of unsteady wakes. In the atmospheric boundary layer, the non-local effects dominates and modify the turbulence anisotropy which changes the dispersion process.

In the past two decades Computational Fluid Dynamics (CFD) has become a more popular tool for modelling dispersion. However, a number of modelling issues need to be addressed in order to warrant the use of CFD in urban areas [2]. Many urban dispersion studies are based on the assumption that the flow field is statistically steady and therefore the steady state Reynolds-Averaged Navier-Stokes (RANS) method is widely used (see e.g. [3, 4, 5, 6]). However, results show that even though the mean velocity field can be fairly well predicted using this method, the turbulence kinetic energy is in general underpredicted, which may lead to a poorly predicted mixing process.

Several studies regarding numerical simulation of dense gas dispersion using the Unsteady RANS (URANS) approach have been carried out in the past [7, 8, 9, 10] with fairly good results. The URANS method inherently assumes that the mean flow field is statistically unsteady. This assumption is better suited for flows involving bluff body shedding which occurs downstream building structures. Another approach that naturally includes the flow unsteadiness is Large Eddy Simulation (LES), which resolves the inherent unsteadiness of the large scale turbulence irrespectively of the nature of the averaged flow field. Previous studies using the LES approach for urban dispersion modelling of neutral gases have shown good results [11, 12, 13, 14].

This report describes the work conducted using the Unsteady RANS approach to simulate release and dispersion of neutral and dense gas in geometries with increasing complexity - from a simple

hill configuration to an actual urban area comprising a part of Paris. The purpose of the study is to improve the methodology for high fidelity dispersion models and validate the results against wind tunnel data.

2 Scenario description

A more detailed description of the various scenarios is found in [15] and [16]. The scenarios are designed with increasing complexity to investigate how the dispersion of dense and neutrally buoyant gases interact with an increasingly more complex wind field. It is also of interest to explore different numerical models as to how well they manage to predict the dispersion and wind field. The scenarios are using the same incoming wind field, see Table 2.1. Carbon dioxide is used as dense gas, which has a density of approximately 1.5 times the density of air.

Parameter	Description	
Q	Emission rate	50/100 dm^3/min
d	Source diameter	0.103 m
U_{ref}	Reference velocity at H = 1 m	1 m/s
H	Boundary layer height	1 m
U^*/U_{ref}	Friction velocity	0.055

Table 2.1 *Parameters describing the incoming wind field and dissemination.*

2.1 Two dimensional hill

This scenario features a large smooth hill that covers most of the spanwise length of the wind tunnel. As shown in Figure 2.1, the hill is homogeneous in the spanwise direction. The sources are positioned both on the upstream and downstream side of the crest. This geometry creates an adverse pressure gradient on the upstream side of the crest, and a favorable pressure gradient on the downstream side of the crest. The emission rate of the neutral/dense gas is 100 dm^3/min.

2.2 Backward-facing step

In order to investigate the two-way coupling between a dense gas and a wind field affected by recirculation, the upstream part from the hill scenario is used to create a backward-facing step (see Figure 2.2). In order to get a high enough aspect ratio of the recirculation to provide two dimensional conditions, the floor behind the back-step was lifted. This yielded a back-step height of 0.1 m. The source is located in the recirculation region, just behind the step, with an emission rate of 100 dm^3/min.

2.3 Backward-facing step with cubes

To include separation effects, as well as recirculation, rows of cubes were placed behind the backward-facing step. Two different placements of the arrays are tested (see Figures 2.3 and 2.4). In

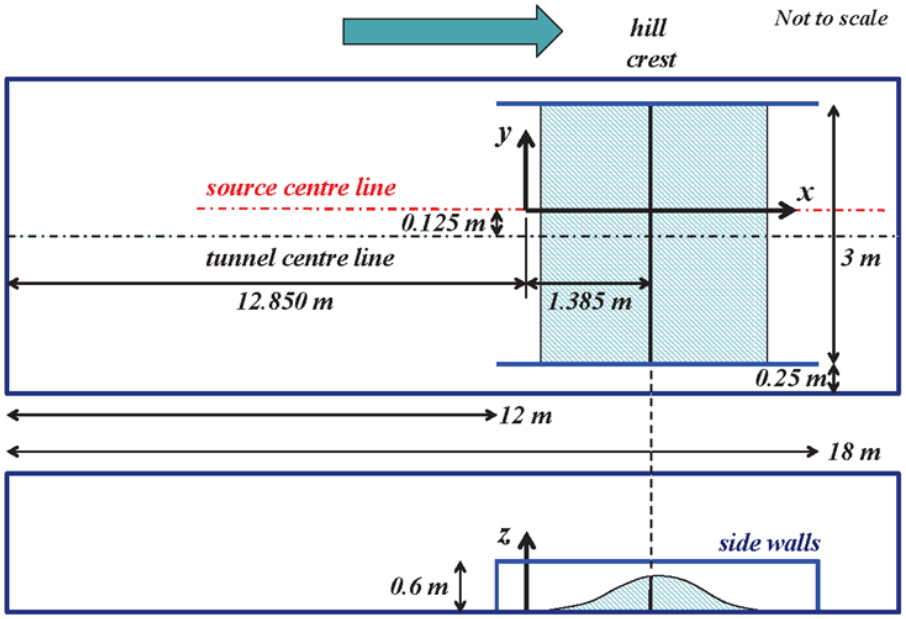

Figure 2.1 *Schematic picture of the hill scenario.*

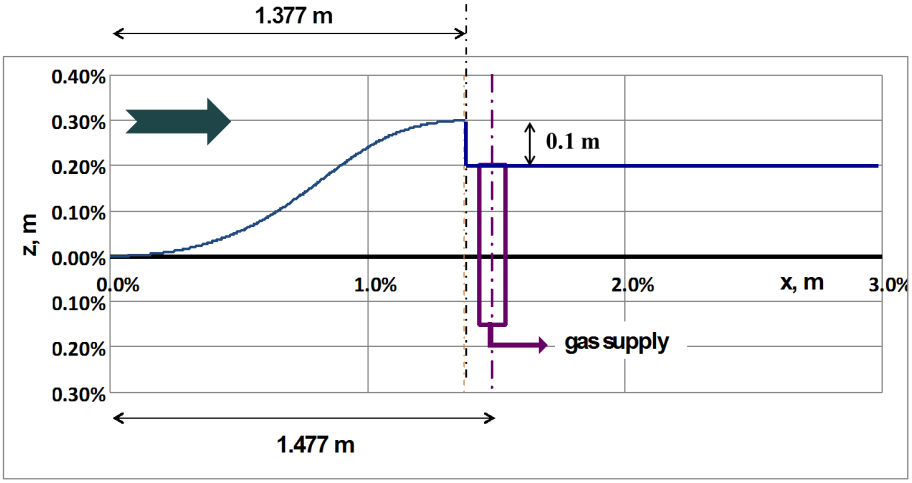

Figure 2.2 *Schematic picture of the back-step.*

array 1 the cubes are located outside of the recirculation region whereas they in array 2 are placed in the recirculation zone. In both cases the source is located behind the back-step and releases 100 dm^3/min.

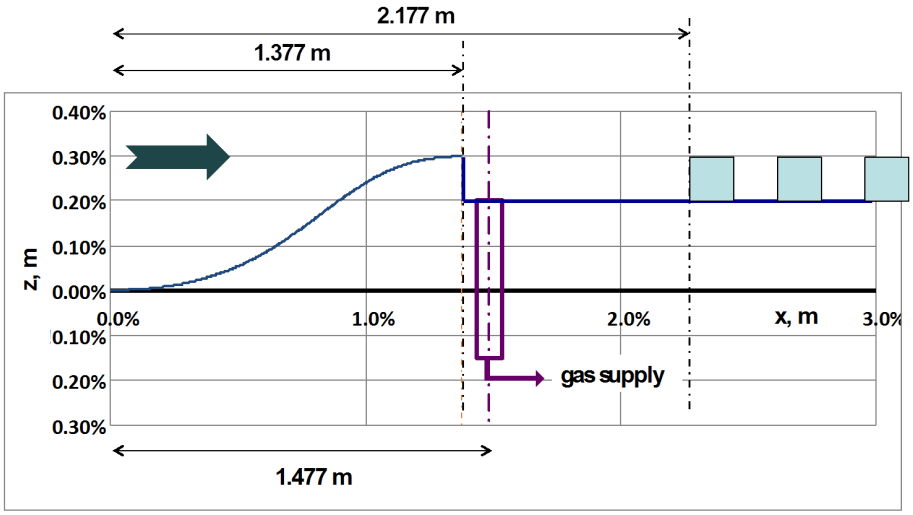

Figure 2.3 *Schematic picture of Back-step with cubes. Array 1.*

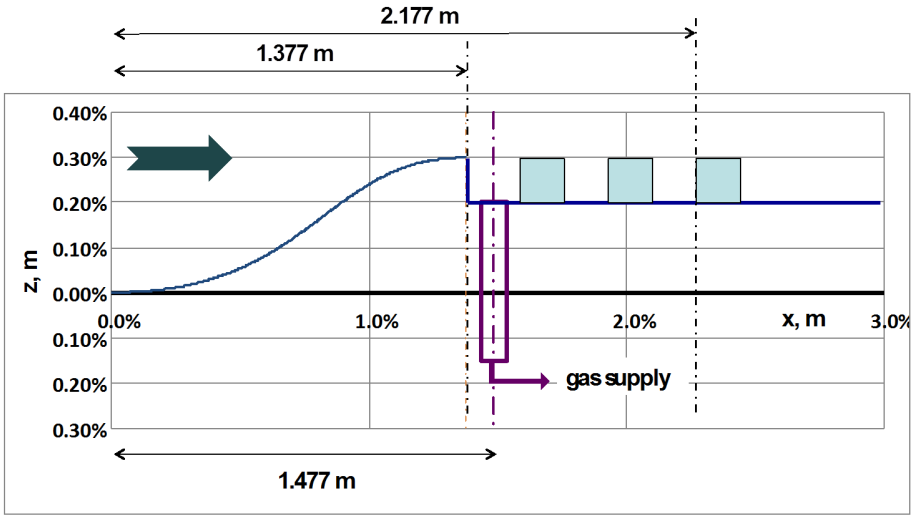

Figure 2.4 *Schematic picture of Back-step with cubes. Array 2.*

2.4 Simple array

Four cubes are used to resemble a simple urban street canyon with vortex shedding, separation, and recirculation. Three sources are placed upstream as seen in Figure 2.5. A separate study is also conducted where the four blocks are rotated 45 degrees. The cube height is 0.110 m, and the emission rate is 50 dm^3/min.

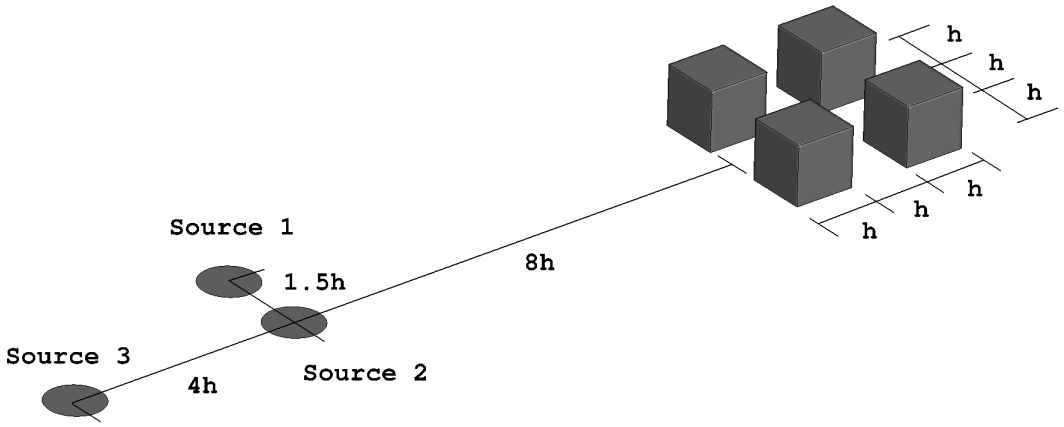

Figure 2.5 *Schematic picture of Simple array.*

2.5 Complex array

The complex array (see Figure 2.6) have models of buildings with four different shapes with trees placed in some of the streets. Three source position are used and two different wind directions. The emission rate is 50 dm^3/min.

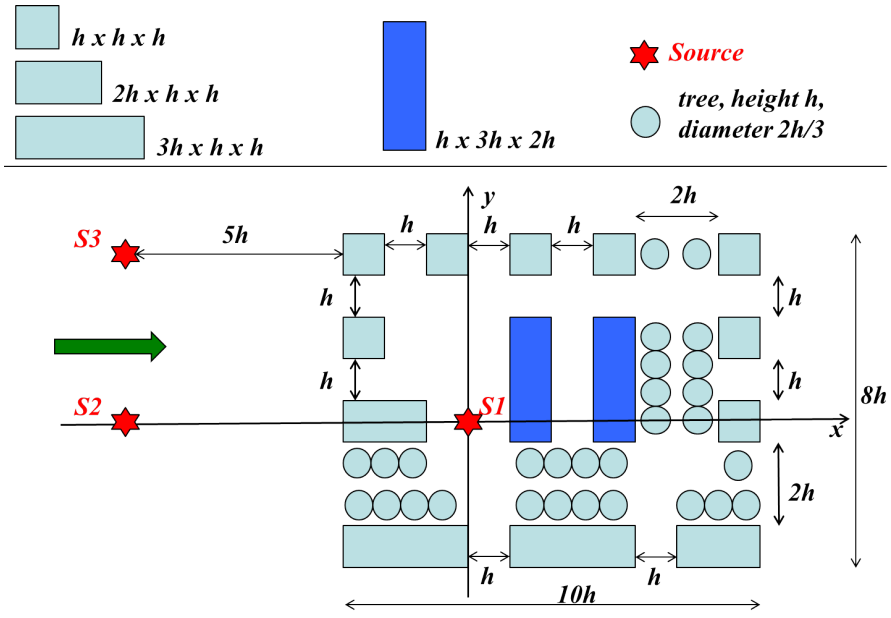

Figure 2.6 *Schematic picture of the complex array. Sources are marked by red stars and trees with light blue circles.*

2.6 Paris

A section of Paris is used to represent a large urban area. The model scale is 350 times smaller than full-scale with an averaged building height of 0.077 m. Irregular avenues and buildings creates an environment that produces a very complex wind field. Three different source locations are as seen in Figure 2.7. The emission rate is 50 dm^3/min. More information about the different Paris cases is found in Table 2.2.

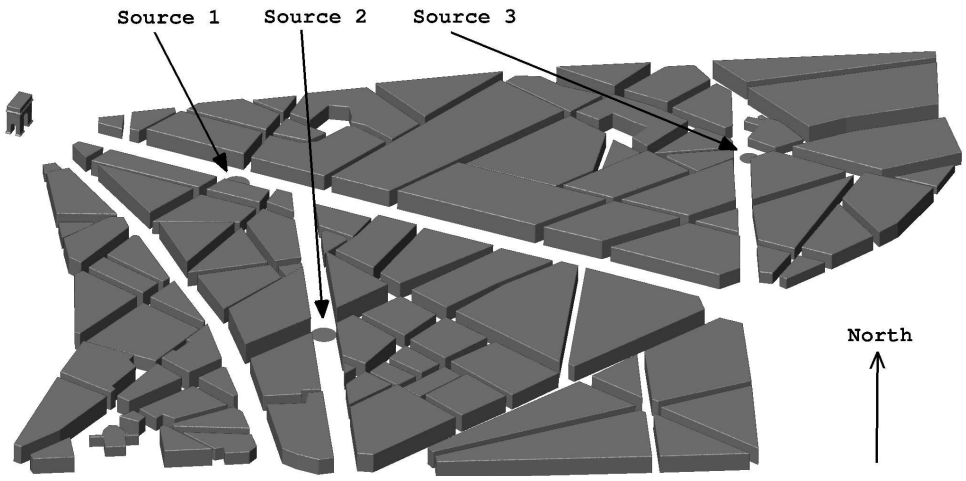

Figure 2.7 *Schematic picture of Paris*

Source number	Wind direction	Source diameter
1	300°	0.1143 [m]
2	220°	0.1143 [m]
3	40°	0.0857 [m]

Table 2.2 *Parameters describing the incoming wind field and dissemination.*

3 Wind tunnel experiment

The wind tunnel experiments are conducted in the meteorological wind tunnel at the Environmental Flow Research Center (EnFlo). The center is located at the University of Surrey. The tunnel has a working section of $20 \times 3.5 \times 1.5$ m with a overall length of 27 meters. See [16] for a more detailed description regarding the wind tunnel experiments.

Figure 3.1 *The Paris model inside the meteorological wind tunnel at the University of Surrey.*

4 Work conducted by DGA

This chapter is authored by DGA who is also responsible for the quality validation.

4.1 Objectives

We want to assess the ability of the software Saturne (EDF) to handle realistic atmospheric conditions and release of dense gas for urban environments. The validation process will use the scenarios named below and experimental data provided in the scope of this project.

- Flat ground
- Two dimensional hill
- Backward-facing step (with and without buildings)
- Simple array
- Complex array (with and without trees)
- Paris

4.2 Mathematical modelling

4.2.1 Dispersion modelling

The Eularian convection – diffusion equation is used to model the transport of gas using the mass fraction ϕ. In this particular study, we choose the "dry atmosphere" option for Saturn in order to deal with varying density when releasing dense gas (usually the "constant density" model is adapted for neutral atmosphere). The density is calculated with

$$\rho = \frac{\rho_{air}}{1 - \phi + \frac{\phi \rho_{air}}{\rho_{CO_2}}} \tag{4.1}$$

using the local mass fraction ϕ.

4.2.2 Turbulence modelling

The software uses RANS with the high Reynolds $k - \varepsilon$ turbulence model with a linear production (corrects the known flaw of the standard $k - \varepsilon$ model which overestimates the turbulence level in case of strong velocity gradients). The turbulent production gravity term, defined as

$$G = \frac{1}{\rho(\mu_t/\sigma_t)\nabla\rho g} \tag{4.2}$$

is included in the $k - \varepsilon$ equations. Saturne also proposes an Algebraic/Differential Flux Model for turbulent fluxes that would also be worth testing when dealing with density stratification and strong anisotropy.

4.3 Meshing procedure

The computational domain is orientated with x, y and z-axis aligned with the streamwise, spanwise and wall-normal direction respectively. All meshes have been created using the software Gambit, version 2.4.6 (Windows XP 32 bits). The Paris scenario is prepared in the software Salome (EDF), version 7.2.0 (Linux 64 bits) because Gambit (Windows XP 32 bits) could not handle large meshes due to RAM allocation problems. Almost all cases have been meshed with a wall boundary mesh layer, consisting of 4 prisms vertical layers, starting at about 1 cm (to avoid being under the roughness height of 0.88 mm for the high Re model using inertial wall law). We have also tried a more refined 5 mm first cell size for the flat case in order to capture the lower part of the dense gas boundary layer. For the hill cases, the upstream side of the hill has a 0.8 mm roughness, where the downstream side (with back-step and array) is smooth. The sources were discretized with a 4 layers horizontal boundary layer mesh starting at 0.5 cm (growth rate 1.2).

The min/max y^+-values in Table 4.1 may not be representative of the average value, as the presence of meshed building gives small wall distances (order 1 or less). The $k-\varepsilon$ linear production model asks for y^+ from 30 to 100 and for a thermal boundary layer around 2.5. We don't obey to this and keep y^+ of the order 10 on some parts of the floor. A scalable wall law is used instead of a log law to blend the viscous layer and the inertial one, and still be able to use the high Re turbulence model.

4.4 Boundary conditions

All simulations are performed at wind tunnel scale, using wind profiles from wind tunnel experiments. We use a module included in Saturne which handles and uses atmospheric inputs. The inflow profile has the possibility to vary in time and contains the average velocity, turbulent kinetic energy, dissipation rate, temperature and humidity as a function of height. The profiles are generated and adjusted with experimental wind tunnel data. The velocity fluctuations are defined as

$$k = 0.5(u^2 + v^2 + w^2) \tag{4.3}$$

and the dissipation as

$$\varepsilon = \frac{C_\varepsilon k^{3/2}}{l_m} = \frac{0.4k^{3/2}}{z}, \tag{4.4}$$

where the mixing length for the neutral release is $l_m \sim kz$ and $k \sim 3.32U^{*2}$. For the dissipation, the coefficient 0.4 is very sensitive to the relation between k and U^{*2}, and may be over-estimated.

Both the inlet and outlet boundary are based on the profiles in Figure 4.1. The side walls are considered smooth with standard boundary conditions. The top has symmetry and the floor is using a rough wall law. Simple array, Complex array and Paris have smooth floor, but the wind profile (inflow) is still generated with a roughness height of 0.8 mm. The source boundary condition uses a routine within Saturne called "cs user boundary conditions-atmospheric.f90". By specifying the right inlet parameters (velocity, turbulence, potential temperature, scalar mass fraction) the correct emission rate is obtained. In almost all cases, we release 50 dm^3/min.

The adapted rough wall law uses atmospheric MO theory. It relies on the work by Musson-Genon [17] and Geleyn [18] to reconstruct turbulent fluxes and mean profiles from vertical measurements (taken from the inlet profile) to be used as boundary layer profiles.

Case	**Domain** (x,y,z) (m)	**# cells**	**Δy^+** min – max	**U^* (m/s)** min – max	**Courant** min – max
Flat coarse	(6,3,1.5)	1.54e^5	45–237	0.01–0.06	0.14–6.5
Flat refined	(3.5,2,1)	1.3e^5	1.5–137	0.045–0.07	0.14–6.5
Hill	(7,3,1.5)	4.19e^5	30–200	0.03–0.06	2.5e^{-3}– 3.8
Back-step	(6,3,1.5)	3.19e^5	0.7–228	1e^{-3}–0.07	3.5e^{-3}– 6.7
Back-step w. cubes Array 1, rough	(6,3,1.5)	1.58e^6	1–1.3	0.053–0.2	3.7e^{-3}– 9.3
Back-step w. cubes Array 1, smooth	(6,3,1.5)	1.58e^6	0.29–228	1.5e^{-3}– 0.086	3.7e^{-3}– 9.3
Back-step w. cubes Array 2, rough	(6,3,1.5)	2.24e^6	1–1.3	0.053–0.2	6.3e^{-4}– 20.2
Back-step w. cubes Array 2, smooth	(6,3,1.5)	2.24e^6	0.17–227	1.4e^{-3}– 0.09	6.3e^{-4}– 20.2
Simple array 0°	(3.5,2,0.5)	1.93e^5	1–49	3e^{-3}– 0.076	0.018–47
Simple array 45°	(3.5,2,0.5)	4.55e^5	0.7–71	3.7e^{-3}– 0.088	0.024–65
Complex array 0°	(4.5,2,0.5)	7.71e^5	0.6–70	3e^{-3}– 0.092	8e^{-3}– 78
Complex array 45°	(4.5,2,0.5)	8.95e^5	0.73–76	2e^{-3}– 0.095	0.02–73
Complex array 0° with trees	(4,3,0.5)	8.45e^5	0.013–117	3.2e^{-3}– 0.17	1e^{-3}– 373
Paris	(7.5,6.5,0.4)	2.34e^6	0.12–66	1e^{-3}– 0.16	2.5e^{-3}–327

Table 4.1 *CAD, MESH and computational properties*

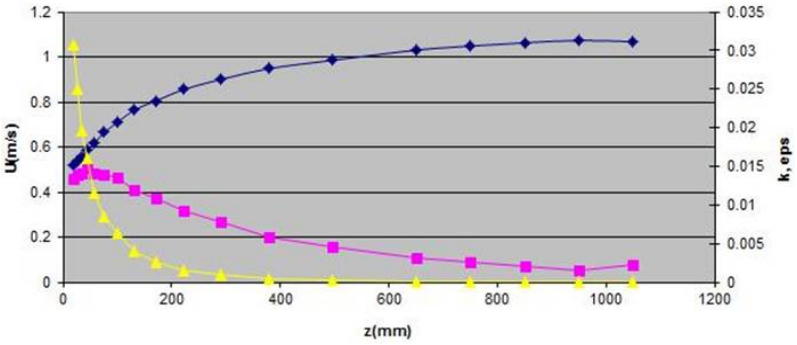

Figure 4.1 *Mean vertical profiles of streamwise velocity (blue), turbulence kinetic energy (pink), and dissipation rate (yellow) used for all scenarios*

4.5 Calculation set-up and control

Four Amd 64 bit linux (Debian 2.6.32) servers with 48 cores total using METIS partitioning tool are used. 64 Gb RAM were available with Intel Xeon 2.5 GHz processors (hexacores). Version 3.0.0 of Saturne is used for all cases accept for Paris, where version 4.0.1 is used due to backtracking issues. Unsteady solver was selected to reach a quasi-stationary state. Travel time to cross the wind tunnel working section is about 5 s. A computational time between 30 s and 60 s is used before taking the results. The results are not averaged due to the solution being quasi-stationary. We follow the residuals until a decrease of at least an order of 2 reached. Mean flow is solved with a second order (centred) scheme. Other scalars are solved with upwind scheme. Pressure-velocity coupling uses SIMPLEC algorithm. Gradient reconstruction is made with a least square method on extended cell neighbourhood. We also check other variables (mean flow, k, ε, scalars) so that no more significant variations are registered. The time step used is about 0.01 s. This is used for all cases, despite the minimum Courant numbers seen in Table 4.1.

4.6 Results

We compare the simulation results against experimental values for the same experimental sensor locations. We had to be careful for the Paris case, as origin and orientation of the model had changed from the original CAD (in the simulation, origin at Rond-Point des Champs Elysees). In the wind tunnel the model is placed in order to get origin at the source, and then turned to fit the orientation relative to the wind tunnel main flow direction. Results are presented in normalized units ($C^* = CU_{ref}/Q \cdot 10^{-6}$), where C is the concentration expressed in parts per million (PPM). For neutral release $C_{air} \cdot 10^{-6} = \phi$ and for dense gas release $C_{co_2} \cdot 10^{-6} \sim 0.66((\phi\rho_{air})/\rho_{co_2})$.

4.6.1 Flat case

The flat case is interesting as it determines the flow profiles for the other more complicated cases (Hill, Arrays, Paris). Over the distance from the inflow boundary to the first building, turbulent

profiles are difficult to maintain which is relevant for dispersion. We first check the mesh adequacy for the high-Re turbulent model ($k-\varepsilon$-linear). We started with a rough mesh (about Δ=1 cm for the min mesh size, around the source and first vertical cell). Then, we proceeded with a finer mesh (0.5 cm) to present the results. As the roughness height was 0.8 mm upstream, we did not want to refine more in order to use the log law for the mean velocity profile. We finally had to use a scalable wall law Figure 4.2 where the viscous layer is blended to the inertial layer. We see that in the refined case shown in y^+-values are around 10 and appear a bit too fine to use the log wall law (30 to 70 needed). This value is consistent with $y^* = u^*(\Delta/2)/\nu$.

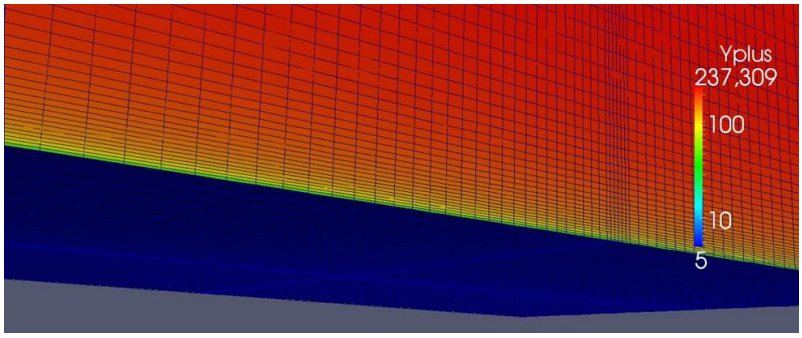

Figure 4.2 *Wall units y^+ for the flat refined case.*

Next, the mean velocity profile (Figure 4.3), and turbulent kinetic energy (Figure 4.4) was checked. The profiles appear to satisfyingly maintaining the turbulence from inlet to outlet .

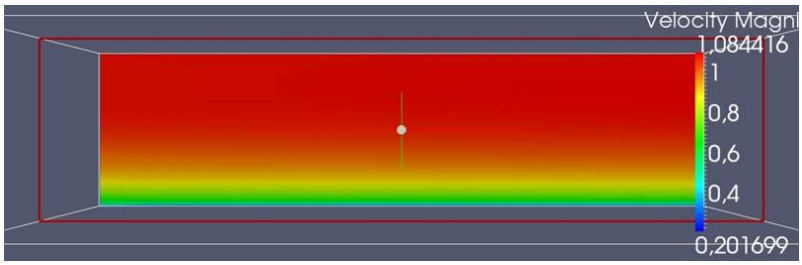

Figure 4.3 *Contours of mean velocity magnitude in the symmetry plane.*

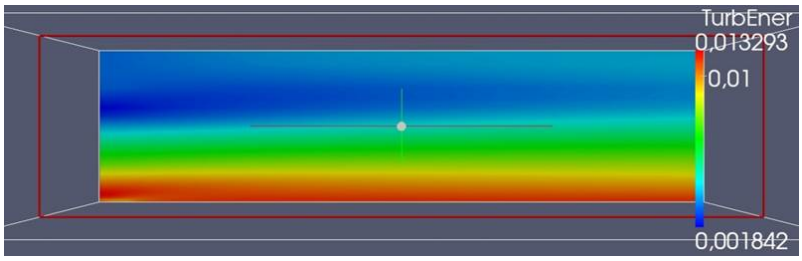

Figure 4.4 *Contours of turbulence kinetic energy, k, in the symmetry plane.*

4.6.1.1 *Neutral gas*

For air dispersed in air (passive dispersion), we have the following turbulent properties (see Table 4.2) reconstructed from the simulation results at one point in space x = 0.75 m and y = 0 m (stationary flow 10 s). The normalized shear rate S^* is about 10 close to the ground, the scale of turbulence being 10 times the characteristic flow time. The vertical turbulent flux $\langle uw \rangle$ is higher than the $-0.3k$ usually observed, but the turbulent viscosity is close to the expected $0.09k^2/\varepsilon$.

z (m)	dU/dz	$S^* = Sk/\varepsilon$	$\langle uw \rangle/k = -2CS^*$	$\nu_t/(k^2/\varepsilon)$
0.025	22.43628	9.29729846	-1.67351372	0.09899115
0.044	3.69173684	2.65418981	-0.47775417	0.09903517
0.064	2.65685	2.63985589	-0.47517406	0.09501636
0.083	0.98326316	1.04784838	-0.18861271	0.09600302
0.103	1.00785	1.16593145	-0.20986766	0.09592544
0.122	1.00789474	1.27025885	-0.22864659	0.09464647
0.142	0.99225	1.36940285	-0.24649251	0.09302924
0.161	1.05942105	1.57409846	-0.28333772	0.09478244
0.181	1.06075	1.721744	-0.30991392	0.09522442
0.2	1.05121053	1.87189714	-0.33694149	0.09443302

Table 4.2 *Vertical profile for air turbulent properties at x=0.75 and y=0*

In Figure 4.5, we show the footprint of mass fraction scalar for the air dispersion, which presents as a narrow plume, still at high concentration levels over the geometry scale (about 3.5m see Table 4.1).

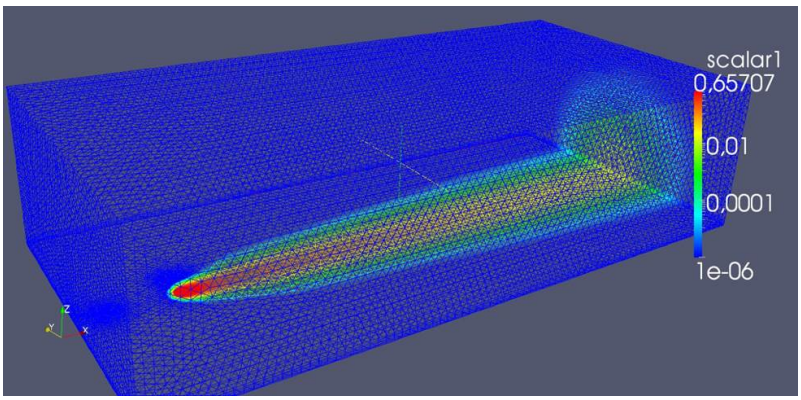

Figure 4.5 *Mass fraction of passive gas (air) for the flat plate case with continuous release.*

The simulation results (dashed lines) at different distances downwind of the source, shown in Figure 4.6, fit rather well compared to the experimental data (bold lines with symbols). Vertical profiles (Figure 4.6b) have a 15% underestimation, but this is only a matter of small lateral shifts of the experimental plumes related to the symmetry line. Experimental plumes are also slightly larger. This seems to come from a slight over-estimation of ν_t by the high Re model.

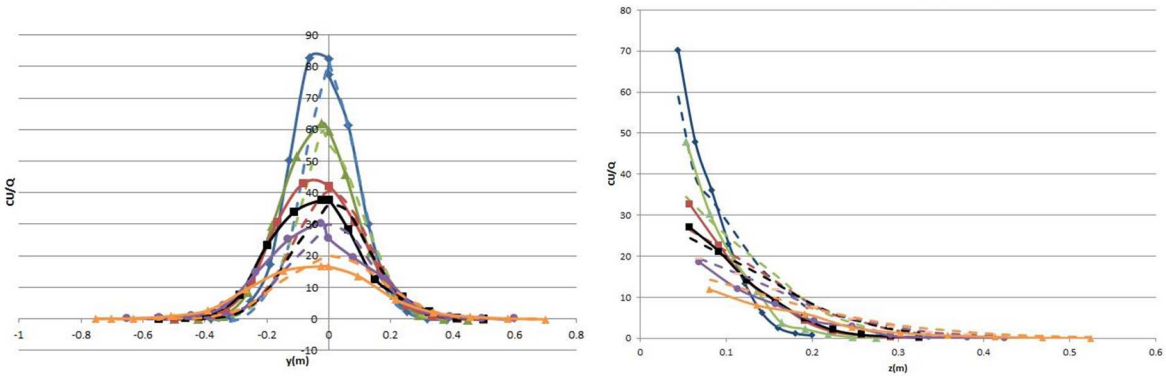

(a) Lateral profiles at z=0.025 m

(b) Vertical profiles at y=0

Figure 4.6 *Profiles of normalized air concentration at different streamwise positions (blue = 0.75, green = 1.036, red = 1.4, black = 1.6, purple = 2 and orange = 3 m). Dashed lines show simulation results whereas solid lines with symbols show the experimental values.*

4.6.1.2 Dense gas

Surprisingly, turbulent properties (see Table 4.3) are quite similar at x = 0.75 m when using dense gas compared to air (density ratio is 1.5).

z (m)	dU/dz	$S^* = Sk/\varepsilon$	$\langle uw\rangle/k = -2CS^*$	$\nu_t/(k^2/\varepsilon)$
0.025	24.37748	10.5006288	-1.89011318	0.09943963
0.044	3.05973684	2.2859031	-0.41146256	0.09825301
0.064	2.092	2.12665473	-0.38279785	0.09439053
0.083	0.84436842	0.91741787	-0.16513522	0.0953365
0.103	0.85395	1.00246906	-0.18044443	0.09538001
0.122	0.85389474	1.08681047	-0.19562589	0.09434954
0.142	0.84735	1.1753251	-0.21155852	0.09307475
0.161	0.96205263	1.43779766	-0.25880358	0.09490736
0.181	0.96445	1.57703304	-0.28386595	0.09539708
0.2	0.96005263	1.72559966	-0.31060794	0.09455732

Table 4.3 *Vertical profile for CO_2 turbulent properties at x=0.75 and y=0*

When we look at the footprint obtained in the simulation (see Figure 4.7), we see a much broader plume than in the passive case (see Figure 4.5), and evidently more diluted after some distance. But the results at different streamwise positions are dramatically changed (see Figure 4.8). Close to the ground, we almost over-estimate the experimental results by a factor of 2, in intensity as well as in plume width estimation. It gets even worse as we go higher (vertical profile). We also notice the appearance of a double peak shape in the experimental data, that is not captured in the simulations. Clearly, some physical aspect linked to dense gas is not handled by the high Re turbulent model, although the gravity term is activated in the turbulence $k - \varepsilon$ equation. We may not be in the right regime when turbulence is suppressed by density stratification [19] when we

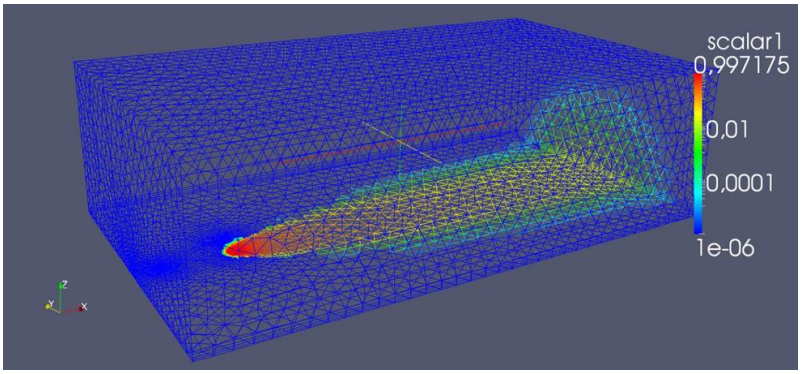

Figure 4.7 *Mass fraction of dense gas (CO_2) for the flat plate case with continuous release.*

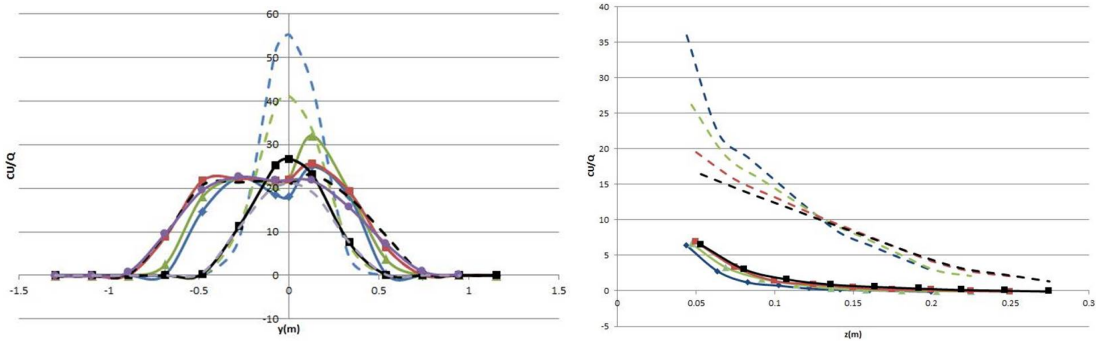

(a) Lateral profiles at z=0.025 m **(b)** Vertical profiles at y=0

Figure 4.8 *Profiles of normalized CO_2 concentration at different streamwise positions (blue = 0.75, green = 1.036, red = 1.4, black = 1.6, and purple = 2 m). Dashed lines show simulation results whereas solid lines with symbols show the experimental values.*

expect to have relaminerization with high values of S^* (here about 10). We have tried at the very end of the analysis to use a low Re turbulence model for the dense gas dispersion, and we notice a slight improvement, as can be seen in Figure 4.9. The double peak is captured, the concentration levels slightly lower, and the plume broader (the purple dashed curve is with a scalable wall law). The turbulent viscosity is also reduced by a factor of 3 by using the low Re model (see Figure 4.10).

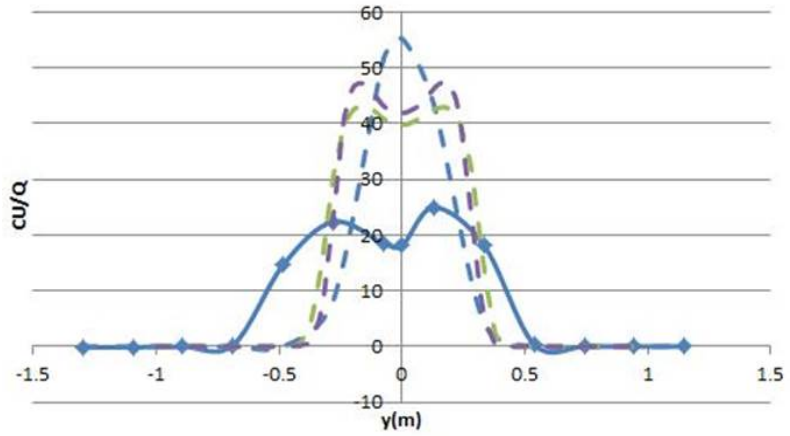

Figure 4.9 *Lateral profiles of normalized CO_2 concentration at x = 0.75 m and z = 0.025 m for different turbulent models. $k-\varepsilon$-linear(dashed blue), $k-\omega$-sst (dashed green) and $k-\omega$-sst with scalable wall function (dashed purple).*

All the following results have unfortunately been obtained with the $k-\varepsilon$-linear model (important remark for the dense gas dispersion).

4.6.2 Hill case

The hill case has been carefully designed to produce a flow field at the edge of separation for the neutral release. Upstream from the crest, the flow is following the streamwise direction and downstream, it almost separates for the velocities used in the wind tunnel. It was also expected that no separation occurs when using CO_2. The y^+-values (see Figure 4.11) are the same or smaller ($y^+ \sim 6$) than for the flat case upstream of the crest, where roughness 0.8 mm has been imposed, and a bit higher in the accelerated region downstream where the floor is smooth ($y^+ \sim 40$). Two sources are being tested. Source 1 is positioned upstream from the crest, in the middle of the slope and source 2 just after the crest, in order to look at the plume interaction with a turbulent or stratified boundary layer. The origin is placed at the foot of the hill. This is also a very demanding case, although the geometry looks simple, especially for RANS models that are not well suited to deal with anisotropic turbulent fluxes.

4.6.2.1 Neutral release from source 1

First we look at neutral dispersion from source 1 (upstream from the crest). Figure 4.12 shows the mean streamwise velocity in a plane at the symmetry line. Here, we don't notice any strong

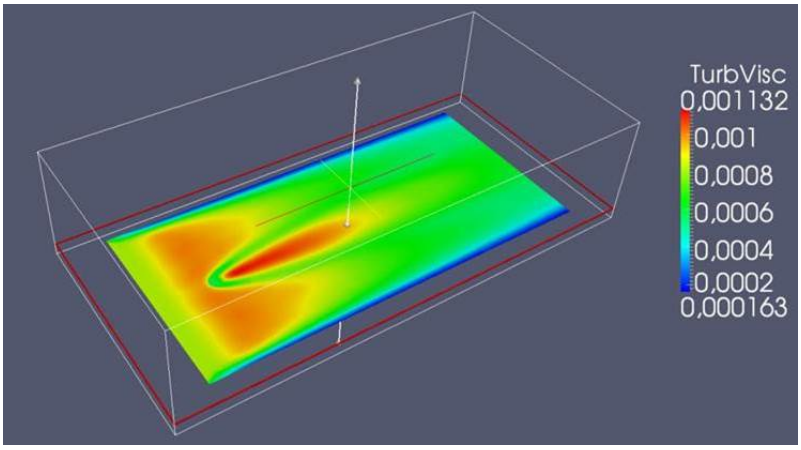

(a) $k - \varepsilon$ linear

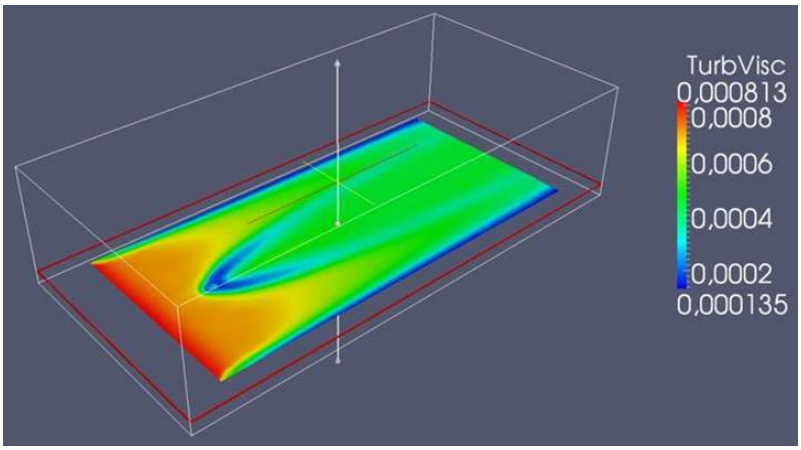

(b) $k - \omega$ sst

Figure 4.10 *Contours of turbulent viscosity in a plane close to the ground for two different turbulence models.*

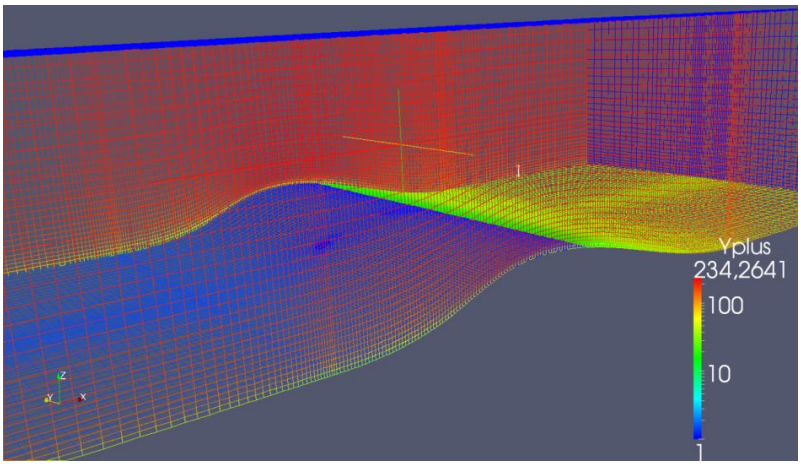

Figure 4.11 *Wall units y^+ for the hill case (rough and smooth regions visible).*

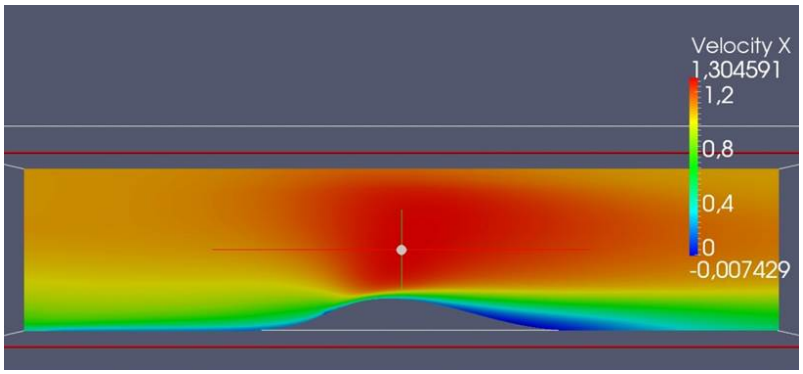

Figure 4.12 *Mean streamwise velocity in the symmetry plane for the hill case with neutral release from source 1.*

recirculation downstream of the hill crest. The flow is just accelerated and decelerated to small values close to the floor. A mass fraction iso surface of 10^{-6} is shown in Figure 4.13. The plume is slightly thinner (0.2 m) upwind from the top compared to the flat case ($\sim$ 0.4 m, Figure 4.7), but reaches the same lateral extension further downstream ($\sim$ 1 m). We see in Figure 4.14a that

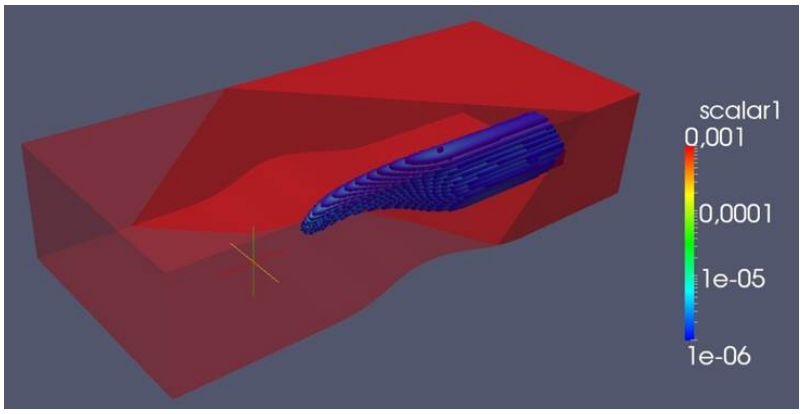

Figure 4.13 *Iso contour of mass fraction of air for the hill case with neutral release from source 1.*

we overestimate the concentration by at most 20% close to the ground (better agreement as we go further downstream), but the results get worse as we look at higher up where 50% error are encountered (see Figure 4.14b). Indeed we know the mesh is coarser there. But this discrepancy between vertical concentration profiles for experimental and simulation results partly comes from the lateral plume shift.

4.6.2.2 Dense gas release form source 1

For this case where CO_2 is released from source 1, only close to the source can we see a small backward flow (see Figure 4.15). No separation occurs downstream. Figure 4.16 shows the mass fraction iso surface of 10^{-6} for the CO_2 release. We see a much larger broadening of the plume compared to the neutral case. The dense gas effect is effectively changing the dispersion, and it is partially taken care of by the model. However, we notice on the results in Figure 4.17a (lateral

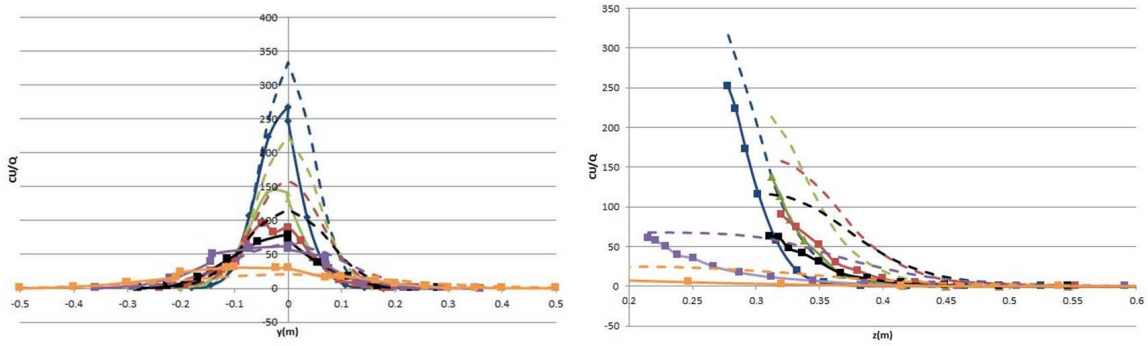

(a) Lateral profiles at different vertical positions

(b) Vertical profiles at y=0

Figure 4.14 *Profiles of normalized passive gas concentration at different streamwise positions (blue = 1.05, green = 1.2, red = 1.4, black = 1.6, purple = 2.05, and orange = 3 m). Dashed lines show simulation results whereas solid lines with symbols show the experimental values.*

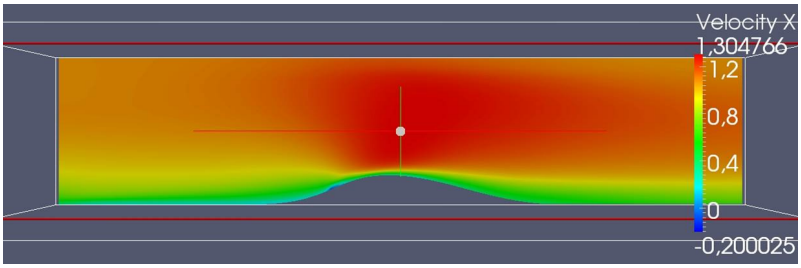

Figure 4.15 *Mean streamwise velocity in the symmetry plane for the hill case with dense gas release from source 1.*

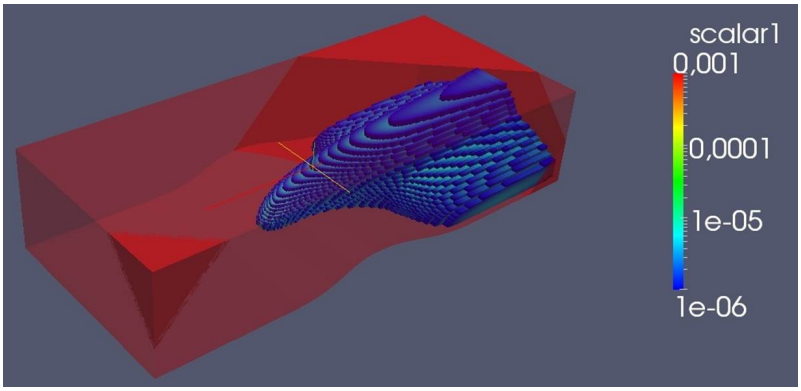

Figure 4.16 *Iso contour of mass fraction of CO_2 for the hill case with dense gas release from source 1.*

results) and Figure 4.17b (vertical results) that we miss some aspects of the dynamics. As we explained in the Flat scenario, the high Re models are unable to compute correctly the damping of turbulence generated by the dense gas, and overestimates turbulent viscosity. The experimental plume is two-sided, much broader, and uniform in intensity when we go further downstream, compared to the simulated plume.

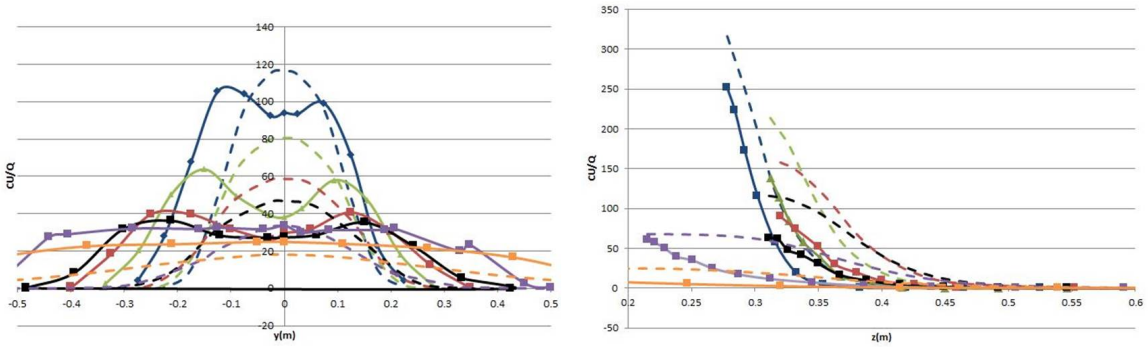

(a) Lateral profiles at different vertical positions

(b) Vertical profiles at y=0

Figure 4.17 *Profiles of normalized dense gas concentration at different streamwise positions (blue = 1.05, green = 1.2, red = 1.4, black = 1.6, purple = 2.05, and orange = 3 m). Dashed lines show simulation results whereas solid lines with symbols show the experimental values.*

4.6.2.3 Neutral release form source 2

For the case where air is released from source 2 (just after the hill crest), we have strong recirculation (see Figure 4.18) and probably separated flow (turbulent viscosity "tongue" in Figure 4.19) that may lead to a lifted plume. Whether this is a genuine effect or not will be investigated in the results below. In Figure 4.20, we see the iso surface representing the mass fraction of 10^{-6} which again

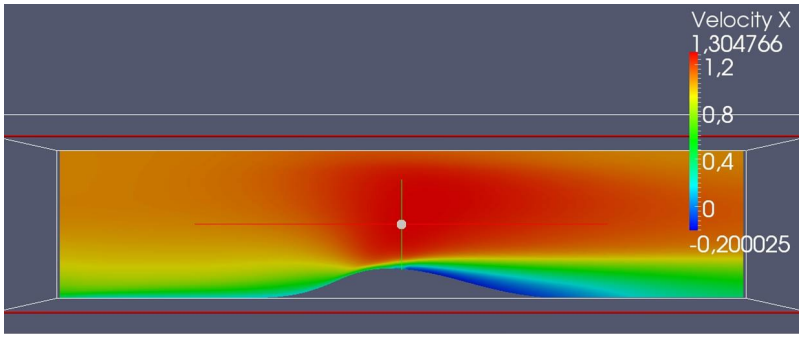

Figure 4.18 *Mean streamwise velocity in the symmetry plane for the hill case with neutral release from source 2.*

shows a wider plume compared to the flat neutral case (0.4 m width) and comparable to the source 1 neutral case (0.2 width). In Figure 4.21a the simulated normalized concentration close to the ground underestimates the experimental results by a factor of 2. Also higher from the ground we

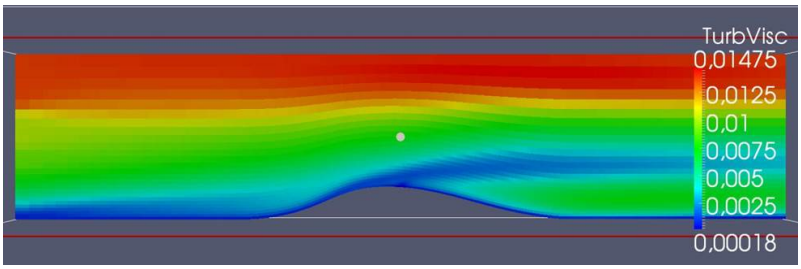

Figure 4.19 *Contours of turbulent viscosity in the symmetry plane for the hill case with neutral release from source 2.*

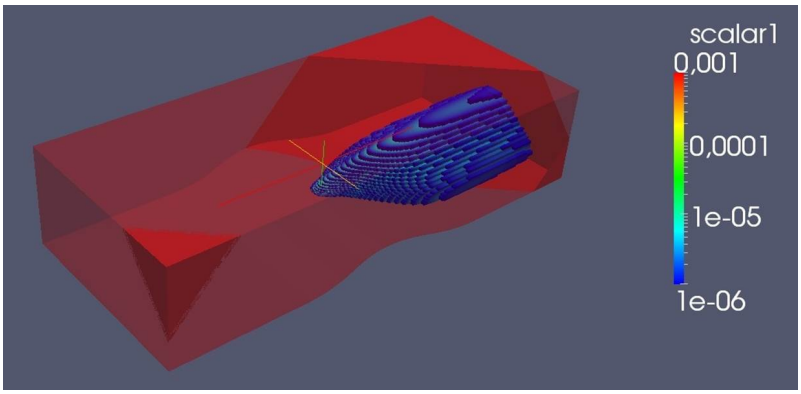

Figure 4.20 *Iso contour of mass fraction of air for the hill case with neutral release from source 2.*

see an overestimation (see Figure 4.21b). Again, we know that the mesh is coarser at higher z levels, which may explain the last remark. We can conclude that the separated flow is not what is really occurring in this case, and probably stems from an overestimation of turbulent viscosity close to the ground. A low Re model would be better suited.

4.6.2.4 Dense gas release form source 2

When we compare the mean velocity field from the dense gas release (see Figure 4.22) to the one with release of air (c.f. Figure 4.18) for the second source location we see dramatic changes, especially close to the ground downstream of the source location. No recirculation is observed close to the source for the dense gas case. The computed turbulent viscosity (see Figure 4.23) is lowered almost everywhere downstream (by turbulent damping), leading to a more pronounced direct gravitational effect on the mean flow and thus of the released gas advection.

The iso surface representing the mass fraction of 10^{-6} shown in Figure 4.24, presents again a broadening of the plume compared to neutral release from source 2.

This enlargement of the plume width is nevertheless underestimated, and the concentration levels overestimated with the two concentration peaks missing (see Figure 4.25a). The overestimation increases further away form the ground and decreases further away from the source location (see Figure 4.25b). The explanation is partly the same as for the Flat scenario. The only difference is that close to the source the agreement between simulation and experiment is rather good and degrades

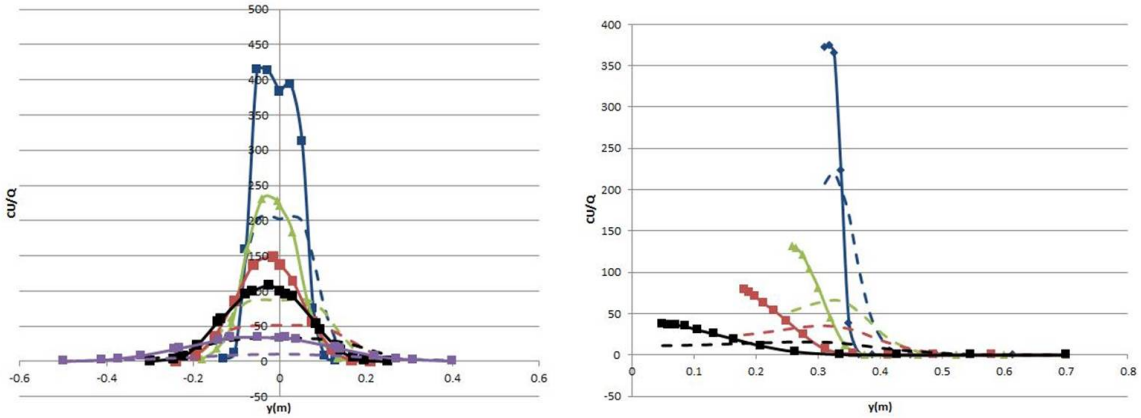

(a) Lateral profiles close to the ground

(b) Vertical profiles at y=0

Figure 4.21 *Profiles of normalized passive gas concentration at different streamwise positions (blue = 1.6, green = 1.75, red = 1.9, black = 2.05, and purple = 3 m). Dashed lines show simulation results whereas solid lines with symbols show the experimental values.*

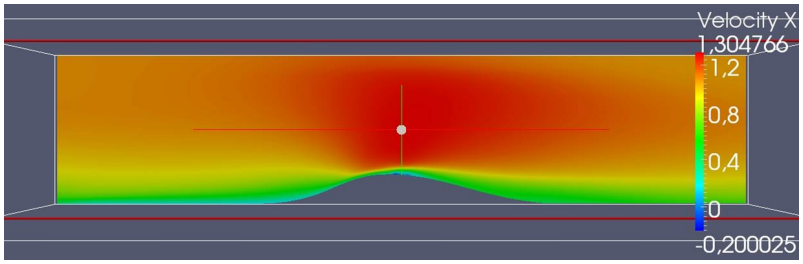

Figure 4.22 *Mean streamwise velocity in the symmetry plane for the hill case with dense gas release from source 2.*

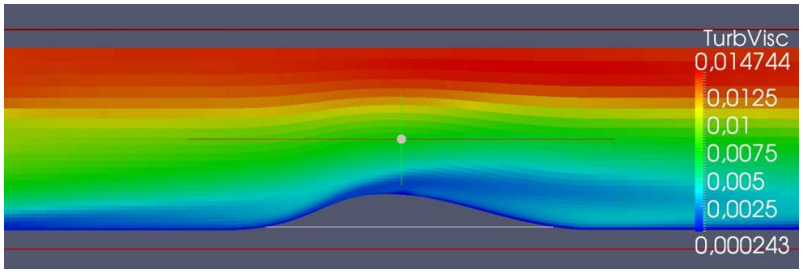

Figure 4.23 *Contours of turbulent viscosity in the symmetry plane for the hill case with dense gas release from source 2.*

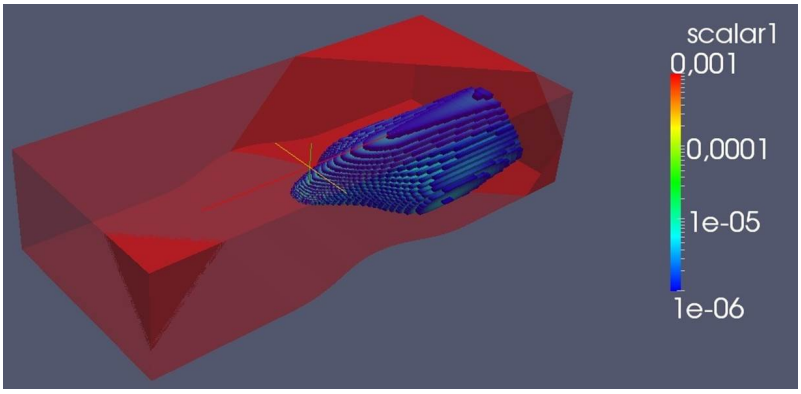

Figure 4.24 *Iso contour of mass fraction of CO_2 for the hill case with dense gas release from source 2.*

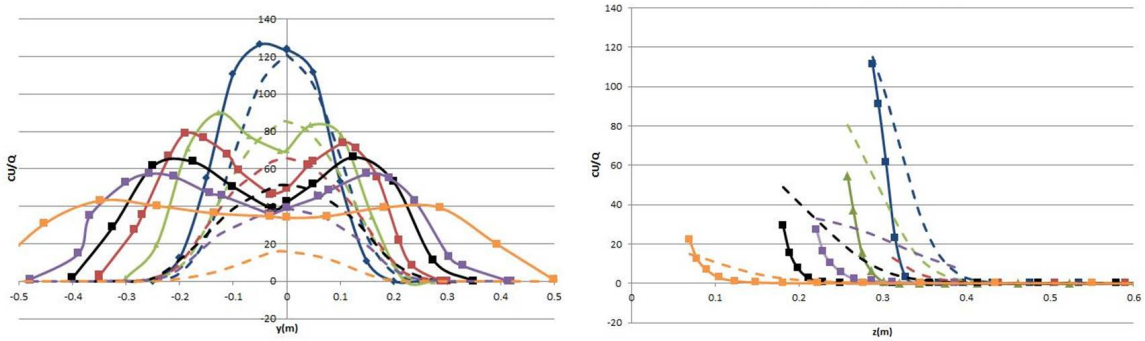

(a) Lateral profiles close to the ground

(b) Vertical profiles at y=0

Figure 4.25 *Profiles of normalized dense gas concentration at different streamwise positions (blue = 1.75, green = 1.9, red = 2.05, black = 2.2, purple = (2.35 (a), 2.05 (b)), and orange = 2.7 m). Dashed lines show simulation results whereas solid lines with symbols show the experimental values.*

as we go further downstream. The interaction of plume with the forming stratified boundary layer is partially captured.

4.6.3 Backward-facing step

A back-step is placed after the hill crest at $x \sim 1.4$ m, with a step height of 0.1 m. The source is placed on the ground just behind the step, with diameter 0.1 m. The origin is still placed at the foot of the hill. We expect a strong interaction with the recirculation region due to the back-step, which is known to be a benchmark for CFD models. The mesh (see Figure 4.26) is fine with $\Delta min \sim 5$ mm. The RANS model use is the linear $k - \varepsilon$ model.

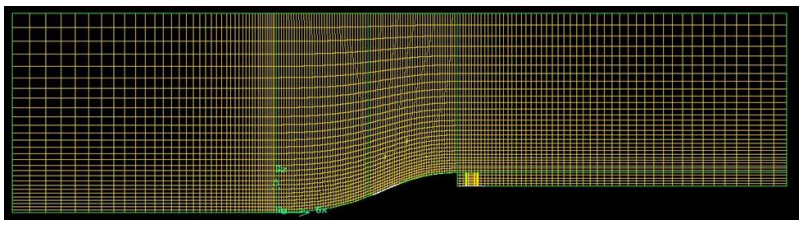

Figure 4.26 *Mesh of the backward-facing step.*

4.6.3.1 Neutral release

The computed mean velocity field exhibits, as expected, a recirculation region behind the step (not explicitly shown in Figure 4.27) and the contour of turbulent viscosity (see Figure 4.28) shows a separation between the mixing layer under the step height and a recovering zone above. We expect the neutral scalar to be well mixed under the mixing height.

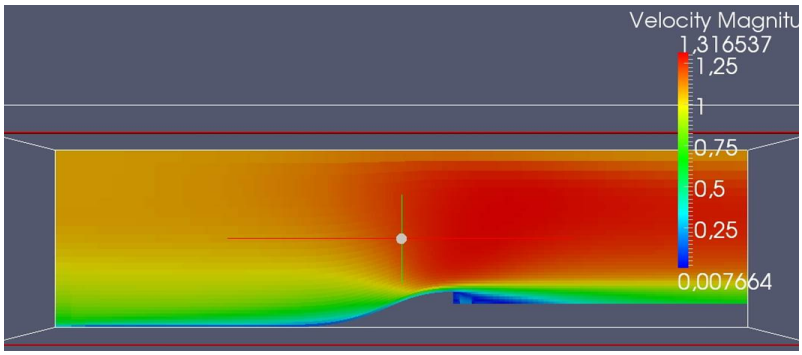

Figure 4.27 *Mean velocity magnitude in the symmetry plane for the back-step case with neutral release.*

The air mass fraction shown in Figure 4.29 is indeed confined below the mixing height (where strong shear exists), at least a few step height distance from the step of the back-step. We also notice lateral spreading of the air which is trapped in the recirculation zone, showing quasi-2D effects.

The lateral variation of normalized concentration of neutral gas at different downwind distances (see Figure 4.30a) show up to 30% underestimation close to the ground, and overestimation above

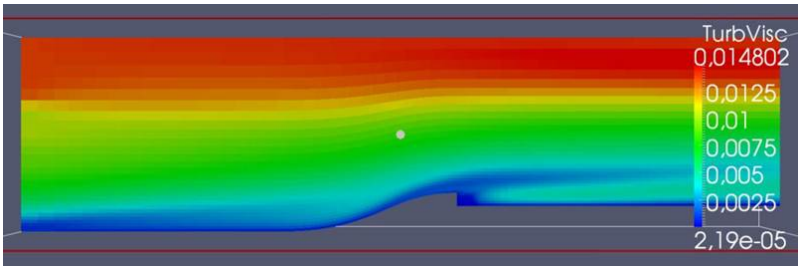

Figure 4.28 *Contours of turbulent viscosity in the symmetry plane for the back-step case with neutral release.*

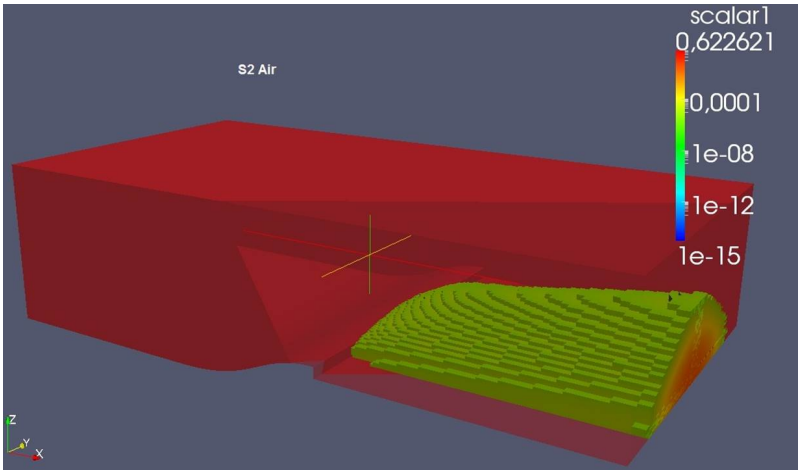

Figure 4.29 *Mass fraction of air for the back-step case with neutral release.*

the mixing height (~0.3 m, see Figure 4.30b). The results agree better further downstream. The simulation has a tendency to overestimate the vertical mass transfer. The use of LES models to capture the right 3D effects may improve the results.

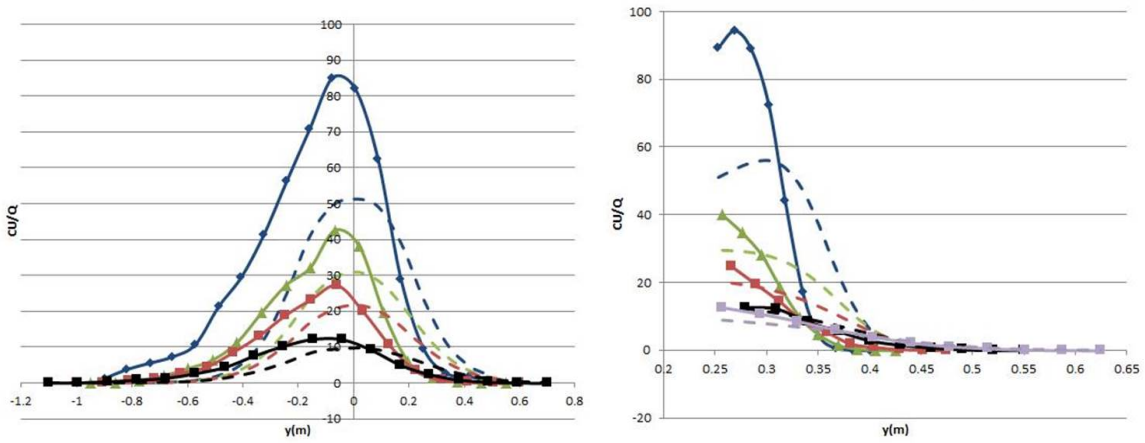

(a) Lateral profiles close to the ground

(b) Vertical profiles at y=0

Figure 4.30 *Profiles of normalized neutral gas concentration at different streamwise positions (blue = 1.75, green = 2.05, red = 2.35, black = (3.5 (a), 2.85 (b)), and purple = 3.5 (b)). Dashed lines show simulation results whereas solid lines with symbols show the experimental values.*

4.6.3.2 Dense gas release

Differences on flow field appear when using CO_2. The recirculation region seems smaller (see Figure 4.31) than for neutral release. The stratification damps the turbulence in the so-called mixing region, which exhibits a much smaller turbulent viscosity as seen in Figure 4.32.

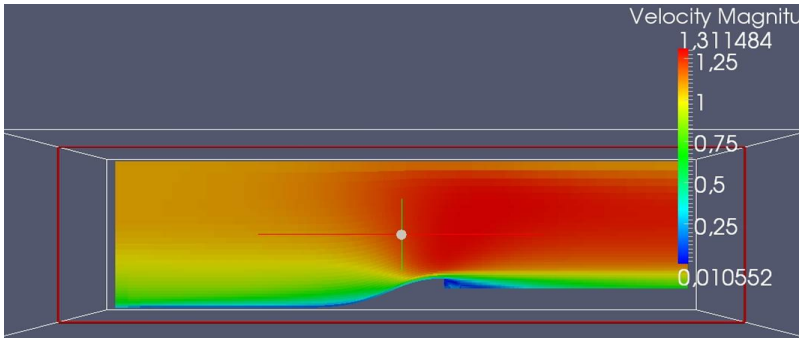

Figure 4.31 *Mean velocity magnitude in the symmetry plane for the back-step case with dense gas release.*

Due to the turbulent damping, a more pronounced lateral dispersion of CO_2 is apparent compared to air (see Figure 4.33).

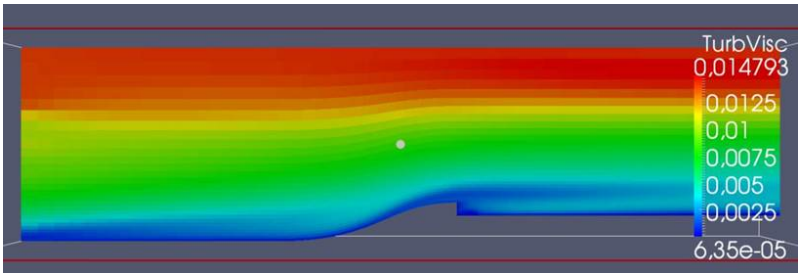

Figure 4.32 *Contours of turbulent viscosity in the symmetry plane for the back-step case with dense gas release.*

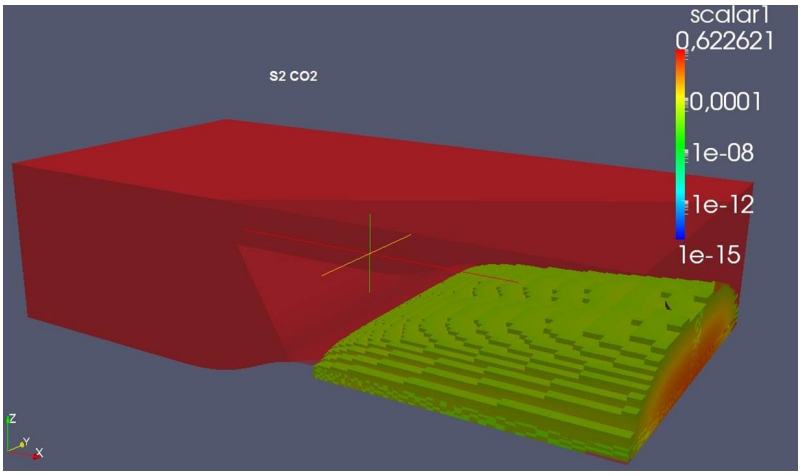

Figure 4.33 *Mass fraction of CO_2 for the back-step case with dense gas release.*

Although the simulated concentration levels are smaller and the quasi 2D-plume larger than for the neutral case, we highly overestimate (factor of 3) the experimental results (see Figure 4.34a). The observed plumes are much more bi-dimensionalized than the simulated. The stratification confines the CO_2 concentration under the back-step height, and only small amounts cross this virtual limit. On the contrary (see Figure 4.34b) the simulation shows a more pronounced vertical transport outside this "limit".

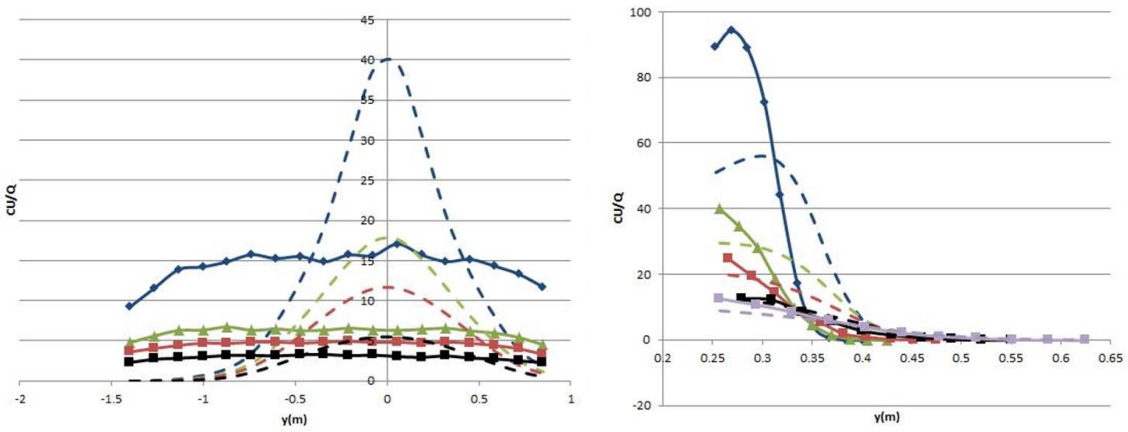

(a) Lateral profiles close to the ground

(b) Vertical profiles at y=0

Figure 4.34 *Profiles of normalized dense gas concentration at different streamwise positions (blue = 1.75, green = 2.05, red = 2.35, black = (3.5 (a), 2.85 (b)), and purple = 3.5 (b) m). Dashed lines show simulation results whereas solid lines with symbols show the experimental values.*

4.6.4 Backward-facing step with array 1

To add further complexity, an array of blocks (3×13) is placed 8 step lengths behind the backward-facing step. The source is placed at y = 0 m, aligned with the centreline of the domain upstream of the middle block. The mesh used for array 1 is shown in Figure 4.35. A fine mesh is created around the source, the blocks, and the step. It is structured upwind and unstructured downwind of the step.

4.6.4.1 Neutral release

The impact of the array, which is placed in the mixing layer of the back-step, is to further decrease the mean flow (see Figure 4.36) and enhance the turbulence viscosity (see Figure 4.37) where it would have otherwise recovered to its flat case state.

The dispersion of air is comparable to the neutral back-step case (see Figure 4.38). We still observe a discrepancy with the experimental values. Underestimating the concentrations below the mixing height (Figure 4.39a), overestimating above (Figure 4.39b), with a better agreement as we go further downstream. This is probably because the high Re model is better to deal with bluff bodies (the blocks) and high levels of turbulent production and dissipation.

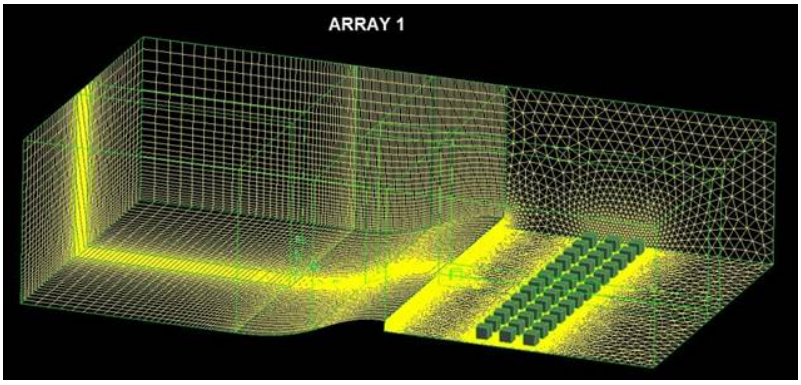

Figure 4.35 *Mesh of the backward-facing step with array 1.*

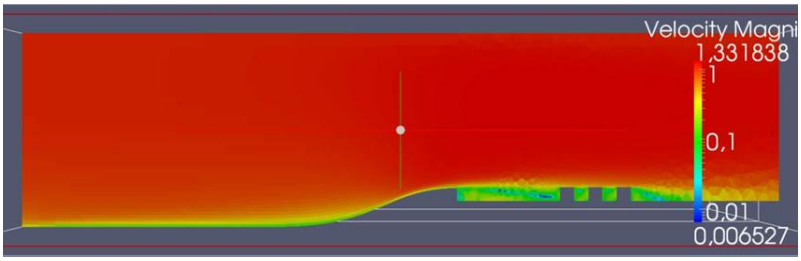

Figure 4.36 *Mean velocity magnitude in the symmetry plane for the back-step with array 1 case with neutral release.*

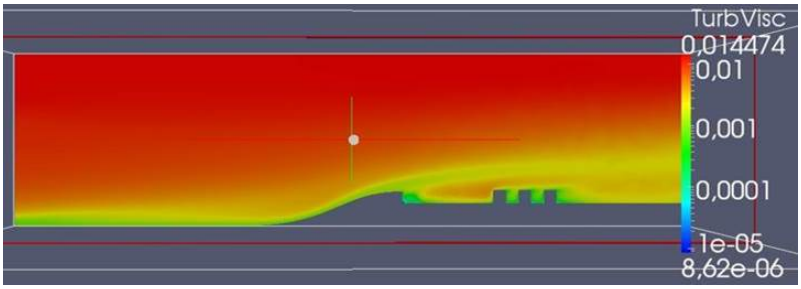

Figure 4.37 *Contours of turbulent viscosity in the symmetry plane for the back-step with array 1 case with neutral release.*

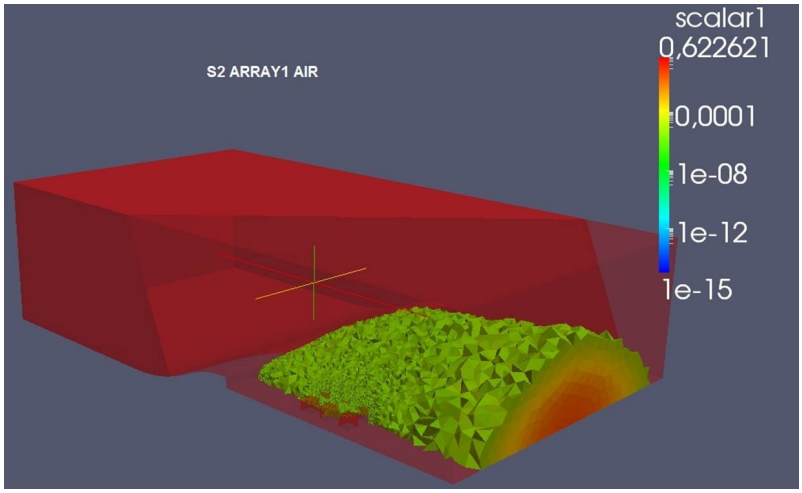

Figure 4.38 *Mass fraction of air for the back-step with array 1 case with neutral release.*

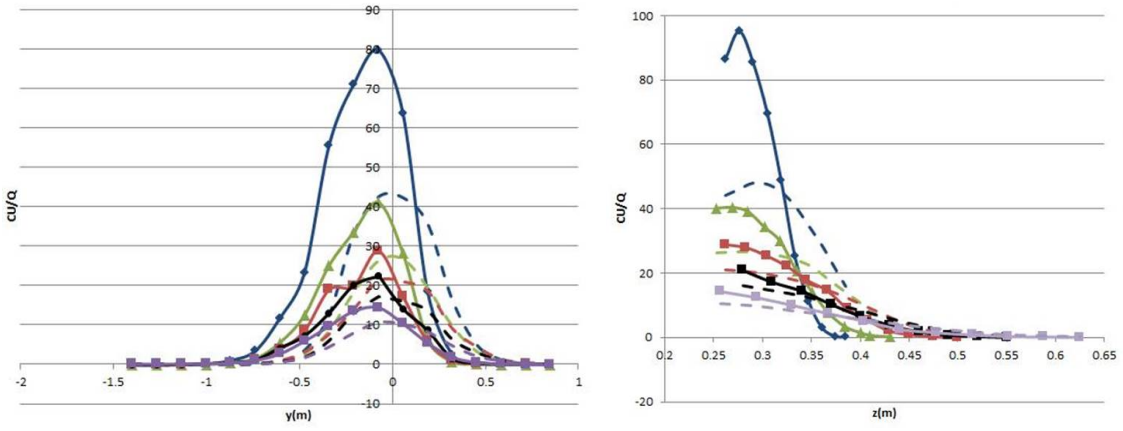

(a) Lateral profiles at z=0.25 **(b)** Vertical profiles at y=0

Figure 4.39 *Profiles of normalized dense gas concentration at different streamwise positions (blue = 1.75, green = 2.05, red = 2.35, black =2.85, and purple = 3.5 m). Dashed lines show simulation results whereas solid lines with symbols show the experimental values.*

4.6.4.2 *Dense gas release*

This case is similar to the back-step CO_2 case. As there is enough distance between the step and the first row of cubes, the dense gas plume spreads laterally behind the step. The simulated mean flow field is shown in a xz-plane in Figure 4.40a and in a xy-plane in Figure 4.40b. The turbulent

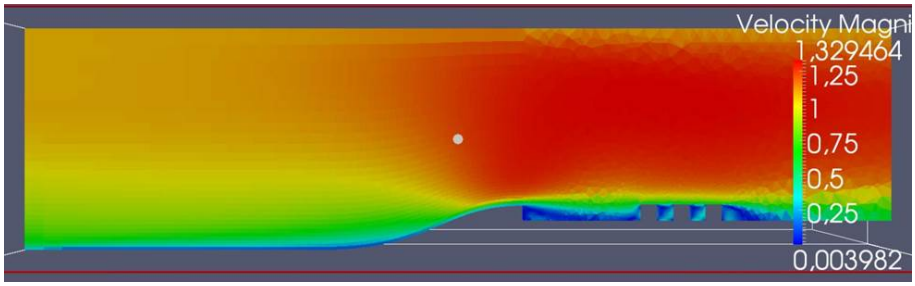

(a) xz-plane

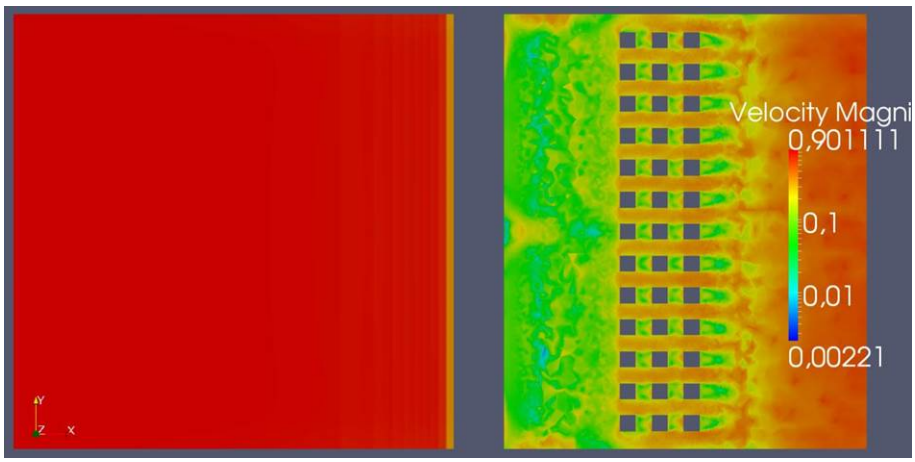

(b) xy-plane

Figure 4.40 *Contours of mean velocity magnitude in two different planes for the back-step with array 1 case with dense gas release.*

viscosity (see Figure 4.41) resembles the dense gas release without array close to the step, and the neutral release further downstream.

As for the CO_2 mass fraction computed by Saturne (see Figure 4.42), we see a flattening of the plume from stratification and the interaction with the recirculation behind the back-step. Still in a lesser extent compared to experiment (see Figure 4.43a and Figure 4.43b). Again, a slight improvement is expected by using a low Re turbulent model.

4.6.5 Backward-facing step with array 2

A second array of blocks (3×13) is placed 4 step heights from the step. This case is quite different: the array 2 is placed inside the recirculation zone and close to the source. The mesh used is shown in Figure 4.44.

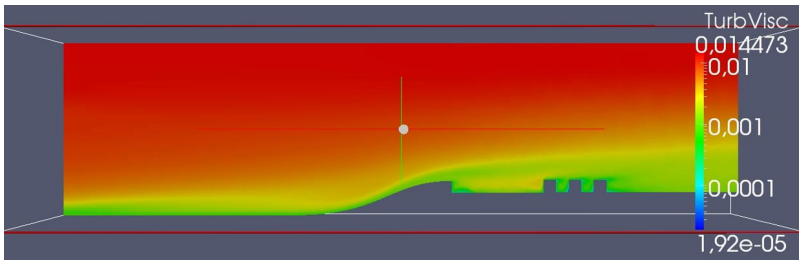

Figure 4.41 *Contours of turbulent viscosity in the symmetry plane for the back-step with array 1 case with dense gas release.*

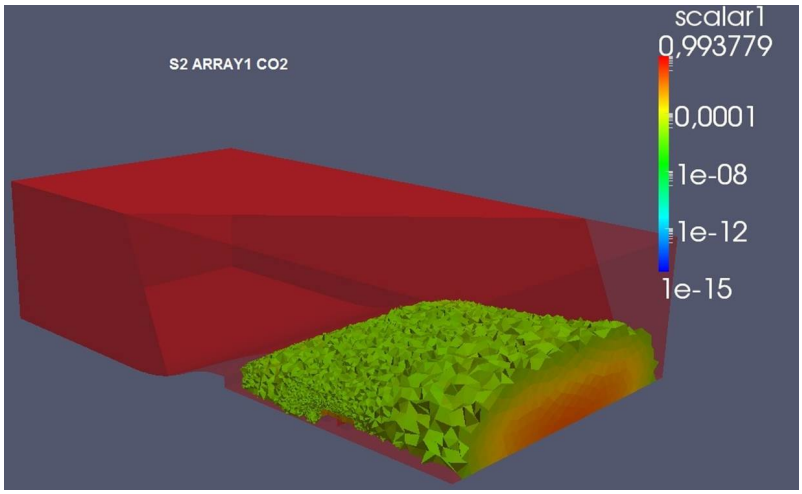

Figure 4.42 *Mass fraction of CO_2 for the back-step with array 1 case with dense gas release.*

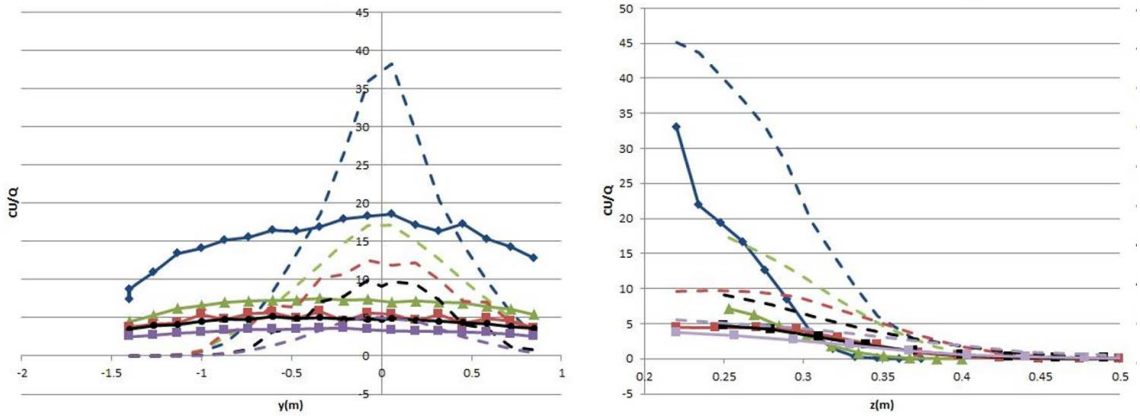

(a) Lateral profiles at z=0.25 **(b)** Vertical profiles at y=0

Figure 4.43 *Profiles of normalized dense gas concentration at different streamwise positions (blue = 1.75, green = 2.05, red = 2.35, black =2.85, and purple = 3.5 m). Dashed lines show simulation results whereas solid lines with symbols show the experimental values.*

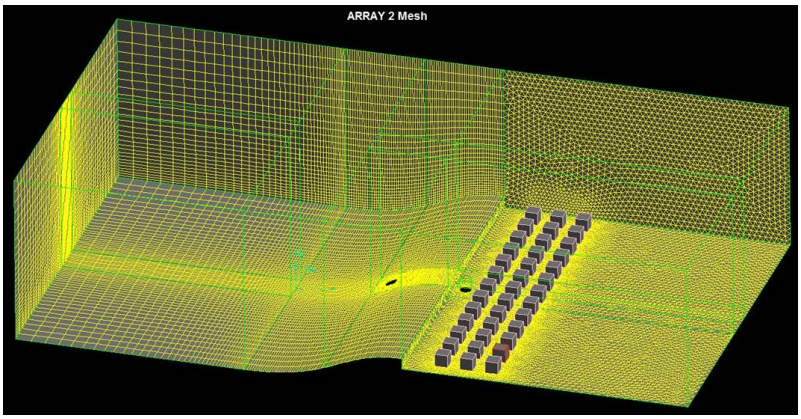

Figure 4.44 *Mesh of the backward-facing step with array 2.*

4.6.5.1 Neutral release

Here, we have a skimming flow and a strong mixing layer (ML) under step height, prolonged by the close array (see Figure 4.45). The mean flow is reduced under the ML and the turbulent viscosity enhanced (see Figure 4.46) especially in between the step and the first row of blocks, and after the blocks where the neutral gas can be trapped and mixed.

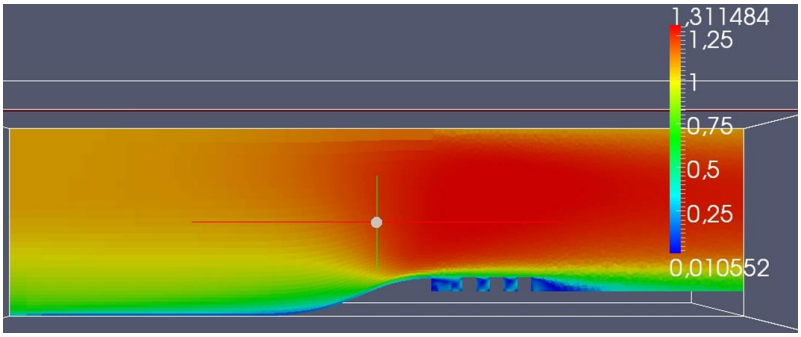

Figure 4.45 *Mean velocity magnitude in the symmetry plane for the back-step with array 2 case with neutral release.*

For this case, we don't have the experimental data, so we show qualitatively the simulation result of the mass fraction in Figure 4.47. It seems that the plume doesn't spread as much in the lateral direction compared to array 1, being strongly mixed with the surrounding air due to the presence of array 2.

4.6.5.2 Dense gas release

Again, the close presence of the array 2 induces a skimming flow and a better mixing than for array 1 with CO_2. Indeed the mean flow results are comparable with the results from the neutral release with array 2 (see Figure 4.48). This is true also for the turbulent viscosity results (see Figure 4.49).

Nevertheless the CO_2 plume encounters strong lateral dispersion (see Figure 4.50). The only experimental results are vertical profiles of the normalized concentration of CO_2 and they show

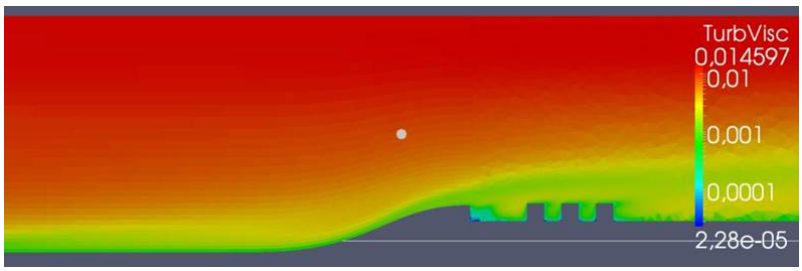

Figure 4.46 *Contours of turbulent viscosity in the symmetry plane for the back-step with array 2 case with neutral release.*

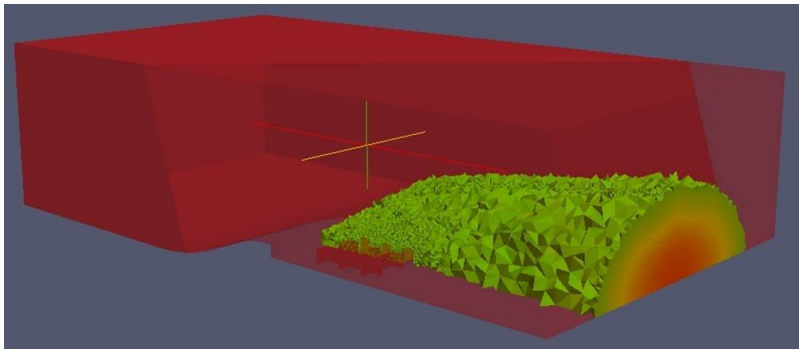

Figure 4.47 *Mass fraction of air for the back-step with array 2 case with neutral release.*

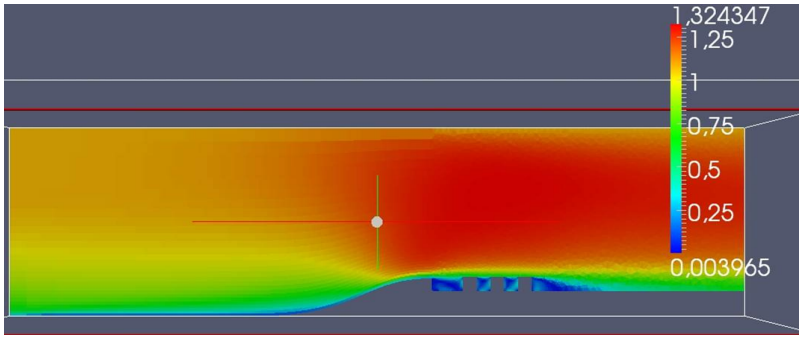

Figure 4.48 *Mean velocity magnitude in the symmetry plane for the back-step with array 2 case with dense gas release.*

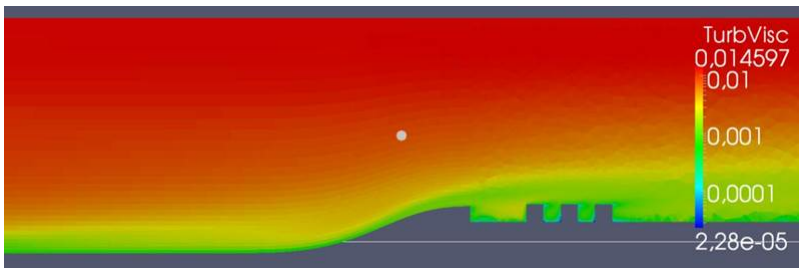

Figure 4.49 *Contours of turbulent viscosity in the symmetry plane for the back-step with array 2 case with dense gas release.*

up to 30% overestimation (see Figure 4.51) close to the ground, again showing that the model underestimates lateral spreading and collapsing of the dense gas.

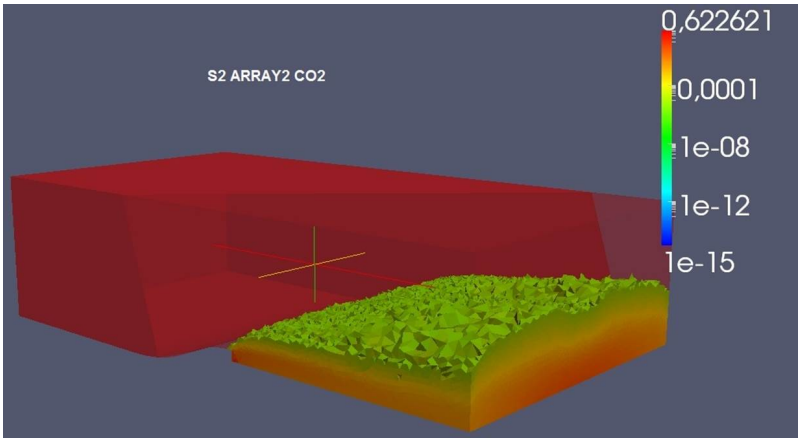

Figure 4.50 *Mass fraction of CO_2 for the back-step with array 2 case with dense gas release.*

4.6.6 Simple array 0°

The Simple Array consists of 4 blocks oriented 0° or 45° relative to the streamwise direction. The objective is to look at the dense gas dispersion closely taking into account blocking and effect of a small array. The sources are placed according to Figure 2.5 in Chapter 2.4. The mesh is finer around the sources and the blocks. A meshed boundary layer is generated on the ground (see Figure 4.52).

The mean flow vectors computed by Saturne are symmetric (see Figure 4.53). We expect to see a plume with a single peak from source 1, and multiple peaks from source 2 and source 3.

4.6.6.1 Neutral release from source 1

Mass fraction of is shown in Figure 4.54. It looks rather undisturbed by the array. We will show results only for the lateral measurements, because the simulated and experimental plumes are shifted which lead to large vertical discrepancy. The lateral normalized concentration is plotted for different distances from the source (see Figure 4.55); upstream of the array (x = 0.75 m, blue lines), in between (x=1.036 m, green lines) and downstream (x = 1.3 m, red lines). We see that globally the concentration and width are well predicted, although shifted. The results improve as we go further downstream.

4.6.6.2 Neutral release from source 2

The mass fraction of passive gas is seen in Figure 4.56 for source 2. The plume stays along the domain centreline with the exception of being enlarged over the array. The result at ground level (z=0.025 m) is shown in Figure 4.57. The 3 peaks we expected by observing the flow field is indeed observed by experiment, but is much less pronounced for the simulation results. Again the results compare better when we go away from the array.

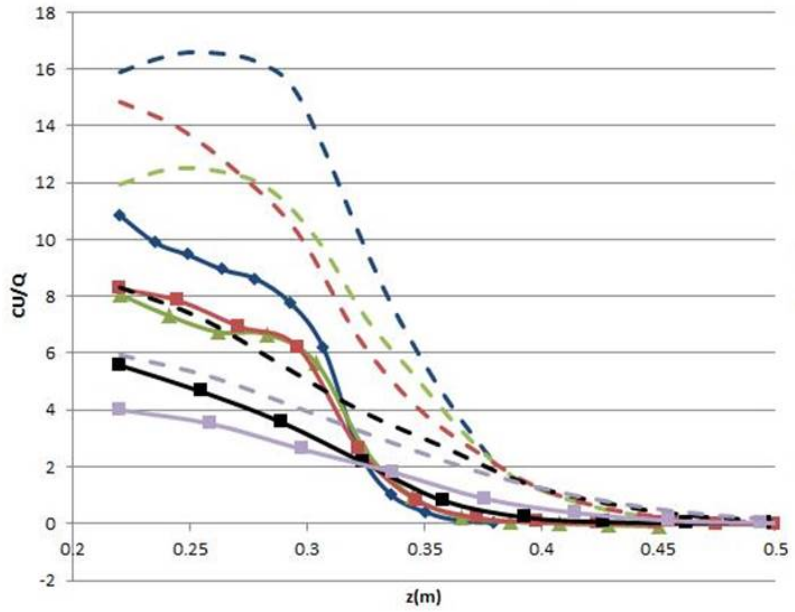

Figure 4.51 *Vertical profiles of normalized dense gas concentration at the centreline at different streamwise positions (blue = 1.91, green = 2.13, red = 2.35, black =2.85, and purple = 3.5 m). Dashed lines show simulation results whereas solid lines with symbols show the experimental values*

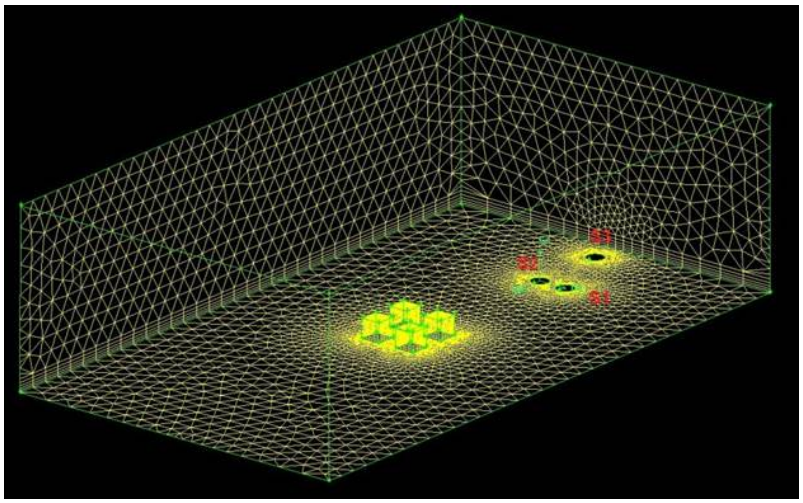

Figure 4.52 *Mesh of the simple array 0°. Sources are placed as shown in Figure 2.5*

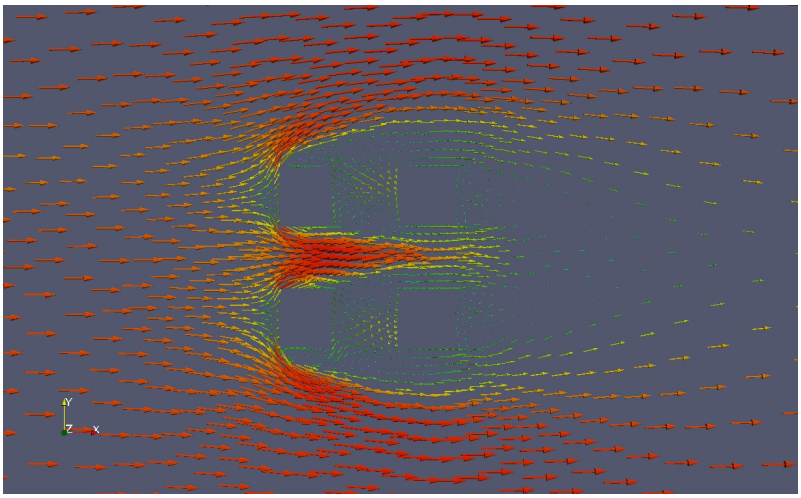

Figure 4.53 *Flow vectors at z=0.025 m for the simple array $0°$.*

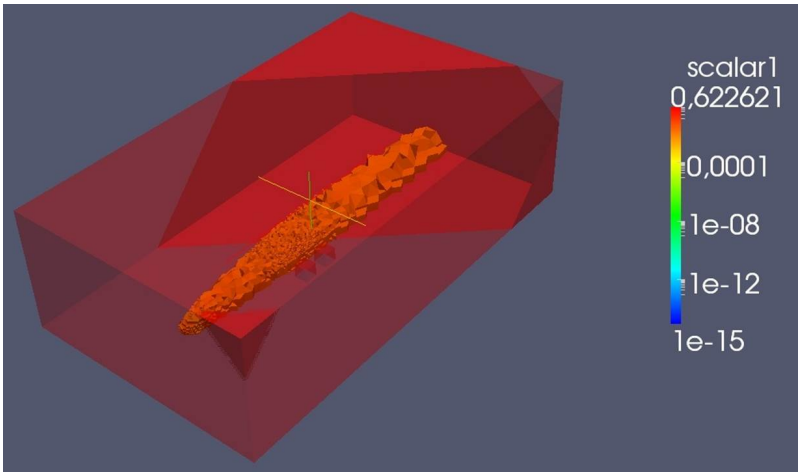

Figure 4.54 *Iso surface of mass fraction ($C = 10^{-2}$) of air in the simple array $0°$ with neutral release from source 1.*

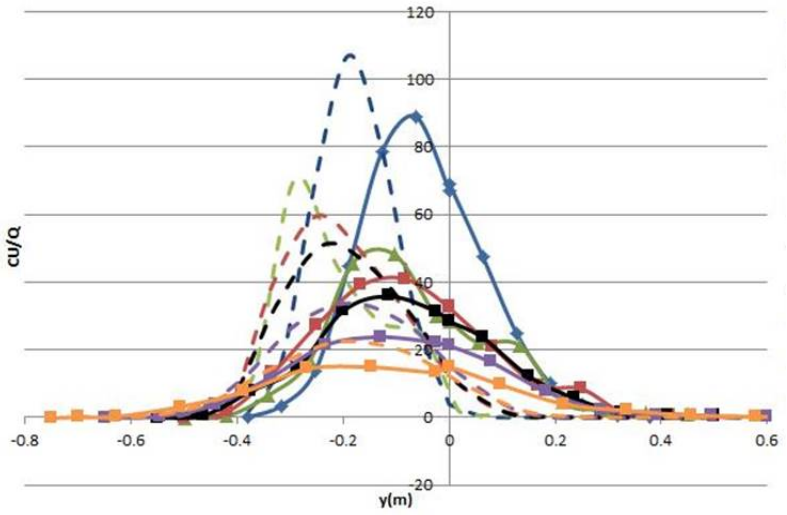

Figure 4.55 *Lateral profiles of normalized concentration of neutral gas at z=0.025 m and at different streamwise positions (blue = 0.75, green = 1.036, red = 1.3, black =1.5, purple = 2, and orange = 3 m). Dashed lines show simulation results whereas solid lines with symbols show the experimental values*

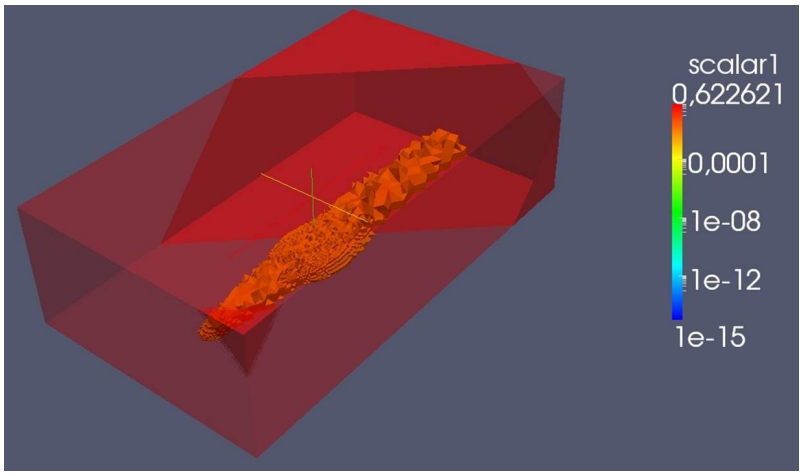

Figure 4.56 *Iso surface of mass fraction ($C = 10^{-2}$) of air in the simple array $0°$ with neutral release from source 2.*

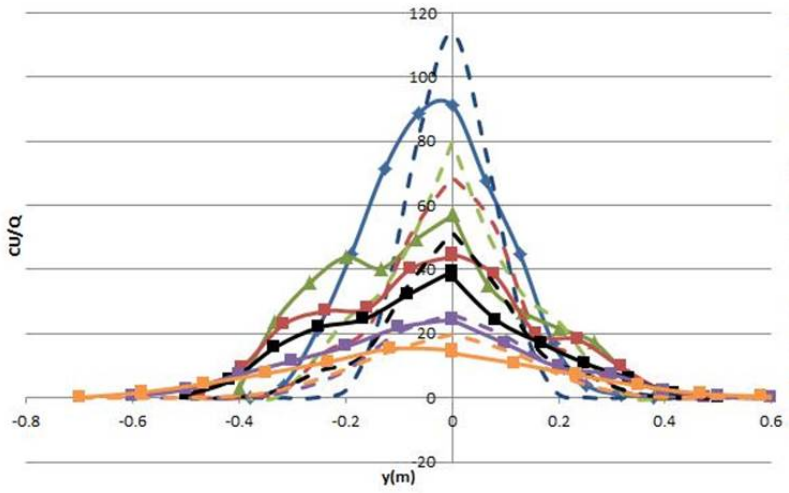

Figure 4.57 *Lateral profiles of normalized concentration of neutral gas at z=0.025 m and at different streamwise positions (blue = 0.75, green = 1.036, red = 1.3, black =1.5, purple = 2, and orange = 3 m). Dashed lines show simulation results whereas solid lines with symbols show the experimental values*

4.6.6.3 Dense gas release from source 2

The CO_2 case is even more interesting. As seen in Figure 4.58 the large plume is collapsed and remaining closer to the ground compared to the neutral release. This means the gas either goes right,

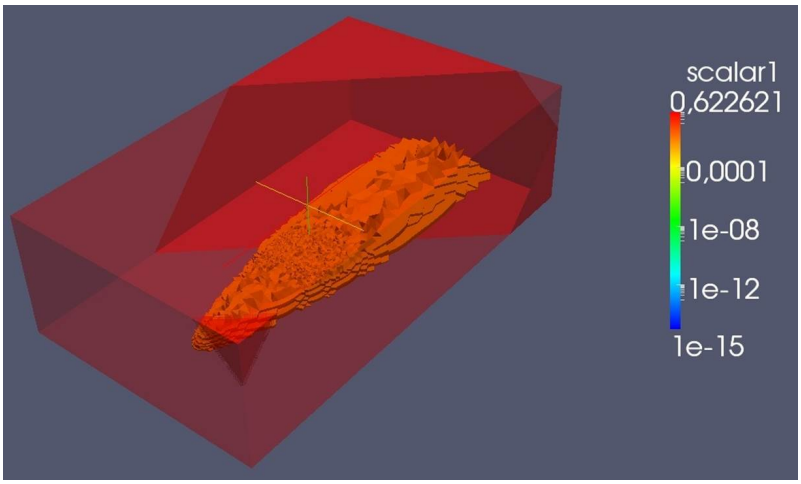

Figure 4.58 *Iso surface of mass fraction ($C = 10^{-2}$) of CO_2 in the simple array $0°$ with dense gas release from source 2.*

in between, or left of the array. The results for normalized concentration against lateral position at ground level (see Figure 4.59); the 3 peaks are very apparent and well separated. Inside the array (x = 1.036 m, green lines), the experiment and the simulation agrees rather well, although the inlet concentration profiles are different (x = 0.75 m, blue lines). As we go further downstream, the central peak disappears for the experimental results, while the simulation only preserves the central

peak. This problem may again be solved using a low Re turbulent model and a finer mesh inside the dense gas boundary layer.

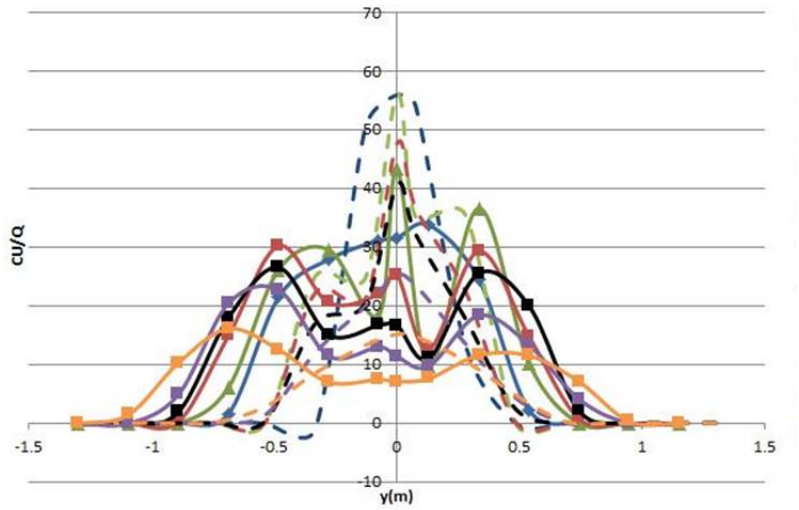

Figure 4.59 *Lateral profiles of normalized concentration of CO_2 at z=0.025 m and at different streamwise positions (blue = 0.75, green = 1.036, red = 1.4, black =1.6, purple = 2, and orange = 3 m). Dashed lines show simulation results whereas solid lines with symbols show the experimental values*

4.6.7 Simple array 45°

We turn the Simple array 45 degrees. The mesh used is shown in Figure 4.60 with refinement around the sources and the blocks. The flow vectors are visualized in Figure 4.61. The symmetric

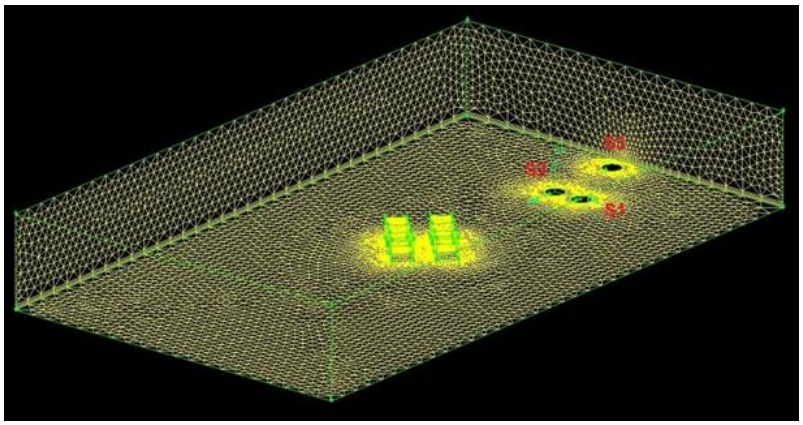

Figure 4.60 *Mesh of the simple array 45°. Sources are placed as shown in Figure 2.5*

flow separates into 4 paths with complicated recirculation patterns. We expect strong mixing of scalar and a dispersion less sensitive to small orientation shifts of the inlet profiles compared to the 0° scenario.

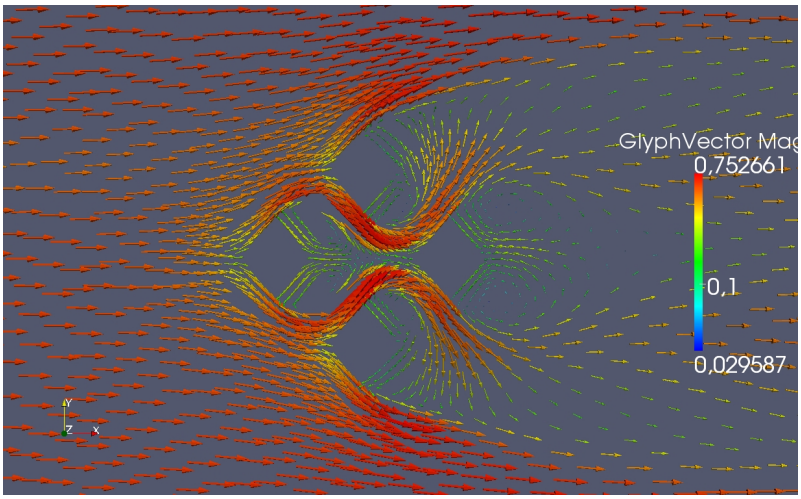

Figure 4.61 *Flow vectors at z=0.025 m for the simple array* 45°.

4.6.7.1 Neutral release from source 1

The air released from source 1 shows almost the same features as the 0 degree scenario (see Figure 4.62) except a broadening of the plume in the same direction the source is shifted in. Good

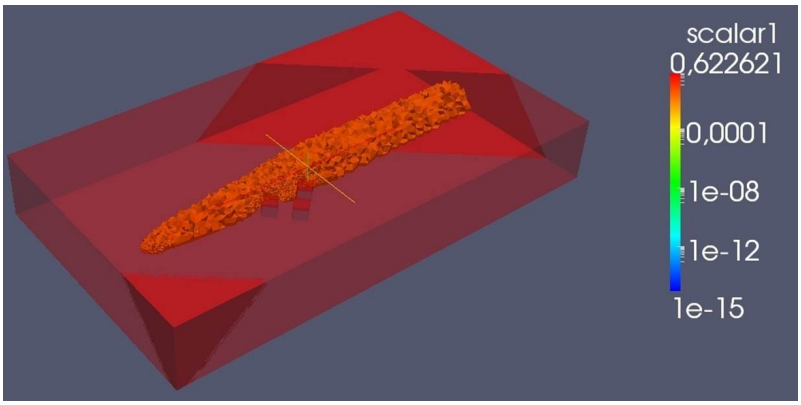

Figure 4.62 *Iso surface of mass fraction ($C = 10^{-2}$) of air in the simple array* 45° *with neutral release from source 1.*

agreements between experimental and simulated results are seen in Figure 4.63, once a 10 cm lateral shift is applied. Concentration and plume width are similar. The lateral spreading is underestimated by the simulation. This brings us to think that a good inlet prediction is sufficient to validate such a model for passive release.

4.6.7.2 Dense gas release from source 1

The next scenario considered here is the CO_2 release from source 1. We see in Figure 4.64 the strong effect the dense gas has on dispersion; a 2 sided plume going around (and slightly over) the

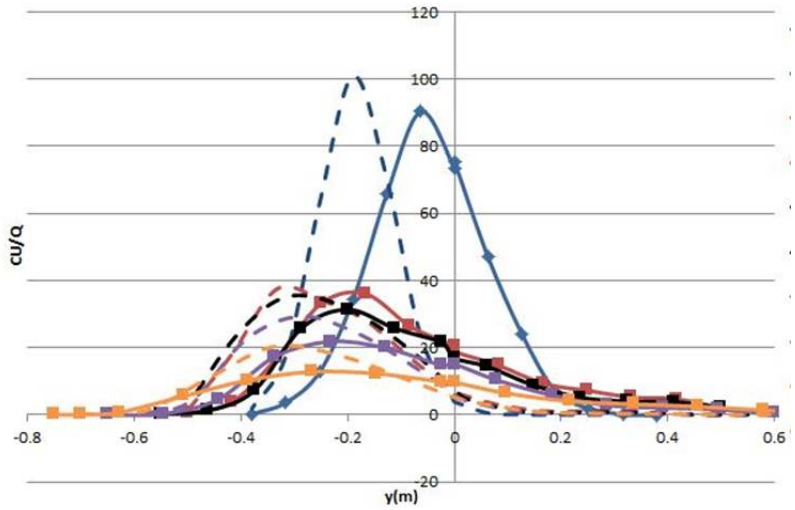

Figure 4.63 *Lateral profiles of normalized concentration of neutral gas at z=0.025 m and at different streamwise positions (blue = 0.75, red = 1.4, black =1.6, purple = 2, and orange = 3 m). Dashed lines show simulation results whereas solid lines with symbols show the experimental values*

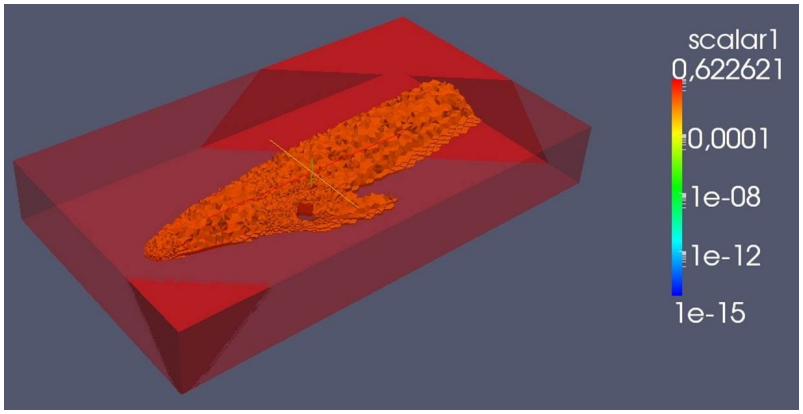

Figure 4.64 *Iso surface of mass fraction ($C = 10^{-2}$) of CO_2 in the simple array $45°$ with dense gas release from source 1.*

blocks. The two peaks resulting from the two sided plume are clearly visible in the experimental results (see Figure 4.65). These are a little lower in concentration for the simulation, although the shape is also captured. Further downstream, the dis symmetry in both cases is captured, and concentration is comparable. Again, a better inlet profile for concentration would improve the results. That brings us to the fundamental problem of dense gas release on flat ground that we mentioned in 4.6.1.2.

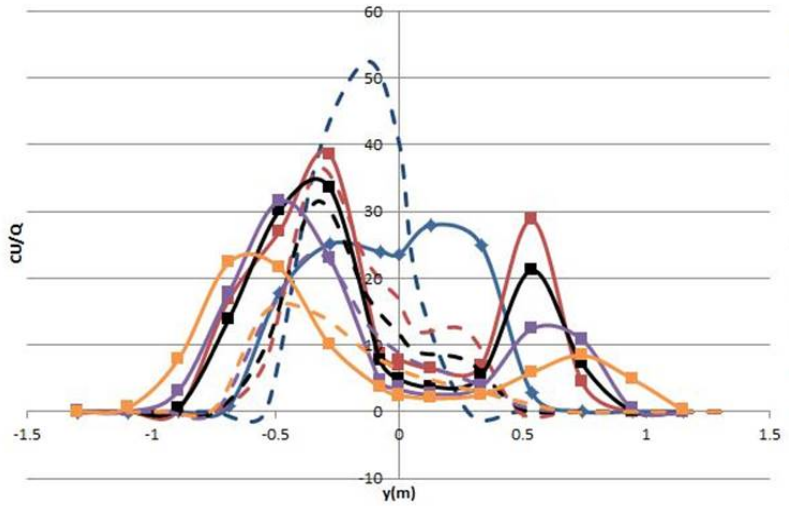

Figure 4.65 *Lateral profiles of normalized concentration of CO_2 at z=0.025 m and at different streamwise positions (blue = 0.75, red = 1.4, black =1.6, purple = 2, and orange = 3 m). Dashed lines show simulation results whereas solid lines with symbols show the experimental values*

4.6.8 Complex array 0°

The next case concerns a more complex array, with dissymmetry in blocks shapes and heights. It can be viewed as an idealized urban area in scale 1:200 oriented 0 degrees from the main flow direction. Source 1 is located inside the array, source 2 outside but on the centreline and source 3 outside but off centreline. A portion of the mesh is shown in Figure 4.66 with refinement around the sources, the blocks and the ground. The finest mesh size is 5 mm.

4.6.8.1 Neutral release from source 1

The stationary average flow field at z = 0.025 m is shown in Figure 4.67. The flow field contains cavity zones, recirculation zones and accelerated flow. The recovery length is of the order of the array width. The iso surface of the air mass fraction ($C = 10^{-2}$) is shown in Figure 4.68. The plume is first enlarged rapidly by the turbulence produced by the source, and then advected as a single plume along the main bottom street (see Figure 4.69a). Vertically, the plume rises upstream before being advected over the blocks (see Figure 4.69b).

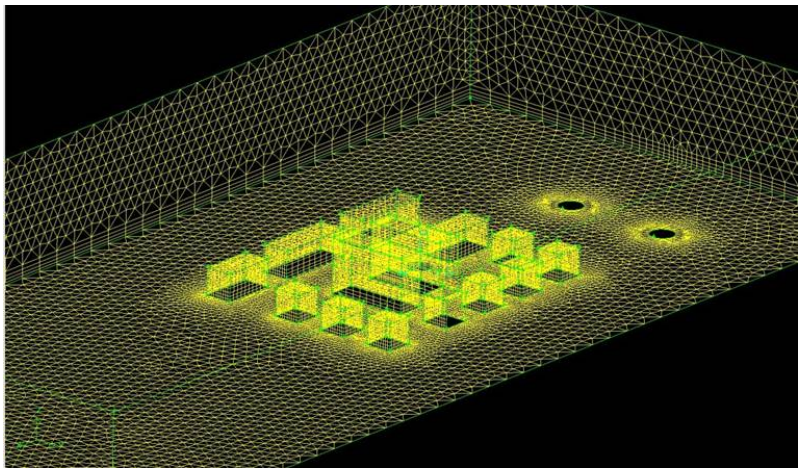

Figure 4.66 *Mesh of the complex array $0°$. Source 1 is placed inside the array, source 2 outside on the symmetry line and source 3 outside and slightly of the symmetry line, c.f. Figure 2.6*

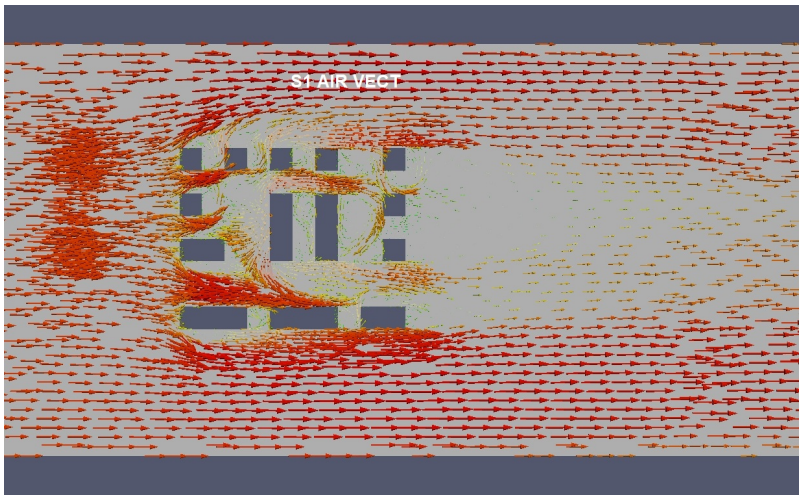

Figure 4.67 *Flow vectors at z=0.025 m for the complex array $0°$ with neutral release from source 1.*

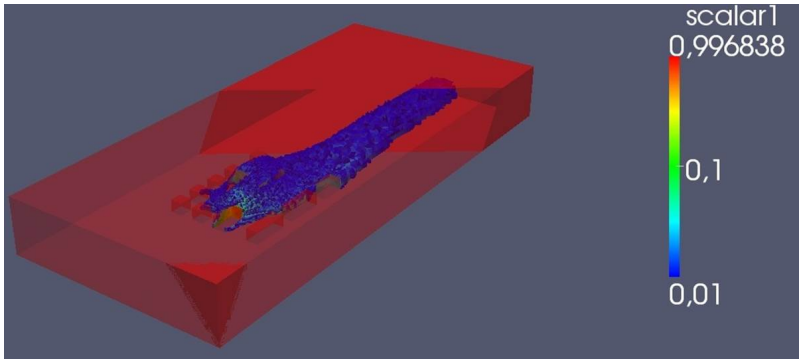

Figure 4.68 *Iso surface of mass fraction ($C = 10^{-2}$) of air in the complex array $0°$ with release from source 1.*

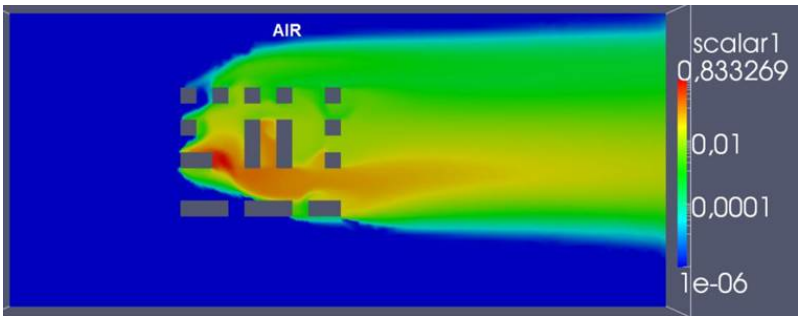

(a) z=0.25

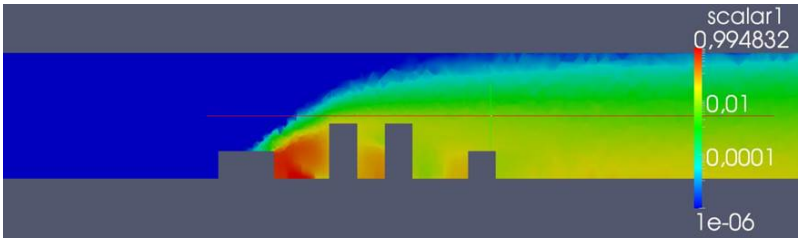

(b) y=0

Figure 4.69 *Contours of mass fraction of neutral gas in complex array* $0°$ *with release from source 1*

Comparing against the experimental plume, the shift of the single air plume is correctly estimated (see Figure 4.70). But the concentration levels are overestimated by a factor of 2. An underestimated vertical turbulence could be the reason for this. When we look at the turbulent properties at roof height (see Figure 4.71), where the vertical mixing is important, the hypothesis of isotropic turbulent fluxes (through the turbulent viscosity) may not be valid. Although the linear $k - \varepsilon$ production model correct some flaws of the standard $k - \varepsilon$ model, anisotropic flux models (Algebraic Flux Model for instance) might work better.

4.6.8.2 Dense gas release from source 1

We next look at the CO_2 release from source 1. The flow field close to the ground is affected by the density stratification (see Figure 4.72), compared to the release of air (c.f. Figure 4.67).

The simulated plume resulting from this flow is shown in Figure 4.73 and Figure 4.74. We see a tunneling effect through the larger street in the bottom of the figure, and a much fainter one on the upper side. The CO_2 tends to stay on the ground and go around the blocks, contrary to the neutral gas dispersion (c.f. Figure 4.68). When we look at the normalized concentration levels, the simulation reproduces quite satisfyingly the experimental results (see Figure 4.75). The measurement points are all placed behind the array. Although a bit narrower, the simulated plume exhibits the principal peaks, and also the secondary fainter one on the other side of the array.

4.6.8.3 Neutral release from source 2

The mean flow field is comparable to the source 1 case (see Figure 4.76). There are cavity and recirculation zones behind each block, horseshoe zones ahead of the first blocks and interaction

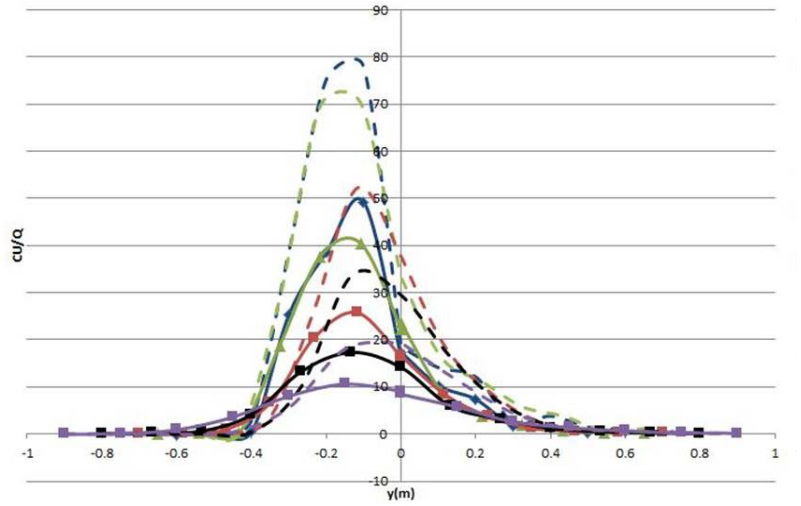

Figure 4.70 *Lateral profiles of normalized concentration of air at z=0.025 m and at different streamwise positions (blue = 0.8, green = 1 red = 1.5, black =2, and purple = 3 m). Dashed lines show simulation results whereas solid lines with symbols show the experimental values*

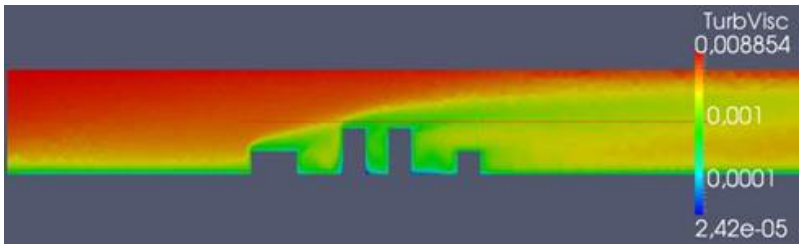

(a) Turbulent viscosity

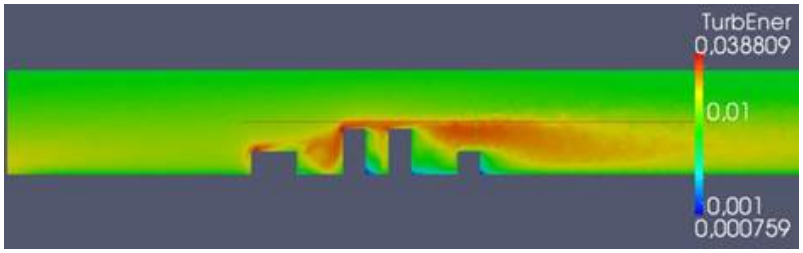

(b) Turbulence kinetic energy

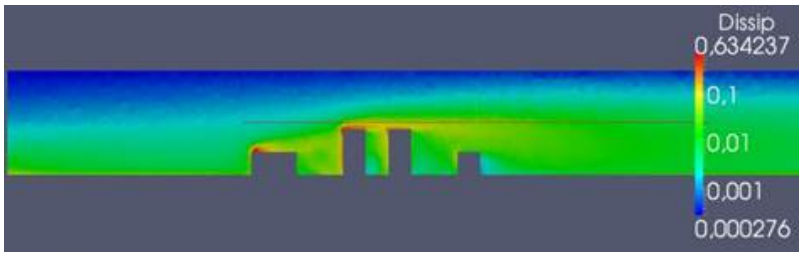

(c) Turbulence dissipation

Figure 4.71 *Turbulent properties for neutral release from source 1 in complex array* $0°$.

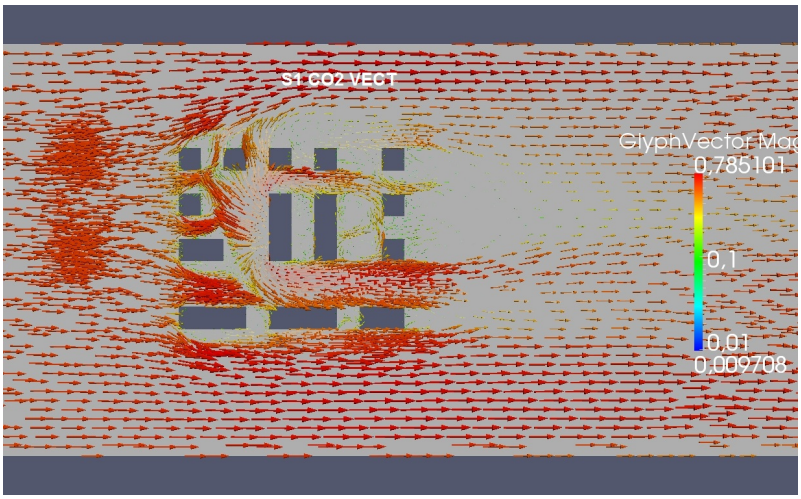

Figure 4.72 *Flow vectors at z=0.025 m for the complex array $0°$ with dense gas release from source 1.*

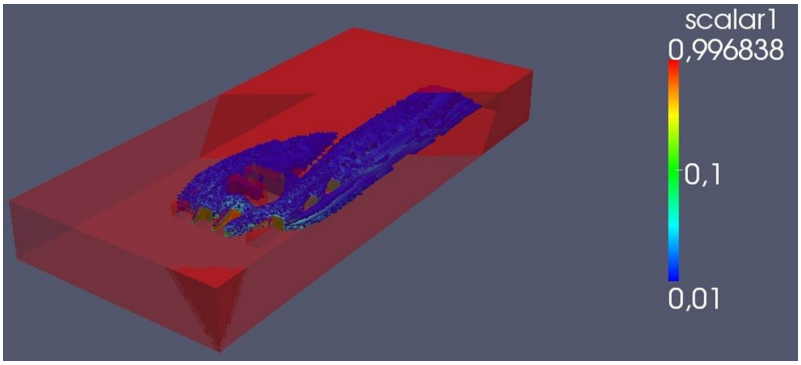

Figure 4.73 *Iso surface of mass fraction ($C = 10^{-2}$) of CO_2 in the complex array $0°$ with release from source 1.*

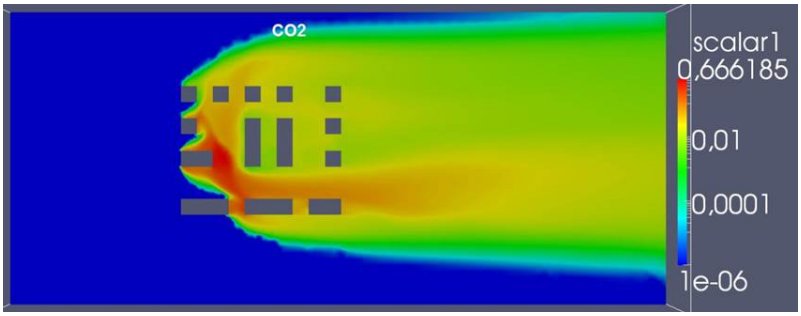

Figure 4.74 *Contours of mass fraction of CO_2 at z=0.025 m in the complex array $0°$ with release from source 1.*

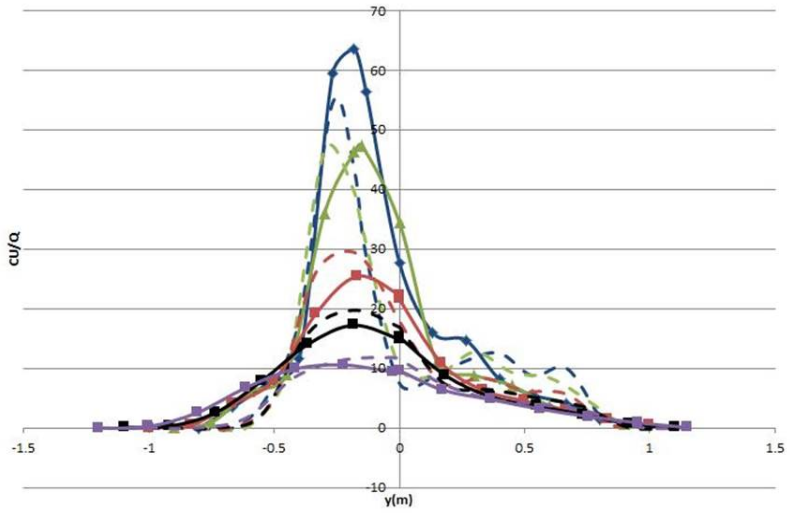

Figure 4.75 *Lateral profiles of normalized concentration of CO_2 at z=0.025 m and at different streamwise positions (blue = 0.8, green = 1 red = 1.5, black =2, and purple = 3 m). Dashed lines show simulation results whereas solid lines with symbols show the experimental values*

between wakes. The air plume from source 2 (see Figure 4.77) is channeled through the main

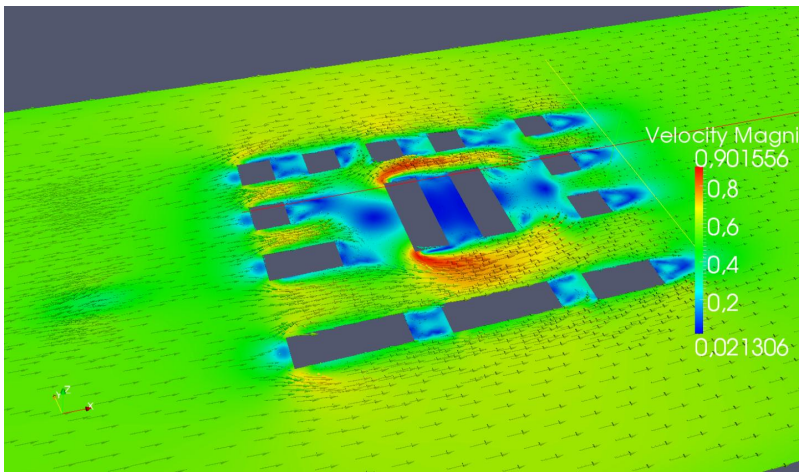

Figure 4.76 *Flow field visualization at z=0.025 m for the complex array 0° with neutral release from source 2.*

street. Also side streets are affected. The consequence is a shifted main concentration peak, with a small secondary peak. In Figure 4.78, we indeed see these features (lateral shift from x = 0.5 m to the intermediate position inside the array x = 0.935 m). The experimental concentrations are reproduced before and inside the array (x = 0.5 m (blue lines) and x = 0.935 m (green lines)), but overpredicts by a factor of 2 after the array (x = 1.75 m, red lines). Again, vertical turbulent transfer outside the urban mixing layer seems under predicted.

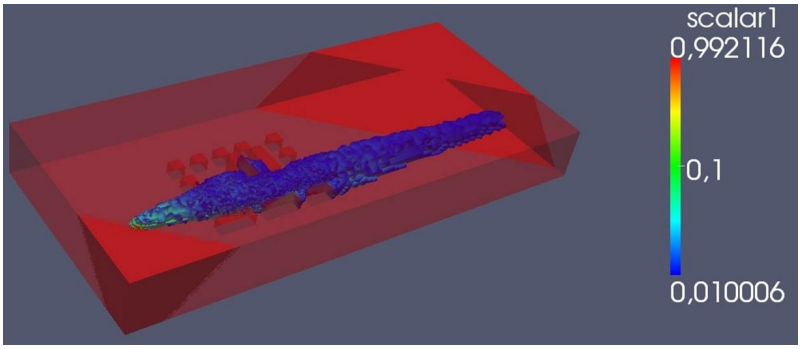

Figure 4.77 *Iso surface of mass fraction ($C = 10^{-2}$) of air in the complex array $0°$ with release from source 2.*

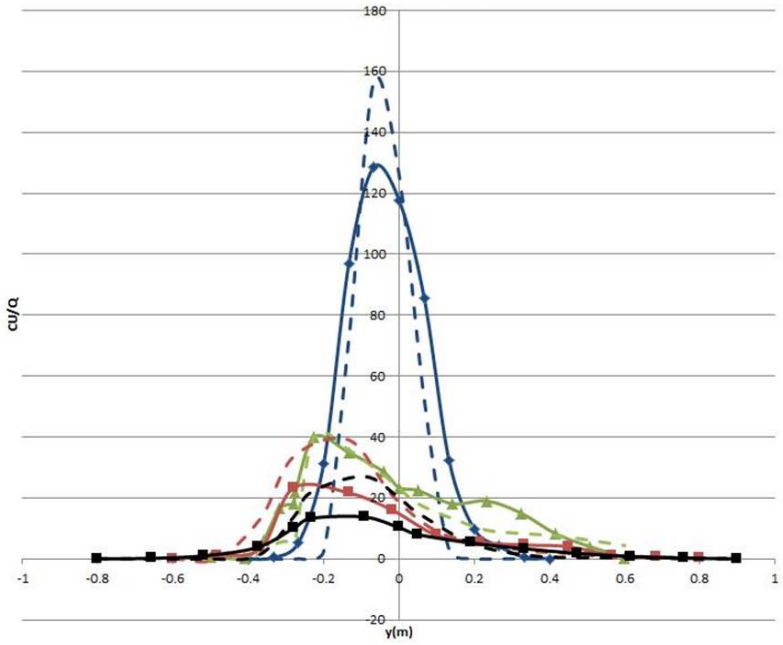

Figure 4.78 *Lateral profiles of normalized concentration of air at z=0.025 m and at different streamwise positions (blue = 0.5, green = 0.935 red = 1.75, and black =2.5 m). Dashed lines show simulation results whereas solid lines with symbols show the experimental values*

4.6.8.4 *Dense gas release from source 2*

The CO_2 results from source 2 are very different from the air release (see Figure 4.79). The dense gas creeps around the blocks, creating a wider plume.

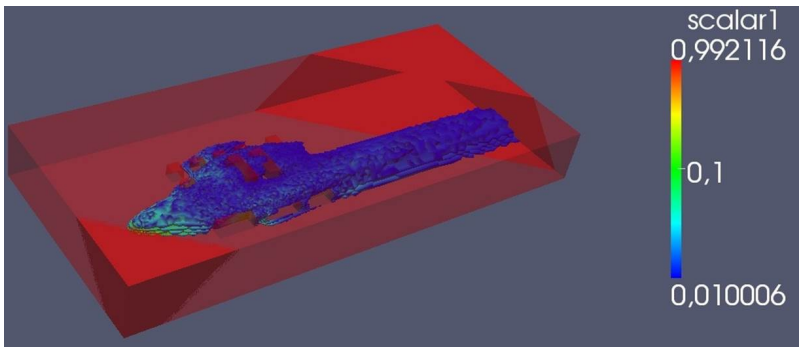

Figure 4.79 *Iso surface of mass fraction ($C = 10^{-2}$) of CO_2 in the complex array $0°$ with release from source 2.*

The concentration results against lateral positions for different streamwise positions (see Figure 4.80) are effected by a CO_2 plume that already is badly simulated once reaching the first blocks (x = 0.5 m, blue lines). The 2 peaks visualized in the experimental results are amplified or channeled through the lateral streets, which the simulation cannot predict. Nevertheless, we see separation into 2 peaks further downstream, starting at x = 0.935 m (green lines, inside the array). The reduced concentration and the wider plume compare to the air release is captured. Concentration against the lateral position for different z positions (inside and behind the array) is shown in Figure 4.81. The simulation overestimates the experiment by a factor of 2, getting worse as we look at higher z levels and the correlation gets slightly better from inside the array. To conclude on this case, a better definition of the inlet plume (before the array entrance) would probably improve the agreement, as we got better results when the source is placed directly inside the array.

4.6.8.5 *Neutral release from source 3*

Source 3 is placed upstream of the array and off the centreline. In Figure 4.82 the iso contour 10^{-2} of the air mass fraction (corresponding to 12 in normalized units) is shown to be apparently diverted outside the array. But we observe that some contaminant penetrate sideways into the array.

Actually, what happens can be seen on the concentration results in Figure 4.83. The plume is shifted in the positive y direction (upper-left direction in Figure 4.82). The correlation between simulation and experimental results are satisfying even if a slight overestimation exists.

4.6.8.6 *Dense gas release from source 3*

The CO_2 release from source 3 is shown in Figure 4.84. The simulated dense gas collapses and crawls, but mainly outside the array. Again, the experimental concentration profile (see Figure

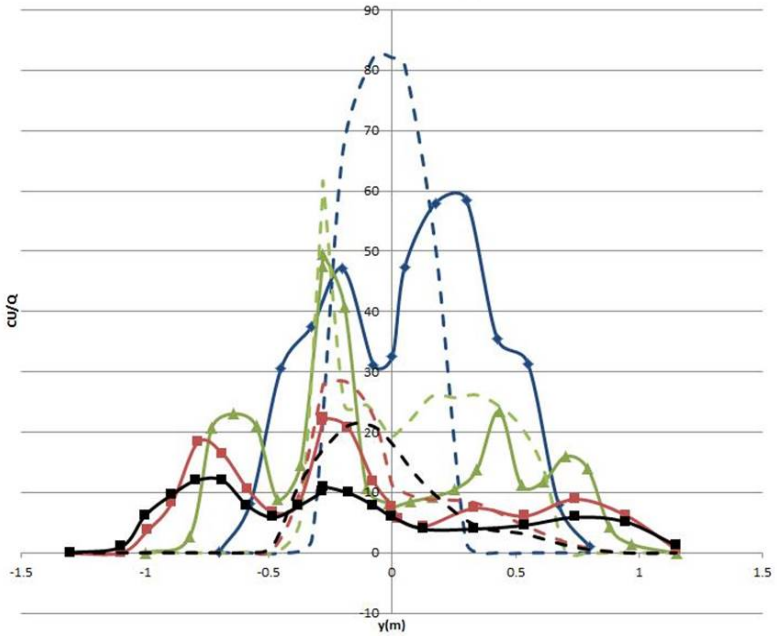

Figure 4.80 *Lateral profiles of normalized concentration of CO_2 at z=0.025 m and at different stream-wise positions (blue = 0.5, green = 0.935 red = 1.75, and black =2.5 m). Dashed lines show simulation results whereas solid lines with symbols show the experimental values*

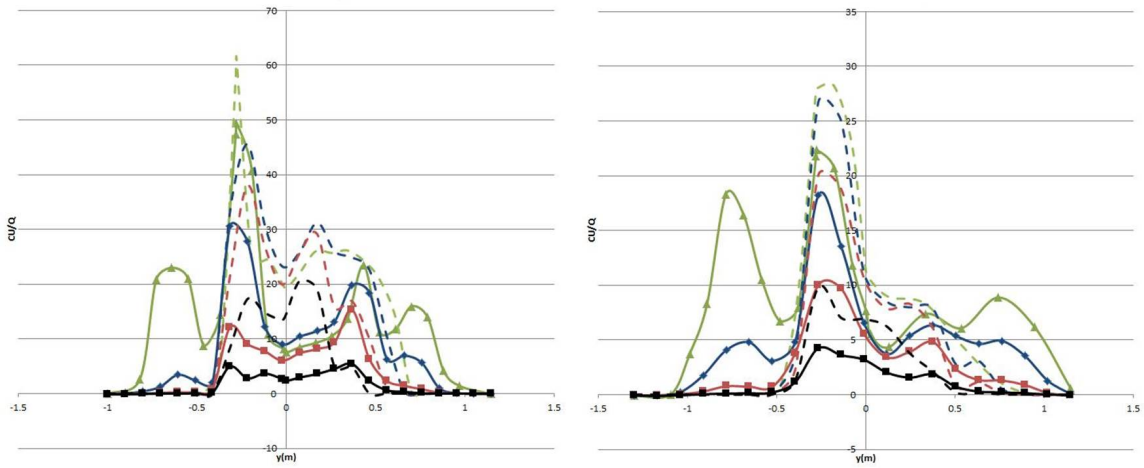

(a) x=0.935 m **(b)** x=1.75 m

Figure 4.81 *Lateral profiles of normalized concentration of CO_2 at different heights (green = 0.025, blue = 0.07 red = 0.13, and black =0.2 m). Dashed lines show simulation results whereas solid lines with symbols show the experimental values*

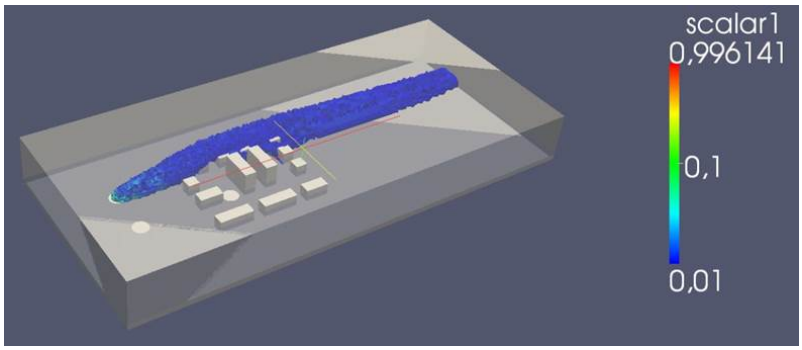

Figure 4.82 *Iso surface of mass fraction ($C = 10^{-2}$) of air in the complex array $0°$ with release from source 3.*

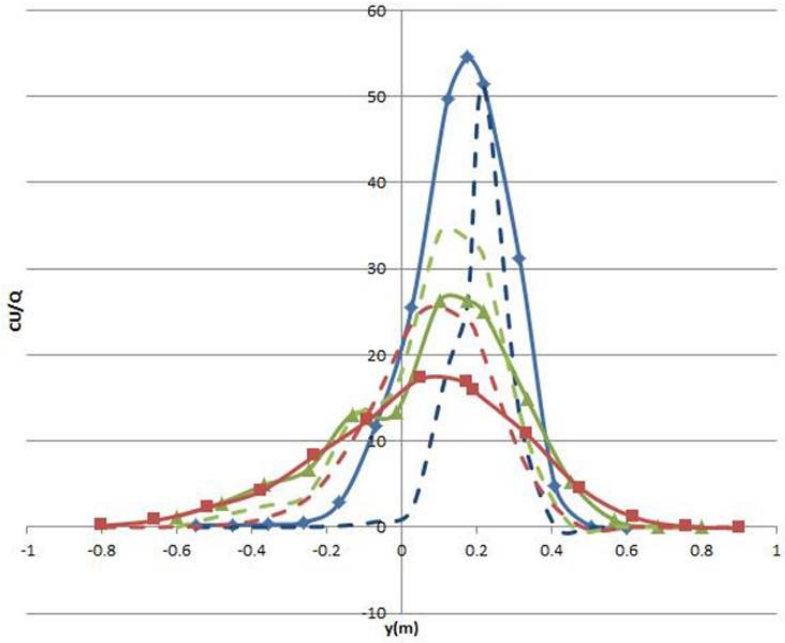

Figure 4.83 *Lateral profiles of normalized concentration of air at z=0.025 m and at different streamwise positions (blue = 0.935, green = 1.75, and red = 2.5 m). Dashed lines show simulation results whereas solid lines with symbols show the experimental values*

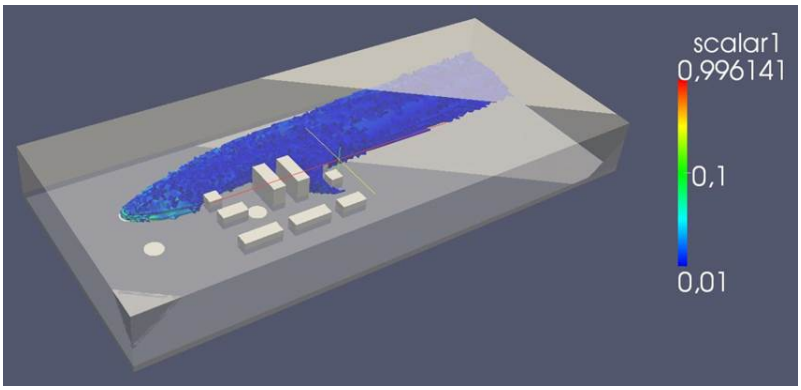

Figure 4.84 *Iso surface of mass fraction ($C = 10^{-2}$) of CO_2 in the complex array 0° with release from source 3.*

4.85) is already distorted at ground level at the beginning of the array, compared to the simulated plume (due to insufficient modelling of the dense gas effect on flat ground between inlet boundary and the array). Furthermore, the initial experimental plume at x = 0.5 m is already shifted from y = 0. The plume gets shifted away from the array, seen by both simulation and experiment. The correlation however gets better as we look further away from the array ($x \geq 1.75$ m). We also notice the broadening of the plume (0.4 m to 0.8 m) from air to the CO_2 release, captured both in the experiment and simulation. We finally see a concentration overestimation before the array exit (gas still dense), and underestimation afterwards (diluted gas).

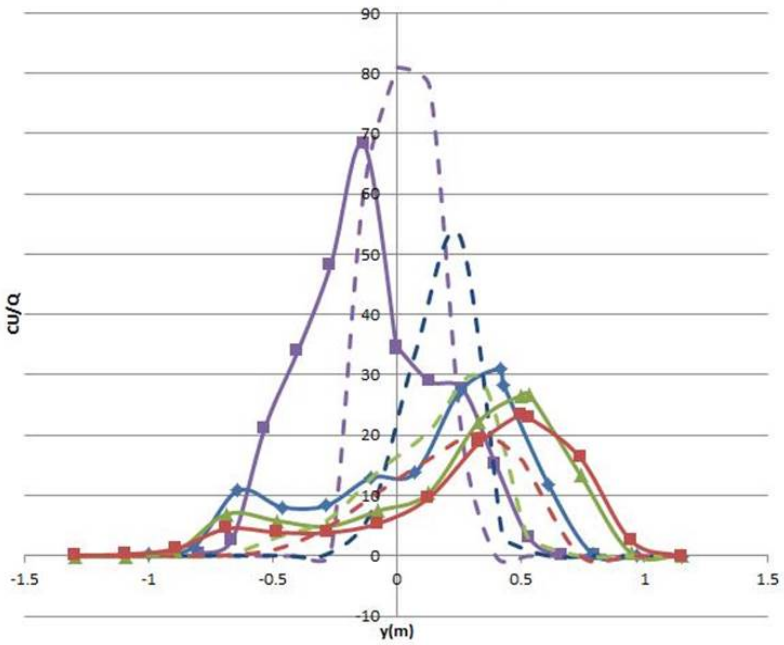

Figure 4.85 *Lateral profiles of normalized concentration of CO_2 at z=0.025 m and at different streamwise positions (purple = 0.5, blue = 0.935, green = 1.75, and red = 2.5 m). Dashed lines show simulation results whereas solid lines with symbols show the experimental values*

4.6.9 Complex array 45°

Here we consider the case of a 45 degree rotated array, and present results from the source 1 release. The mesh used is visible on Figure 4.86. Refinement has been applied around the source and blocks, and a ground boundary layer mesh is created to properly compute and transport the vertical shear stress.

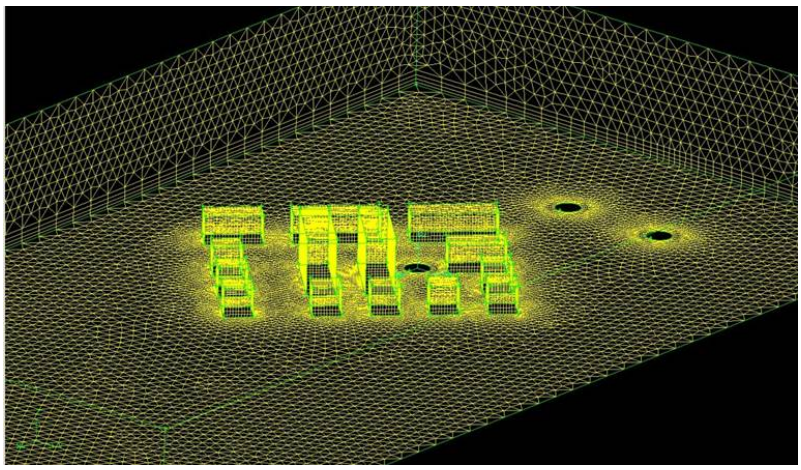

Figure 4.86 *Mesh of the complex array 45°. Source 1 is placed inside the array, source 2 outside on the symmetry line and source 3 outside and slightly of the symmetry line, c.f. Figure 2.6*

4.6.9.1 Neutral release from source 1

Not surprisingly, the plume is channeled along the large blocks (see Figure 4.87). Part of the air moves also upstream thanks to turbulent wakes and recirculation. In Figure 4.88, the agreement

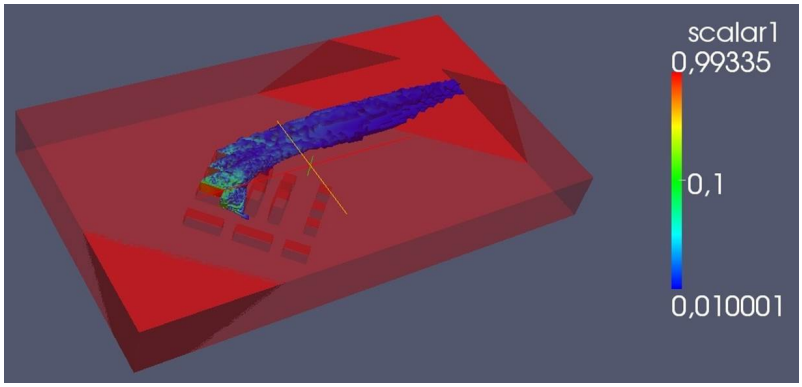

Figure 4.87 *Iso surface of mass fraction ($C = 10^{-2}$) of air in the complex array 45° with release from source 1.*

between simulation and experimental concentration is rather good, although 20-30% overestimation with the simulated plume being larger. The shifted plume position is well captured.

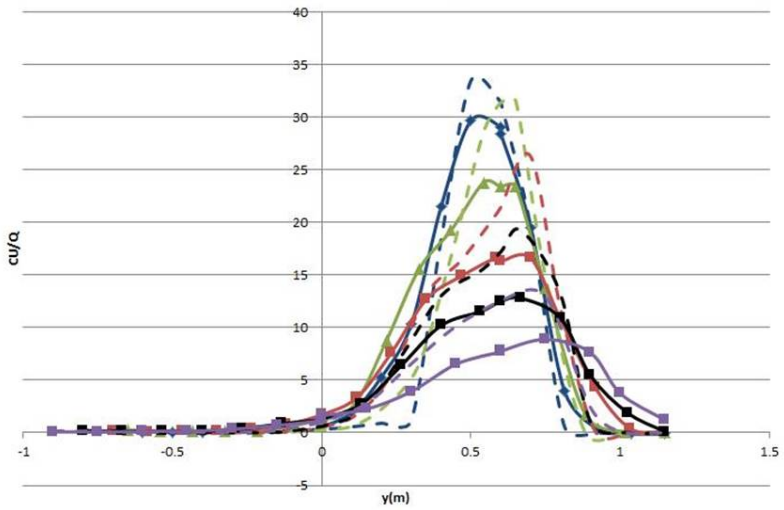

Figure 4.88 *Lateral profiles of normalized concentration of air at z=0.025 m and at different streamwise positions (blue = 0.8, green = 1, red = 1.5, black = 2, and purple = 3 m). Dashed lines show simulation results whereas solid lines with symbols show the experimental values*

4.6.9.2 Dense gas release from source 1

The CO_2 results are very different compared to the neutral release. The dense gas collapses and creeps around and splits the plume, each part taking a 90 degree diagonal paths (see Figure 4.89). The plume separation is more visualized in Figure 4.90, where the correlation between simulation

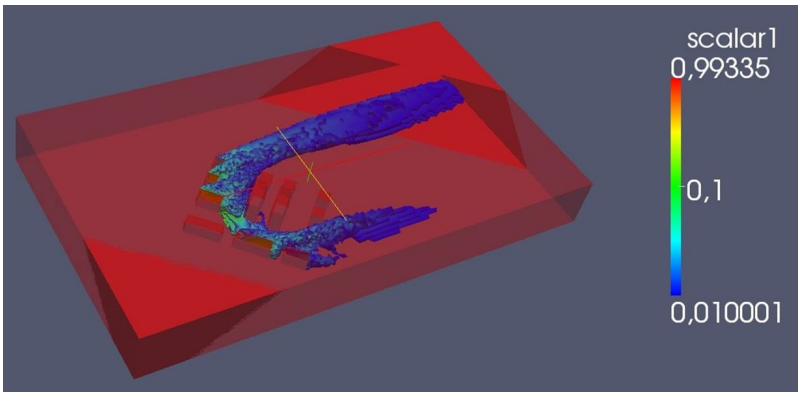

Figure 4.89 *Iso surface of mass fraction ($C = 10^{-2}$) of CO_2 in the complex array $45°$ with release from source 1.*

and experiment can be considered sufficient for dispersion studies. We expect that in a real scenario, a different orientation would distribute the plume parts differently, and assuming different density ratio would lead to different distribution enhanced by street orientation.

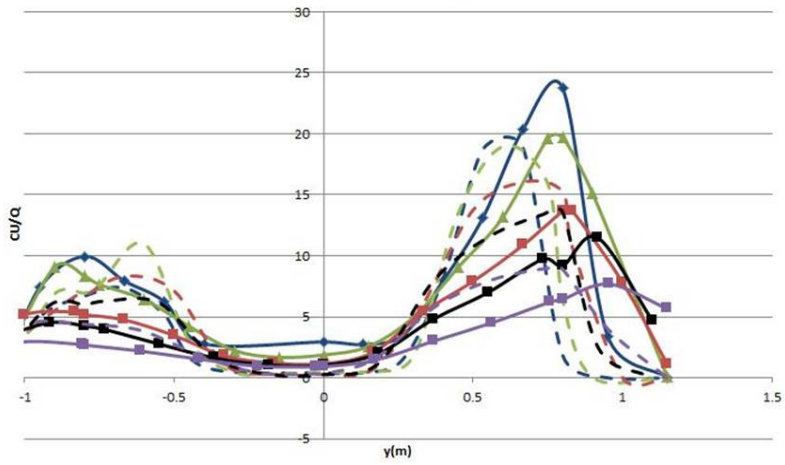

Figure 4.90 *Lateral profiles of normalized concentration of CO_2 at z=0.025 m and at different streamwise positions (blue = 0.8, green = 1, red = 1.5, black = 2, and purple = 3 m). Dashed lines show simulation results whereas solid lines with symbols show the experimental values*

4.6.10 Complex array with trees 0°

To test the effects of trees, the Complex array scenario is used. We had great difficulties generating a suitable mesh as the needed details were extreme ($<$ 1 mm) close to the trees (see Figure 4.91). Three kinds of trees were used: 90 degree crossed plates, wire meshed cylinders and porous wool spheres. We could only compare the crossed plate tree scenario, therefore the conclusions have to be taken with caution.

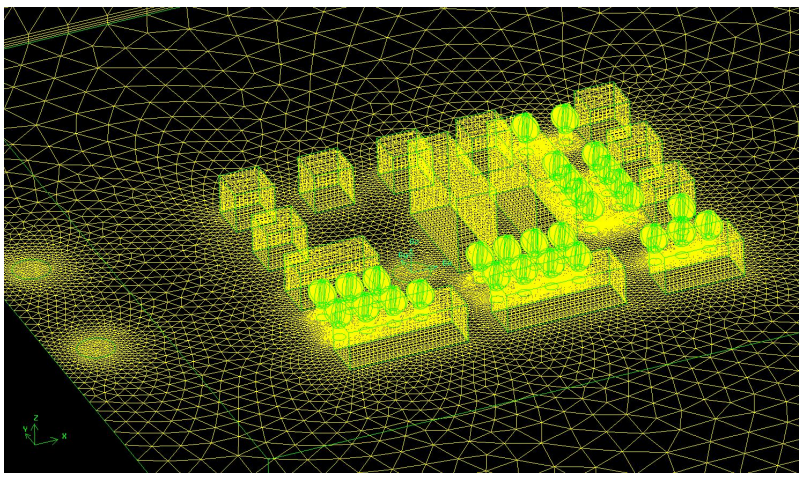

Figure 4.91 *Mesh of the complex array 0° with plate trees. Source 1 is placed inside the array, source 2 outside on the symmetry line and source 3 outside and slightly of the symmetry line, c.f. Figure 2.6*

4.6.10.1 Neutral release from source 1

When we compare the source 1 air release without trees against the one with trees (see Figure 4.92), we notice a complete different dispersion pattern. With trees more pollutant is trapped inside the array. The effect is indeed to slow down the mean flow and generate extra turbulent mixing. In Figure 4.93 the simulation results behind the array for crossed plate trees (blue lines) overestimate the experimental concentration, using meshed trees (red lines). The agreement recovers downstream. As the air is dispersed vertically at the source, it eventually reaches the tree canopy, were a damping

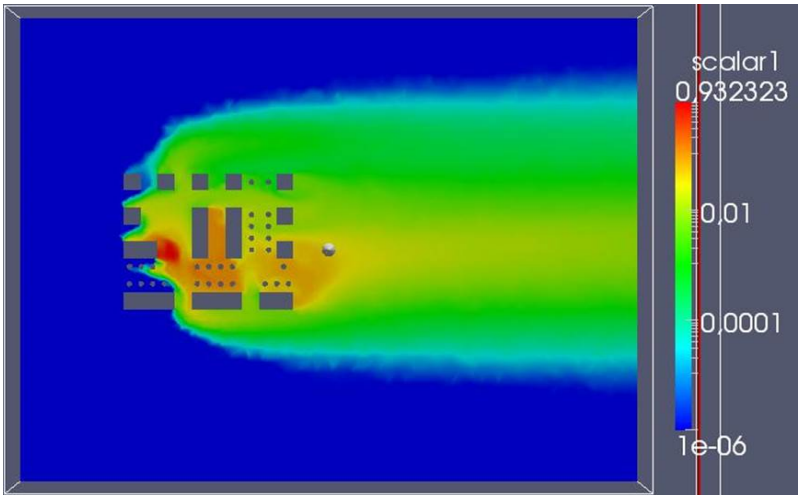

Figure 4.92 *Contours of mass fraction of air in the complex array* 0° *with trees and release from source 1.*

of the flow occurs. More pollutant is trapped in the array. The over estimation could be because the mixing is higher for the porous wool spheres used in the wind-tunnel compared to the crossed plate trees used in the simulation. Or the model used predicting less turbulent. Less mixing will result in higher concentration.

4.6.10.2 Dense gas release from source 1

The CO_2 release from source 1 with trees is shown in Figure 4.94. The shape of the plume is very different compared to the scenario without trees. The same remark as above is valid with gas trapped inside the array by the presence of trees. But this time, the effect is less visible and the agreement between simulation and experiment better (see Figure 4.95). The reason is probably because the dense gas goes under the trees, resulting in a reduced tree effect. Nevertheless, the concentration measured without trees are higher which is probably due to a reduced mixing. It can be concluded for this part that trees affect the dispersion of passive and dense gas, and lead to increased concentration inside and reduced levels outside an array of buildings.

4.6.11 Paris

The Paris case was designed to deal with large scale urban accidents. The release rate is 50 dm^3/min for wind tunnel scale 1:350. This leads to an unrealistic scenario at scale 1:1. Experiment with

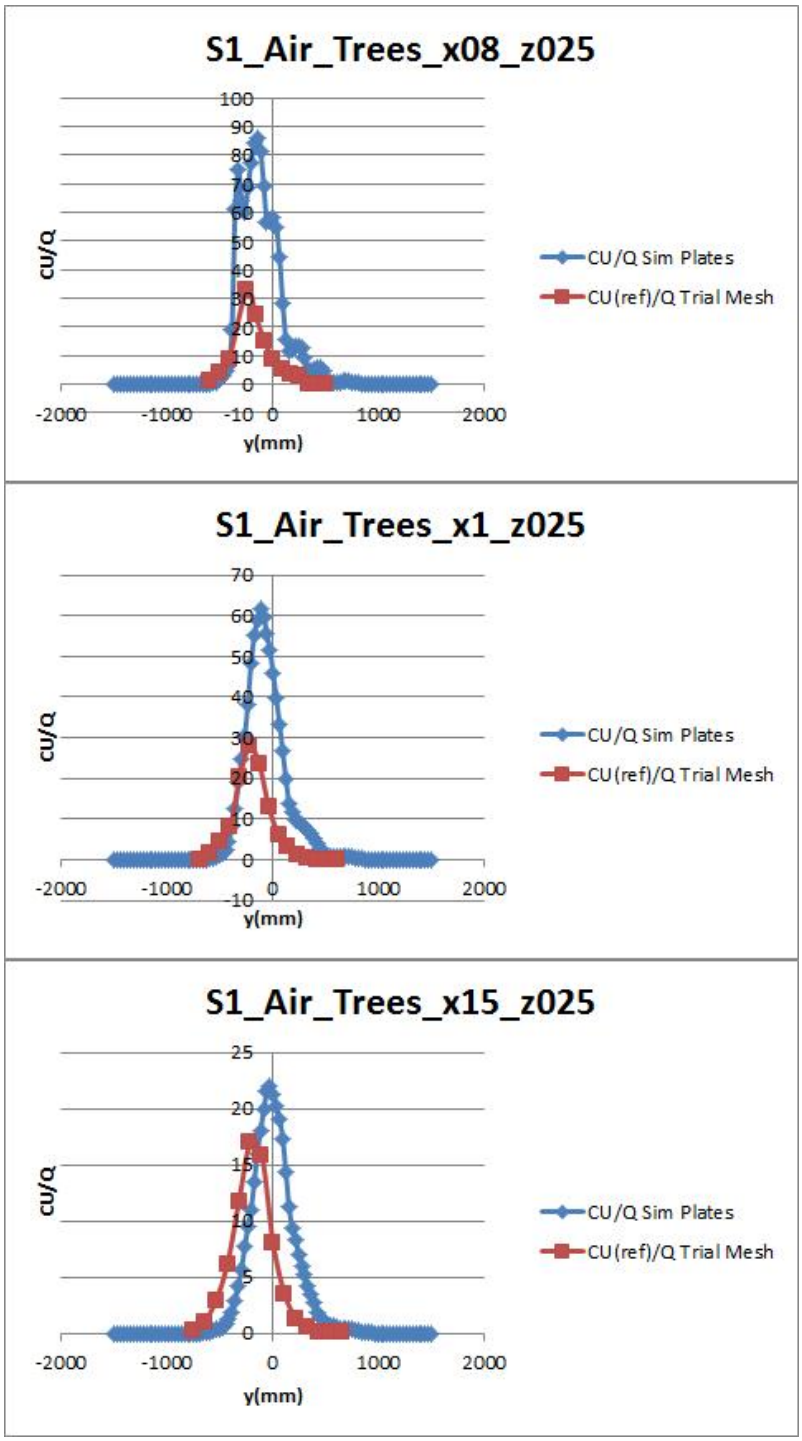

Figure 4.93 *Lateral profiles of normalized air concentration at three different streamwise positions (x=0.8 m (top), 1.0 m (middle), and 1.5 m (bottom)) in the complex array* 0° *with trees and release from source 1. Blue lines represent simulation with plate trees and red lines are experimental values with mesh trees.*

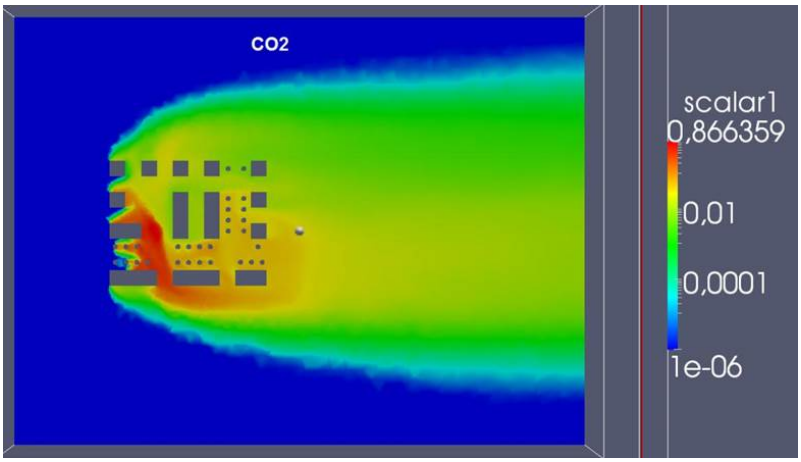

Figure 4.94 *Contours of mass fraction of CO_2 in the complex array 0° with trees and release from source 1.*

smaller release rates or/and wind tunnel velocities have been tested, down to 1.5 dm^3/min (75 m^3/s real scale, which is closer to a realistic scenario. The results presented here concerns only 50 dm^3/min release for air and CO_2, and must be seen only from a validation viewpoint. The mesh projected on the floor is shown in Figure 4.96. It was created with Salome software (EDF) using Netgen mesh generator. We use a vertical boundary layer mesh on the floor and refinement where strong curvature is encountered and around sources. We were not able to refine the mesh correctly along the narrow streets, but we expect the overall effect will be small. The whole domain is 2.6×2.3 km^2 in full scale and contained initially about 300 buildings, which have been merged and simplified to about 90 buildings of mean height of 27 m in full scale. Figure 4.97 shows the y^+-values on the surface. On the ground the mesh is fine ($y^+ = 10$), too fine for RANS models with log law as wall boundary condition. We chose a scalable log law resolving the viscous layer and blending it with inertial layer profiles.

4.6.11.1 Neutral release source 1

Source 1 is placed some distance downstream "Champs Elysees" Avenue (c.f. Figure 2.7 in Chapter 2.6). We see the "Arch of Triumph" upstream. The wind direction is 300°, slightly tilted compared to the "Champs Elysees" orientation. Figure 4.98 shows the positions of the sensors within the street network (z = 0.01 m). Sensors are also placed above the buildings (z = 0.12 m). We see in Figure 4.99 the mean flow field at 0.01 m height. We observe a reduced velocity within the lateral streets compared to streets oriented in the stream-wise direction. Turbulent viscosity close to the ground, shown in Figure 4.100 is not uniform within the domain. The special case of "Champs Elysees" avenue can almost be considered as if it was a bare surface without building, and we expect dispersion to be driven by wall floor turbulence and channeling effect. The normalized air concentration is shown in Figure 4.101. There are high concentrations around the source. Further downstream the concentration reduces rapidly. Gas is penetrating the lateral streets (George V Avenue), but is mainly confined to the "Champs Elysees". CU/Q levels of 10 or more are still predicted far downwind. For the comparison, we compare the simulated versus observed (experimental) normalized concentration, for all experimental measurement (see Figure 4.102a),

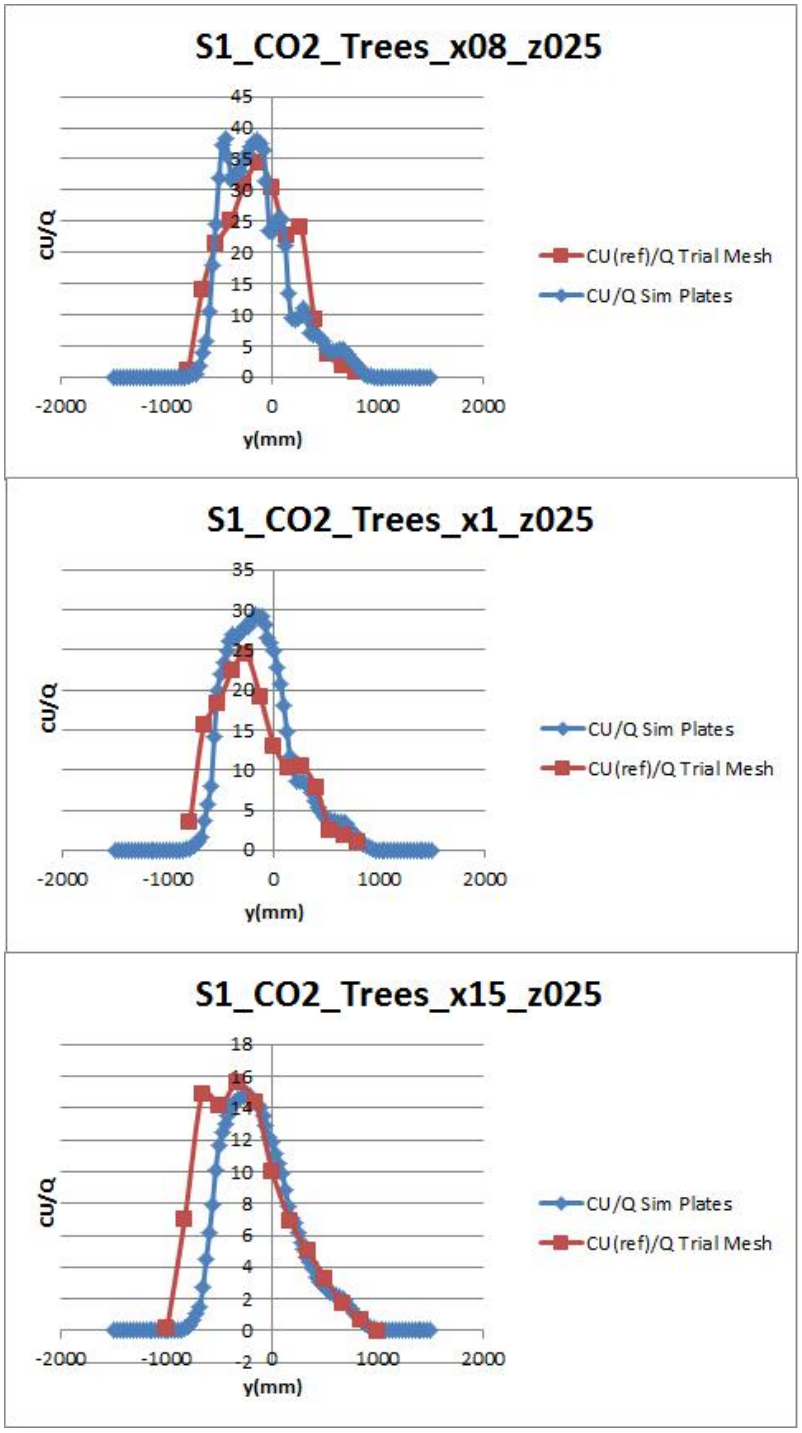

Figure 4.95 *Lateral profiles of normalized CO_2 concentration at three different streamwise positions (x=0.8 m (top), 1.0 m (middle), and 1.5 m (bottom)) in the complex array 0° with trees and release from source 1. Blue lines represent simulation with plate trees and red lines are experimental values with mesh trees.*

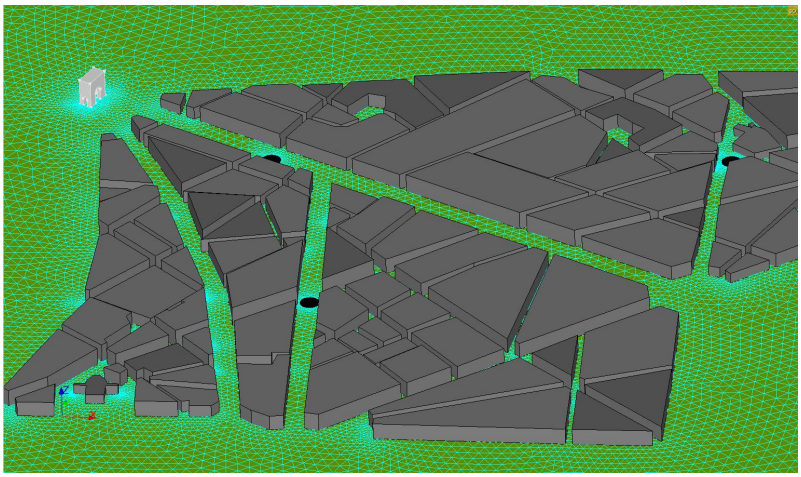

Figure 4.96 *Mesh of the Paris case*

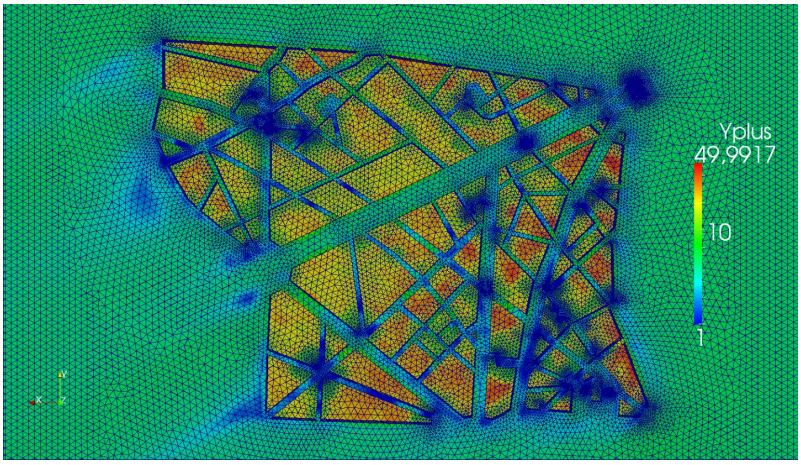

Figure 4.97 *y^+ values on the ground for the Paris case with source 1.*

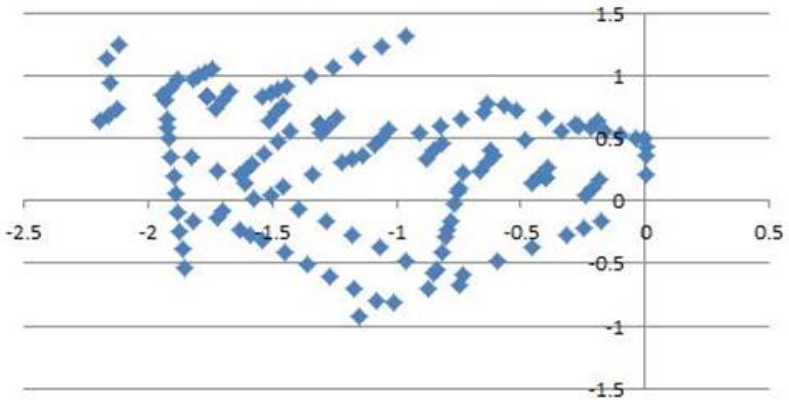

Figure 4.98 *Sensor positions within the street network for source 1 in the Paris case.*

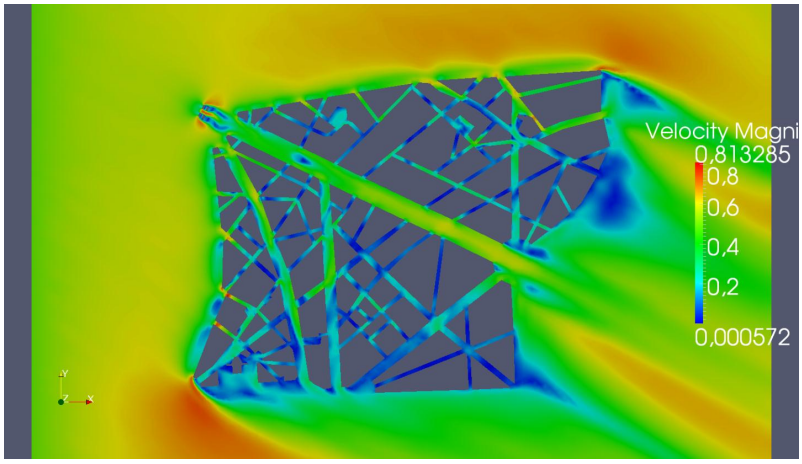

Figure 4.99 *Contours of mean velocity magnitude at z=0.01 m for the Paris case with neutral release from source 1.*

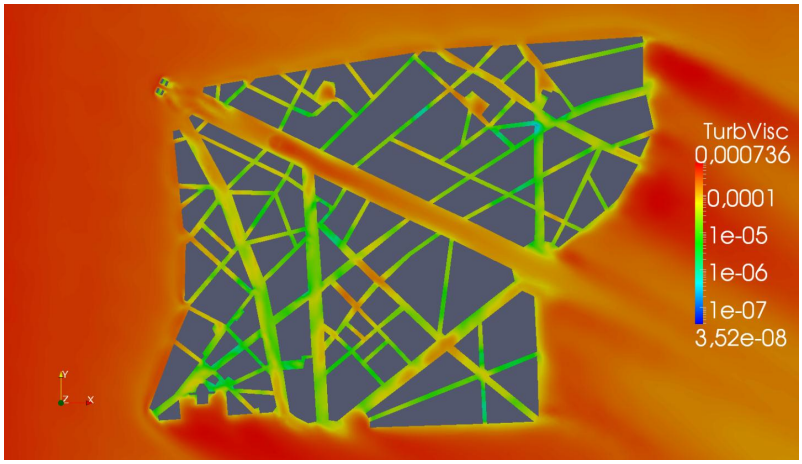

Figure 4.100 *Contours of turbulent viscosity at z=0.01 m for the Paris case with neutral release from source 1.*

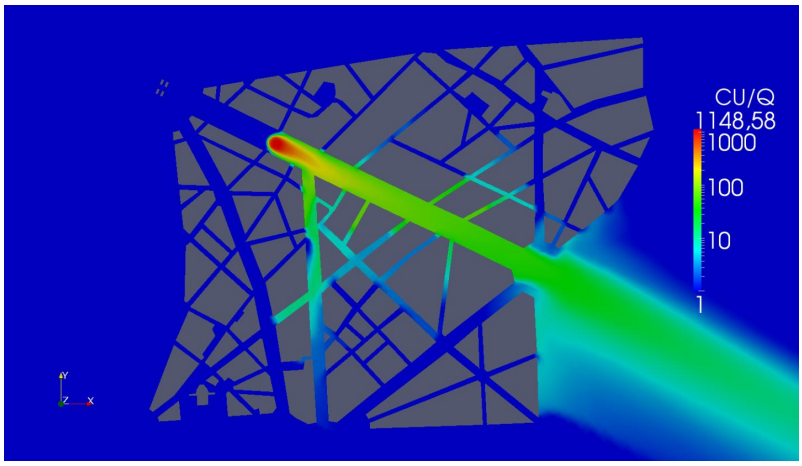

Figure 4.101 *Contours of normalized concentration of air at z=0.01 m for the Paris case with neutral release from source 1.*

street level sensors only (Figure 4.102b), vertical profiles in the “Champs Elysees” only (see Figure 4.102c). These last results are very well correlated, corresponding to a quasi-flat air dispersion case. The street level sensors results show rather good correlation for large values down to 10, after which a tendency to overestimate small values is seen (sometimes by a factor of 100!). We have to mention that very small values (< 0.01) have been cut due to not being significant.

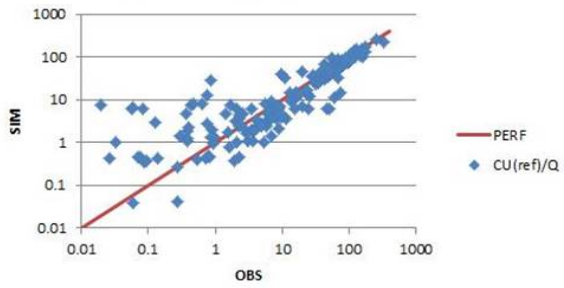

(a) All measurements

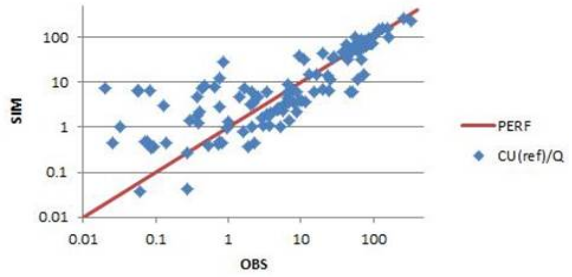

(b) Street level measurements

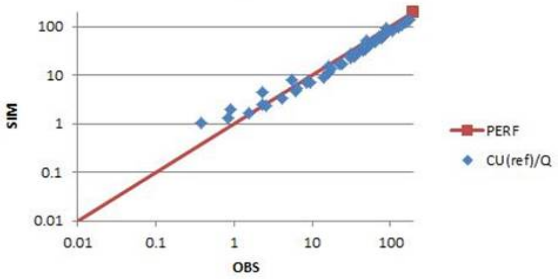

(c) Champs Elysees measurements’

Figure 4.102 *Simulated versus observed (experimental) values in the Paris case with neutral release from source 1.*

We have computed two classical statistical measures: FAC2 and FAC5. FAC2 = 64% and FAC5 = 84%. This is considered satisfying for comparison with real experiment. We also use MOEs as advised in [15]. Analysis rates definitions (Occurrence, Good Analysis, Detection, False Negative and Positive rates) are found in [15] and the results are shown in Figure 4.103. We’ll just point to the MOE1 rate which represents the overlapping of the observed and predicted (simulated) plumes, discretized using all experimental values. The MOE1 stays over 80% for all, except the last interval of threshold concentration (we count overlapping events corresponding to concentrations above the given threshold). The last point (where the orange curve collapses in Figure 4.103) is not significant as there is almost no point there around the source at high levels. When we turn to MOE2s, false positive scores against false negative ones (see Figure 4.104), we find well grouped data points in the 80%-80% region. This means the model is capable of predicting neutral dispersion in an urban environment.

Before getting to the next case, we want to show a comparison made by scaling the results to scale 1:1 according the scaling laws provided by [16]. We know that the scaling by a factor of 350 on geometry doesn’t lead to a realistic scenario ($Q \sim 2500 m^3/s$ and $U = 10$ m/s at 10 m height). y^+-values become enormous and we doubt the flow is well computed. Nevertheless, results remain acceptable (see Figure 4.105). MOE1 (see Figure 4.106) drop to 60% above $CU/Q = 10$, and we

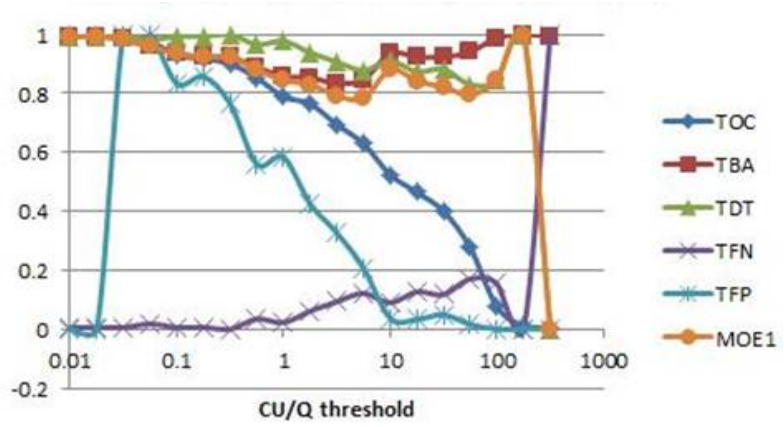

Figure 4.103 *Analyses Rates (among which MOE1 = overlapping) versus threshold normalized concentration for the Paris case with neutral release from source 1.*

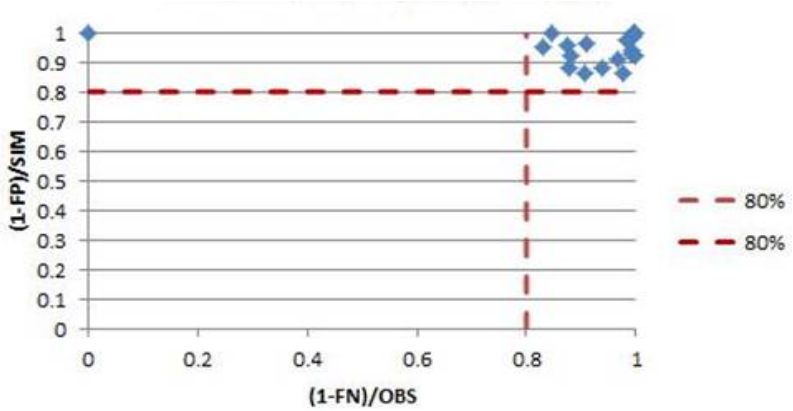

Figure 4.104 *MOE2s representation (False Positive versus False Negative) for the Paris case with neutral release from source 1.*

see more false negative values compared to wind tunnel scale (see Figure 4.107), which is not suitable for risk analysis.

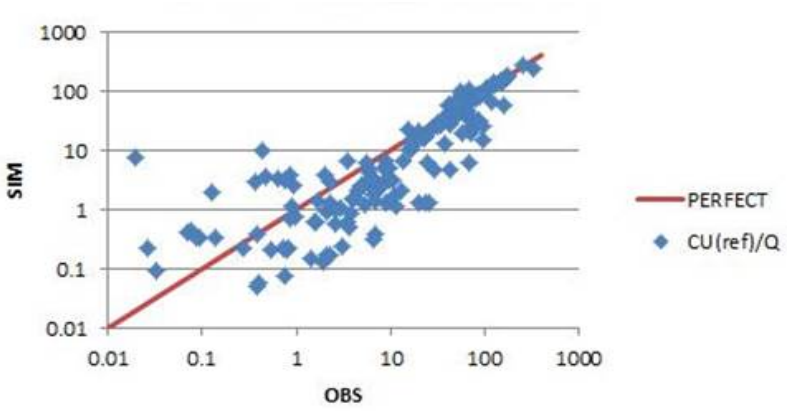

Figure 4.105 *Simulated vs. observed results for the Paris case in full scale (1:1) with neutral release from source 1.*

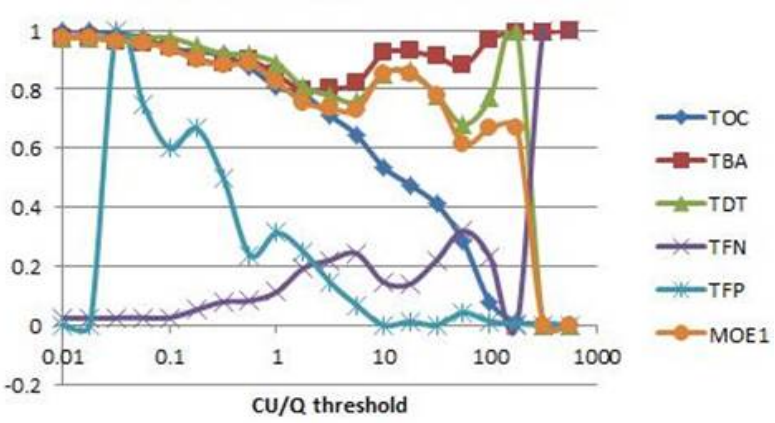

Figure 4.106 *Analyses Rates (among which MOE1 = overlapping) versus threshold normalized concentration for the Paris case in full scale (1:1) with neutral release from source 1.*

Finally, FAC2=48% and FAC5=73%, less than at scale 1:350, but still not so bad. In Figure 4.108 the normalized concentration against the linear distance to source is shown for the simulation (Figure 4.108a) and the experimental values (Figure 4.108b). The upper limits are obtained from other experiments [16].

4.6.11.2 Neutral release from source 2

The second set of results concerns source 2 and wind direction 220°. Source 2 is placed in a streets cross-road, and we expect that a small angle error can make the plume go right or left very easily (c.f. Figure 2.7) Sensor locations are shown in Figure 4.109. The mean flow field close to the ground (see Figure 4.110) shows the same behaviour as for source 1. The flow is mainly developing in large

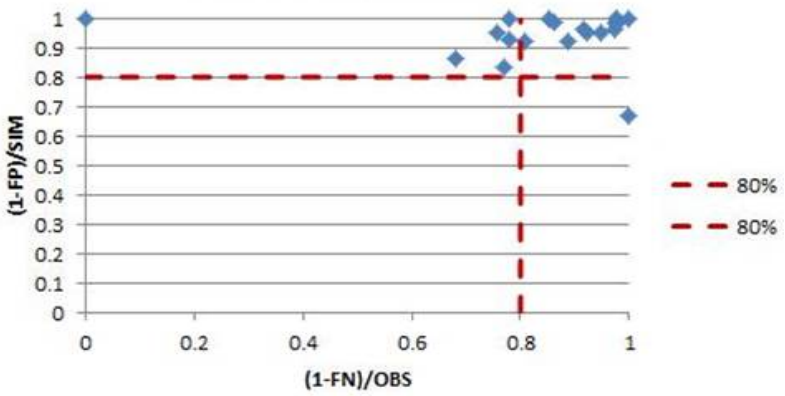

Figure 4.107 *MOE2s representation (False Positive versus False Negative) for the Paris case in full scale (1:1) with neutral release from source 1.*

avenues and damped in narrow streets. We see that almost no important path lead to the "Champs Elysees" avenue, so there is a clear separation between north and south of "Champs Elysees". Close to the source, the flow is weakened and keeps the contaminant concentrated. Turbulent viscosity (see Figure 4.111) is more uniform and weaker than for source 1.

The gas follows the two main streets leading from the source to "Champs Elysees". Beyond this point the concentration is uniform.

The results of simulated versus observed normalized concentrations are shown in Figure 4.113a for all sensors, Figure 4.113b for streets sensors, Figure 4.113c for above roofs sensors, and finally Figure 4.113d for vertical profile sensors [16]. We again observe good correlation close to the source. The small concentration levels above roof (Figure 4.113c) are more dispersed than in the streets (see Figure 4.113b). The vertical profiles (Figure 4.113d) are well captured by the simulation, probably because they are placed in areas with higher concentrations. As a large number of sensors are placed in the small values region, the overall statistics (FAC2=39% and FAC5=66%) is worsened compared to source 1.

The analysis rates, seen in Figure 4.114, and MOE2s, presented in Figure 4.115, show a good behaviour ($> 80\%$), with of lower score in the range between 5 and 100 for MOE1 and some false negative values looking at MOE2s between $60 - 80\%$, but still acceptable.

4.6.11.3 Neutral release from source 3

Source 3 is surrounded by buildings and a wind direction of 40° (c.f. Figure 2.7). Sensors, both street level and roof level, are shown in Figure 4.116.

The mean flow field (see Figure 4.117) is again quite different compared to the other scenarios with a low wind speed around the source. Turbulent viscosity is uniform around the source (see Figure 4.118) and reduces downstream until it reaches the "Champs Elysees" where high levels are encountered.

The dispersion is more isotropic around the source (see Figure 4.119) compared to source 1 and

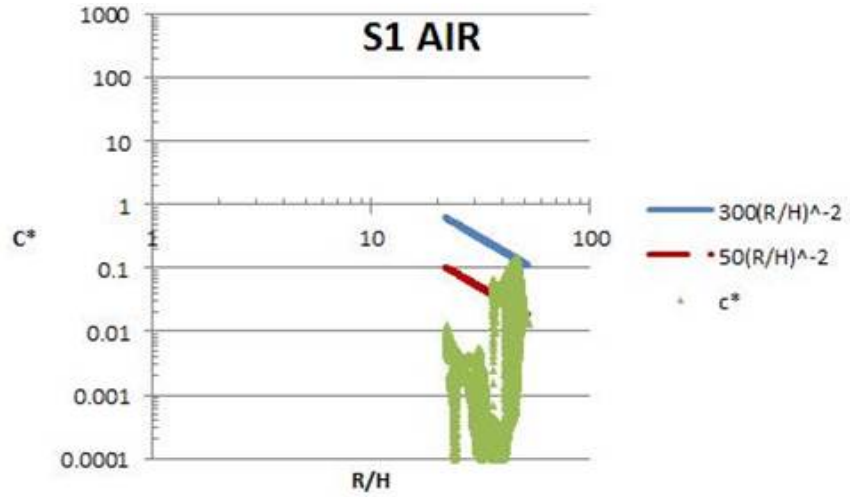

(a) Simulation

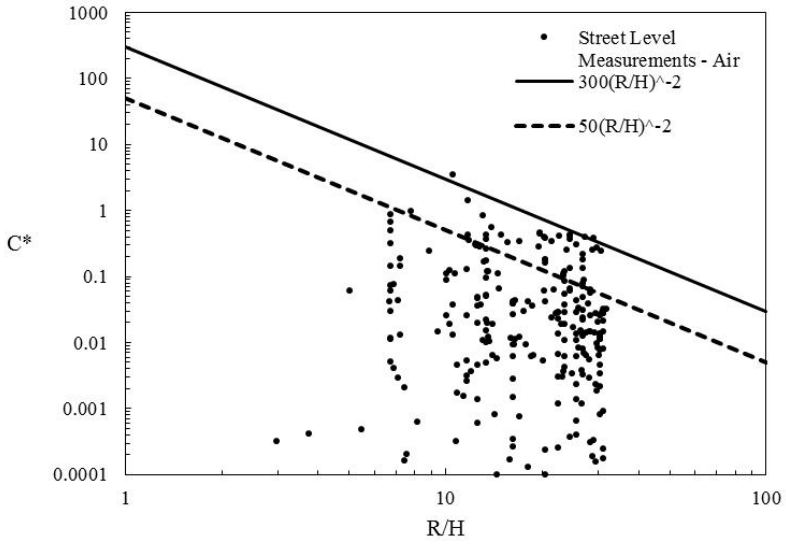

(b) Experiment

Figure 4.108 *Normalized concentration of air vs. linear distance to source in the Paris case with neutral release from source 1. Lines show expected upper bounds from other experiments*

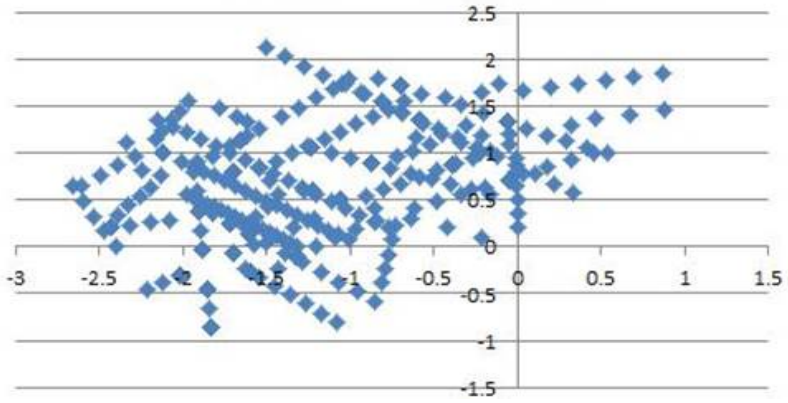

Figure 4.109 *Sensor positions for neutral release from source 2 in the Paris case.*

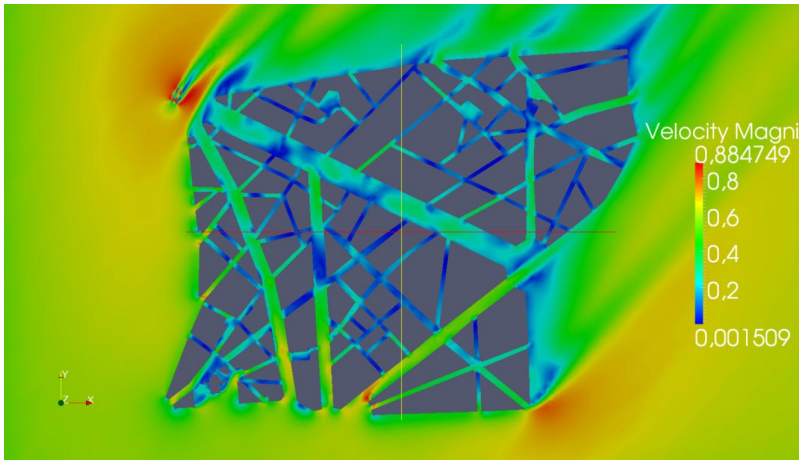

Figure 4.110 *Contours of mean velocity magnitude at z=0.01 m for the Paris case with neutral release from source 2.*

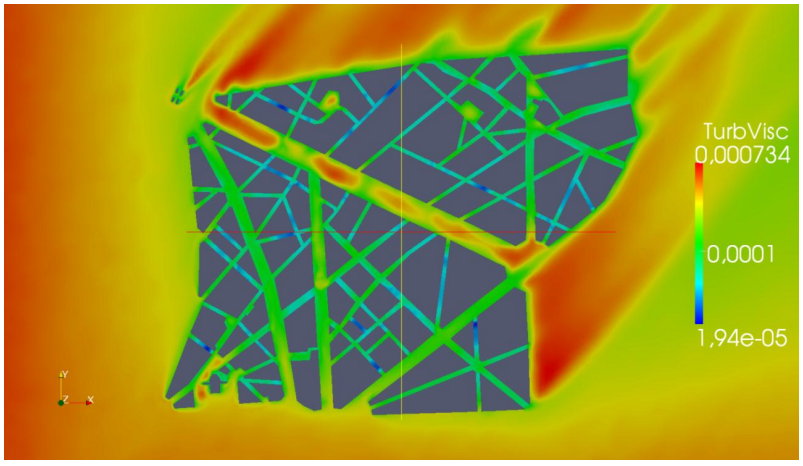

Figure 4.111 *Contours of turbulent viscosity at z=0.01 m for the Paris case with neutral release from source 2.*

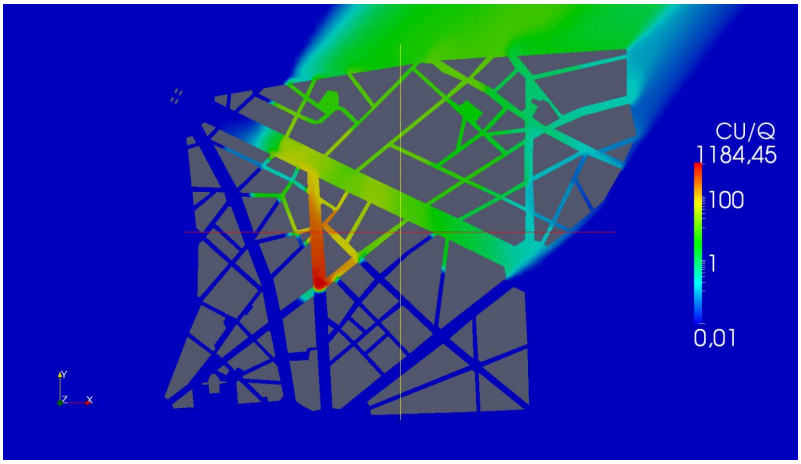

Figure 4.112 *Contours of normalized concentration of air at z=0.01 m for the Paris case with neutral release from source 2.*

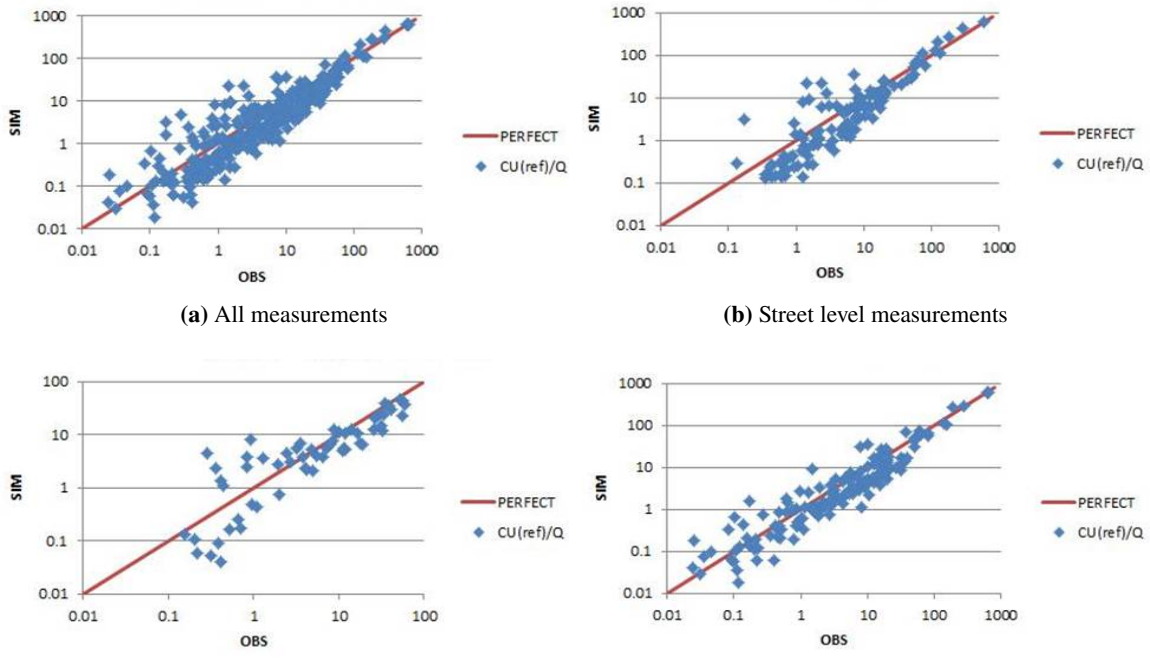

(a) All measurements

(b) Street level measurements

(c) Ropf top measurements

(d) Vertical profile measurements

Figure 4.113 *Simulated versus observed (experimental) values in the Paris case with neutral release from source 2*

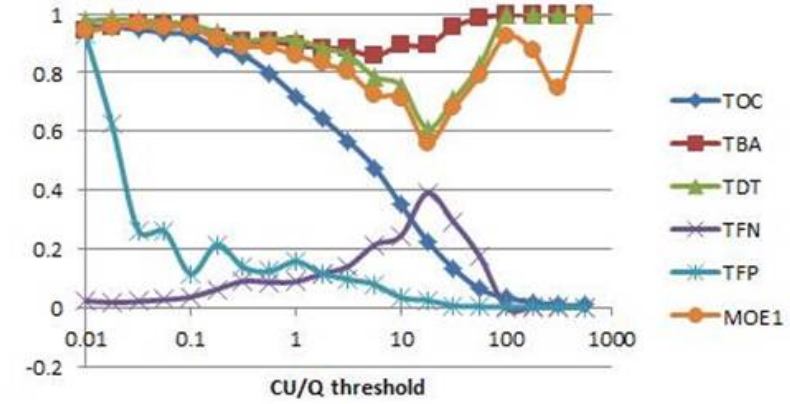

Figure 4.114 *Analyses Rates (among which MOE1 = overlapping) versus threshold normalized concentration for the Paris case with neutral release from source 2.*

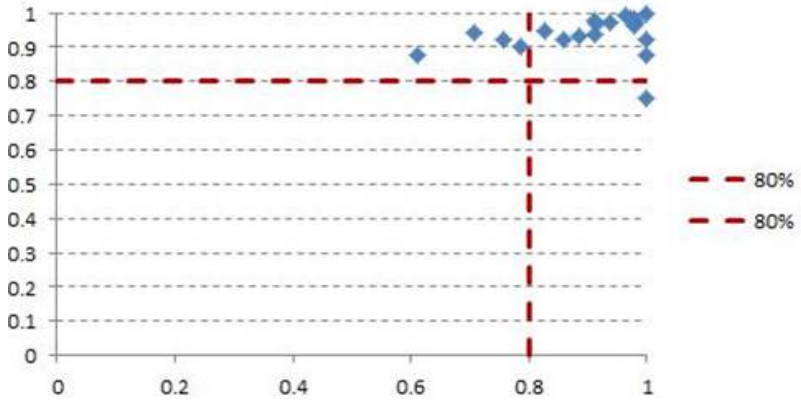

Figure 4.115 *MOE2s representation (False Positive versus False Negative) for the Paris case with neutral release from source 2.*

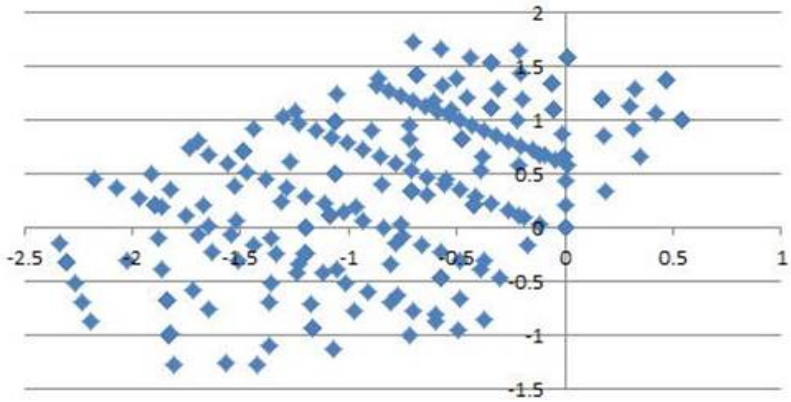

Figure 4.116 *Sensor positions for neutral release from source 3 in the Paris case.*

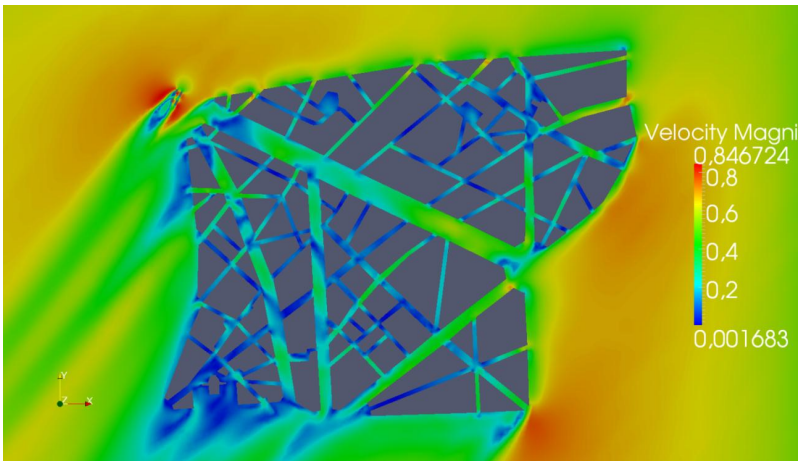

Figure 4.117 *Contours of mean velocity magnitude at z=0.01 m for the Paris case with neutral release from source 3.*

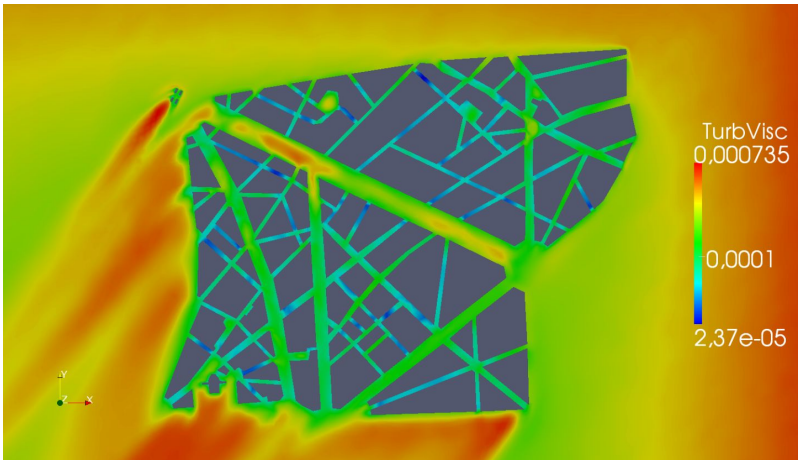

Figure 4.118 *Contours of turbulent viscosity at z=0.01 m for the Paris case with neutral release from source 3.*

source 2. As the plume is broadened at the source, it covers a larger area with relatively high concentration).

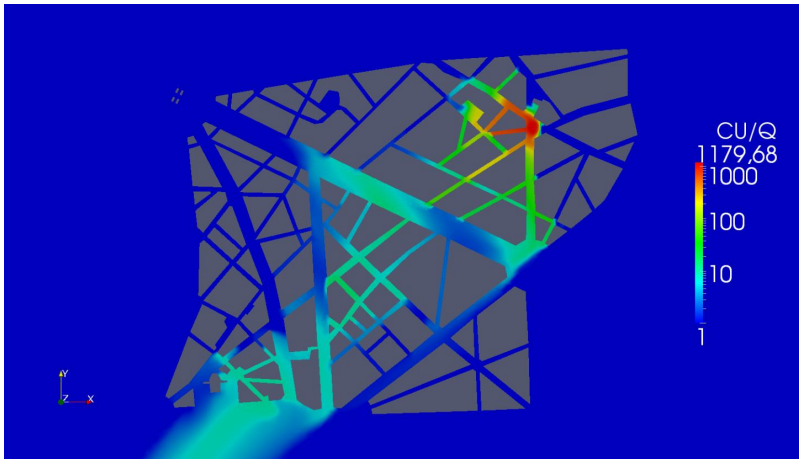

Figure 4.119 *Contours of normalized concentration of air at z=0.01 m for the Paris case with neutral release from source 3.*

The simulated versus observed results (see Figure 4.120) are slightly worse than for source 1 and source 2, but more evenly distributed from low to high values. Street (see Figure 4.120b) or Roof (see Figure 4.120c) concentrations are comparable, which indicates a good modelling of the vertical mixing. Vertical profiles (see Figure 4.120d) at x = 3.3 m, 4.5 m, 5.5 m, 8.3 m from the source location gives good correlation, well within a factor of 5.

We get FAC2=40% and FAC5=79%, which confirms what we just said. Finally, the analysis rates (see Figure 4.121) and MOE2s (see Figure 4.122) are not as good as for the source 1 and source 2, because more points are contributing badly to the statistics (high or low levels). We observe more false negative than false positive events, and overlapping of simulated and observed plume deteriorates at higher values.

4.6.11.4 Dense gas release from source 1

The mesh for the CO_2 release is the same as for the air release but the sensors (see Figure 4.123) have been placed differently.

The mean flow field (see Figure 4.124) is similar to the source 1 air release flow field, except close to the source where we see a decreased velocity (the vertical velocity is 0.11 m/s). The turbulent viscosity (see Figure 4.125) around the source doesn't seem much different to the air release. There may be locally some Kelvin-Helmholtz instability from each side of the dense gas flow leading to shear that would increase turbulent viscosity, which seems unexpected. The overall effect is a reduction turbulent viscosity in the stratified region downstream of the source.

Comparing the plume (see Figure 4.126) to the release of neutral gas we see an obvious widening of the plume that penetrates into many more side streets, and even slightly upwind, with overall comparable concentrations.

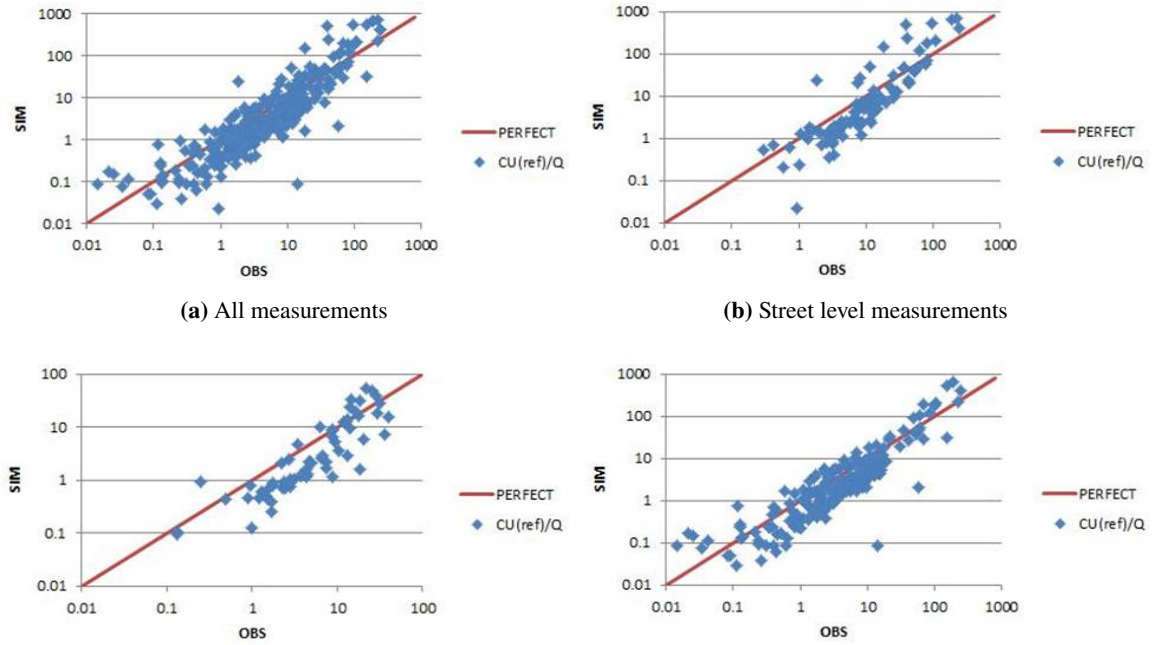

(a) All measurements

(b) Street level measurements

(c) Ropf top measurements

(d) Vertical profile measurements

Figure 4.120 *Simulated versus observed (experimental) values in the Paris case with neutral release from source 3*

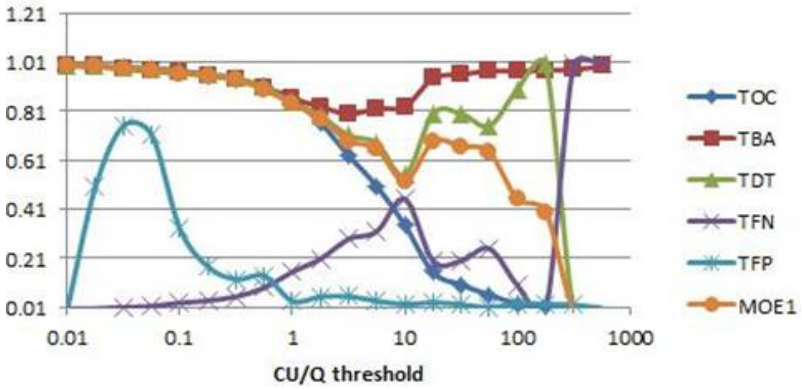

Figure 4.121 *Analyses Rates (among which MOE1 = overlapping) versus threshold normalized concentration for the Paris case with neutral release from source 3.*

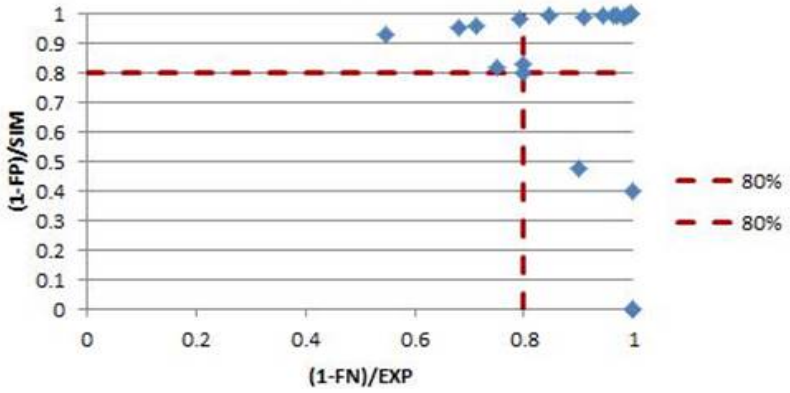

Figure 4.122 *MOE2s representation (False Positive versus False Negative) for the Paris case with neutral release from source 3.*

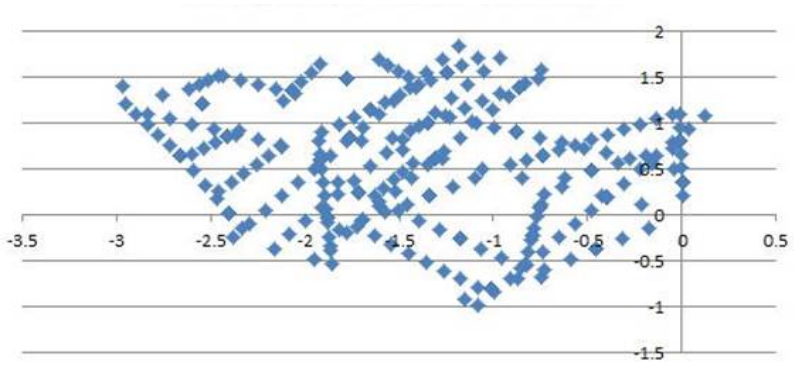

Figure 4.123 *Sensor positions for dense gas release from source 1 in the Paris case.*

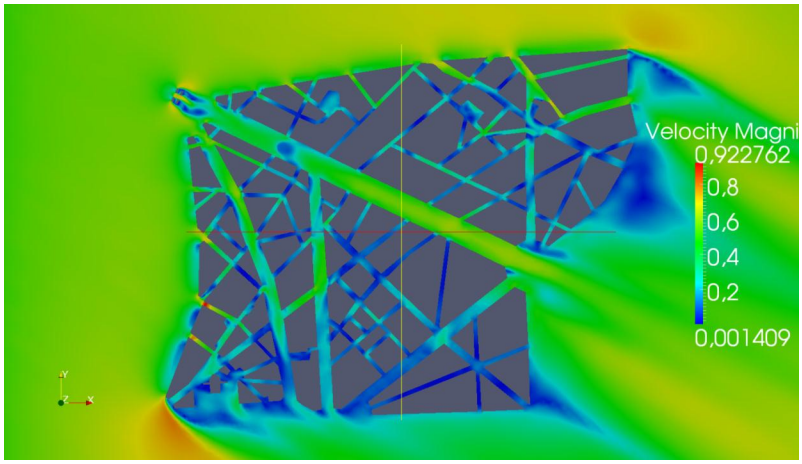

Figure 4.124 *Contours of mean velocity magnitude at z=0.01 m for the Paris case with dense gas release from source 1.*

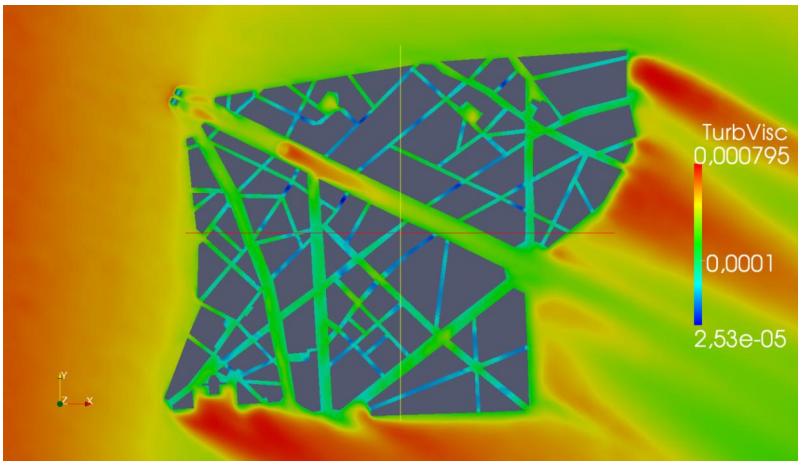

Figure 4.125 *Contours of turbulent viscosity at z=0.01 m for the Paris case with dense gas release from source 1.*

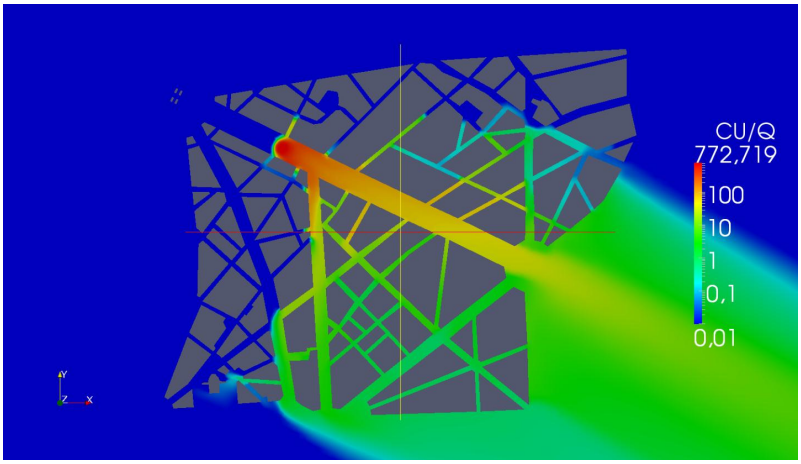

Figure 4.126 *Contours of normalized concentration of CO_2 at z=0.01 m for the Paris case with dense gas release from source 1.*

When comparing the simulation versus observed normalized concentrations, the high values are underestimated for all sensors (see Figure 4.127a). The small values are more dispersed compared against the air release (within a factor of 10, sometimes more). The same kind of results can be shown for the CO_2 release from source 1 at scale 1:1 (see Figure 4.127b).

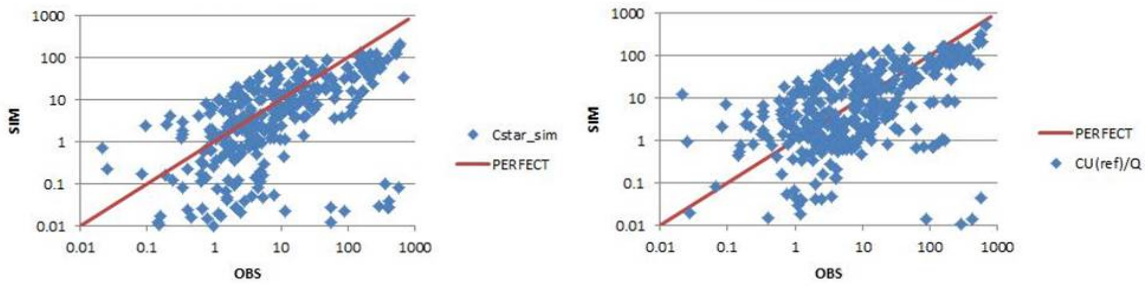

(a) All measurements scale 1:350

(b) All measurements scale 1:1

Figure 4.127 *Simulated versus observed (experimental) values in the Paris case with dense gas release from source 1.*

At street level (see Figure 4.128a), we notice a better collapse of the data, except for some high levels (between 50 and 1000), that are clearly underestimated. This is probably due to the upstream spread, not predicted by the model. The roof level concentrations (Figure 4.128b) are the worse correlated, but we deal here with very small values as the plume doesn't escape the urban canopy height. The vertical profiles (Figure 4.128c), described in [16], give better agreement for high values than low ones. However, there are no vertical measurements close to the source.

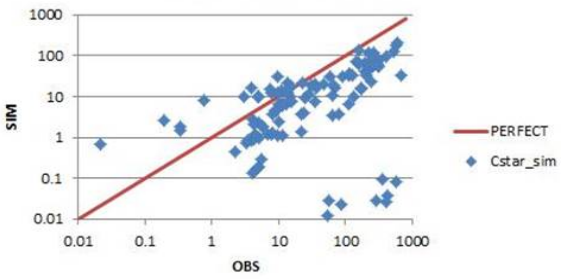

(a) Street level measurements

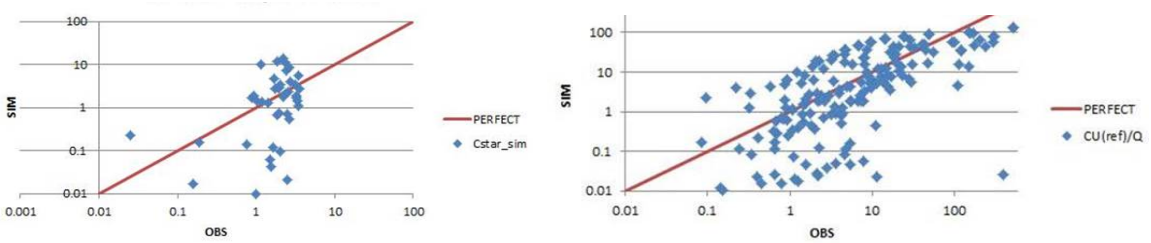

(b) Roof top measurements

(c) Vertical profile measurements

Figure 4.128 *Simulated versus observed (experimental) values in the Paris case with dense gas release from source 1.*

So not surprisingly this case gives worse scores: FAC2=21% and FAC5=47%. We look at analysis rates and MOE2 to get a better understanding. We see in Figure 4.129 that the MOE1 (plumes overlap) is decreasing strongly above the threshold value 50; this means the concentrations around the source are not predicted well. In Figure 4.130, we see a lot of false negative values, meaning the plume is not where it should be.

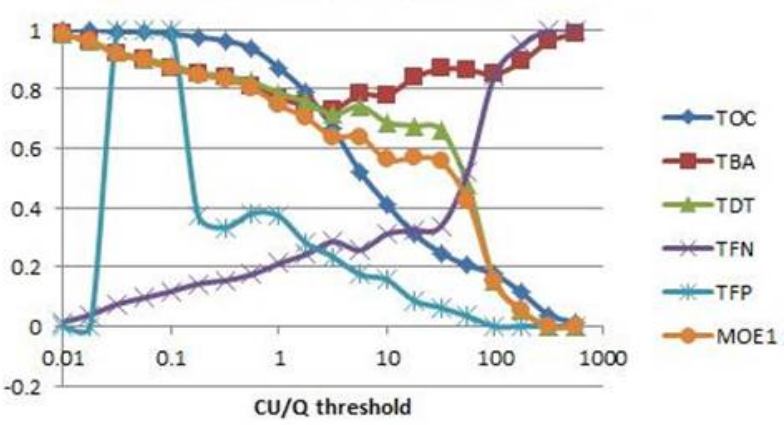

Figure 4.129 *Analyses Rates (among which MOE1 = overlapping) versus threshold normalized concentration for the Paris case with dense gas release from source 1.*

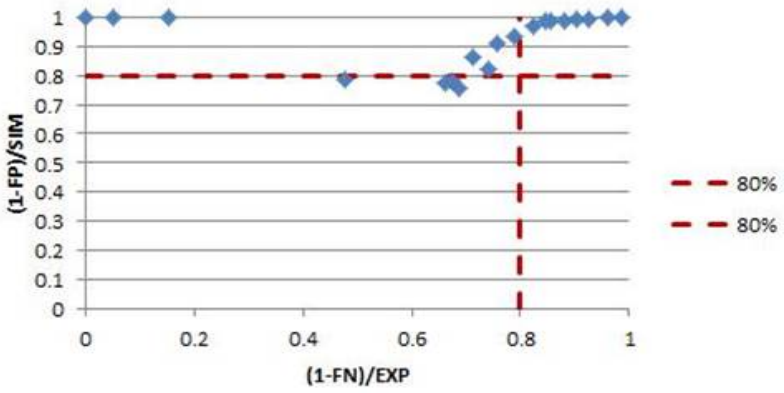

Figure 4.130 *MOE2s representation (False Positive versus False Negative) for the Paris case with dense gas release from source 1.*

4.6.11.5 Dense gas release from source 1 – low Re $k-\omega$ model

In this section the $k-\omega$ turbulence model is tested. Computing the statistics, we get FAC2=25% and FAC5=55%, compared to 21% and 47% for the $k-\varepsilon$ model. Also in Figure 4.131 there are high concentrations from experiment, that is not detected by the simulation.

The analysis rates and the MOE2 are shown in Figure 4.132 and Figure 4.133. Compared to the $k-\varepsilon$ model there is no obvious difference.

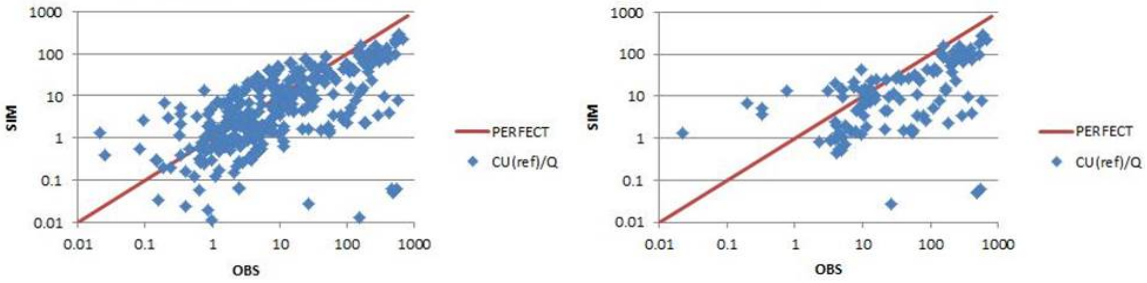

(a) All measurements **(b)** Street level measurements

Figure 4.131 *Simulated versus observed (experimental) values in the Paris case with dense gas release from source 1 using the low Reynolds turbulence model.*

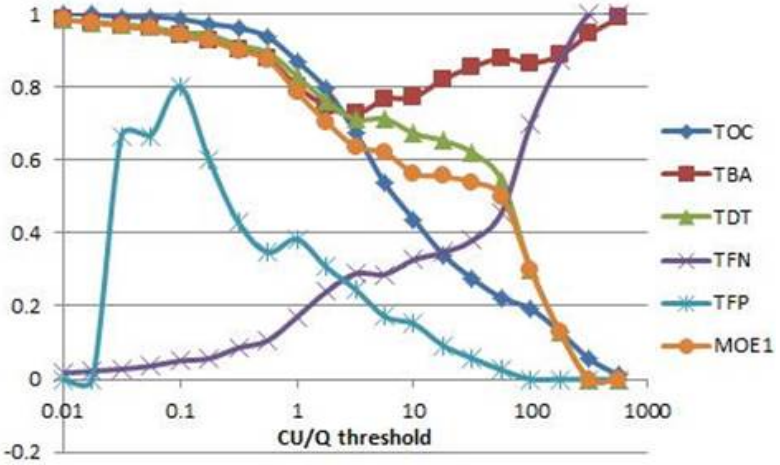

Figure 4.132 *Analyses Rates (among which MOE1 = overlapping) versus threshold normalized concentration for the Paris case with dense gas release from source 1 using the low Reynolds turbulence model.*

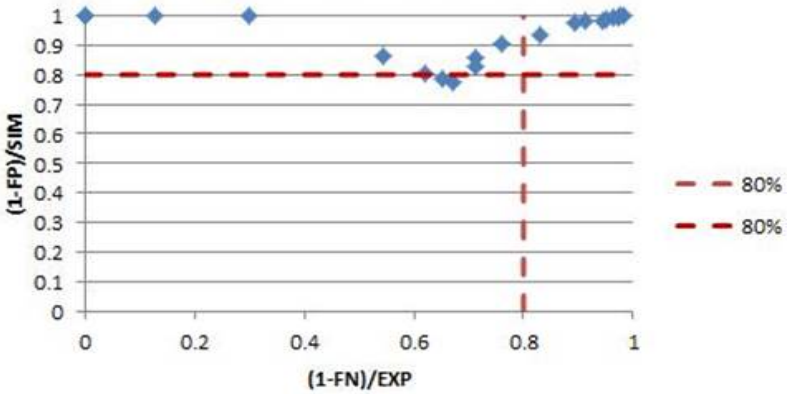

Figure 4.133 *MOE2s representation (False Positive versus False Negative) for the Paris case with dense gas release from source 1 using the low Reynolds turbulence model.*

Finally, the concentration presented against the linear distance from source, together with estimated upper bounds (see Figure 4.134). Results show good agreement for most of the measurements.

4.6.11.6 Dense gas release from source 2

This section presents the results of the CO_2 release from source 2 (c.f. Figure 2.7). The sensor locations are according to Figure 4.135. The mean flow and turbulent viscosity are presented in Figure 4.136 and Figure 4.137. The result is similar to the release from source 1. The normalized concentration is shown in Figure 4.138. Compared to the air release, the concentration covers a larger area.

The simulated versus observed concentrations are shown in Figure 4.139a (all), Figure 4.139b (street level) and Figure 4.139c (roof level) are more consistent than the previous case (source 1 CO_2), especially for high concentration values. Even the vertical profiles (see Figure 4.139d) are satisfying looking back at the difficulties modelling dense gas.

FAC2 = 66% and FAC5 = 87%, which are acceptable in a validation viewpoint. Analysis rates (see Figure 4.140) confirms a reasonable agreement together with a MOE1 (plume overlap) above 60% (the last point isn't significant because the lack of data there). The MOE2s in Figure 4.141 show again some false negative on the highest values, which indicate some discrepancy very close to the source.

4.6.11.7 Dense gas release from source 3

This section presents the CO_2 release from source 3 (c.f. Figure 2.7). The sensors are displayed in Figure 4.142. In Figure 4.143 the mean flow doesn't change that much, compared to the air release. The turbulent viscosity (see Figure 4.144) is locally increased compared to the air release close to the source for the same reasons described in Section 4.6.11.4.

The normalized concentration is shown in Figure 4.145. The plume is broader than for the air release, with more upstream dispersion.

The simulated versus observed normalized concentrations (see Figure 4.146) are rather well collapsed against the perfect curve for all but the roof level data (Figure 4.146c). The vertical profile comparison (Figure 4.146d) is especially convincing.

The statistics brings FAC2 = 54% (close to 60%) and FAC5 = 87%. For the Analysis rates (see Figure 4.147), the MOE1 are above 60% for all but the highest values, for which less points are available. For the MOE2s (see Figure 4.148), there are some false negative values, but most of them stay under 60%, which is acceptable.

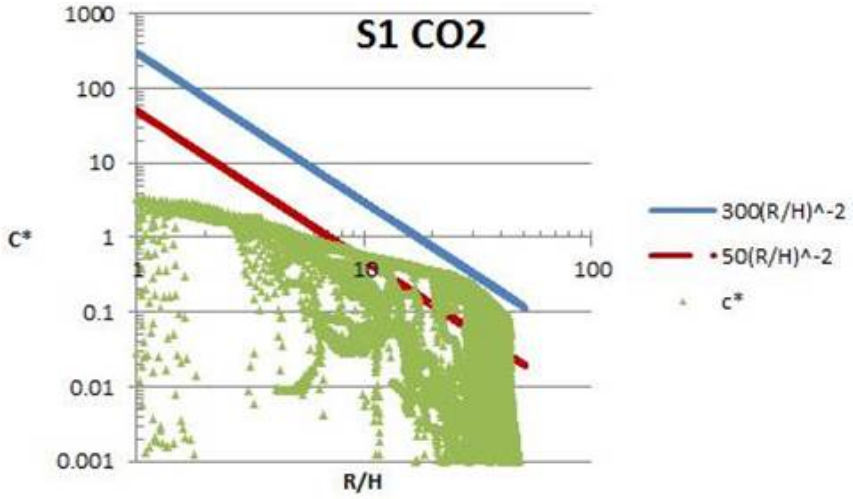

(a) Simulation

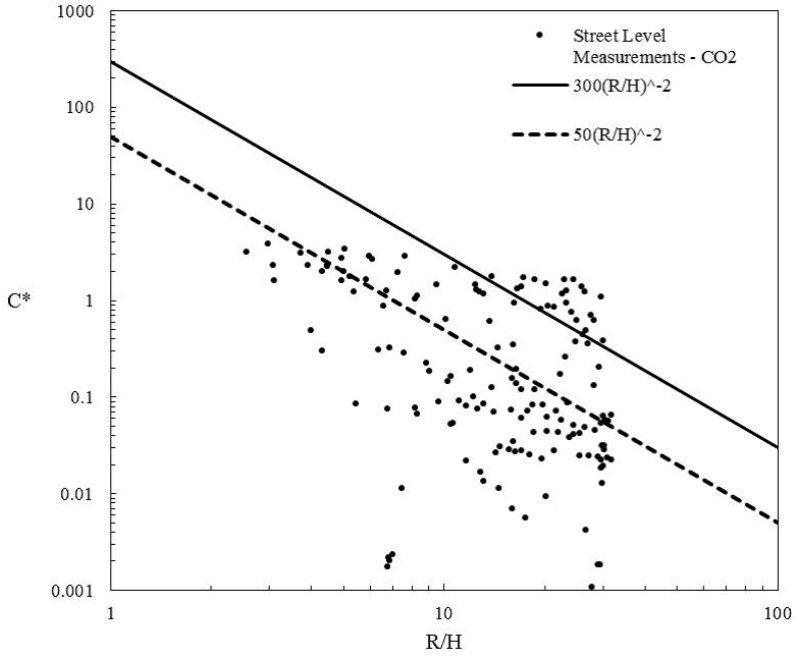

(b) Experiment

Figure 4.134 *Normalized concentration of CO_2 vs. linear distance to source in the Paris case with dense gas release from source 1 using the low Reynolds turbulence model. Lines show expected upper bounds.*

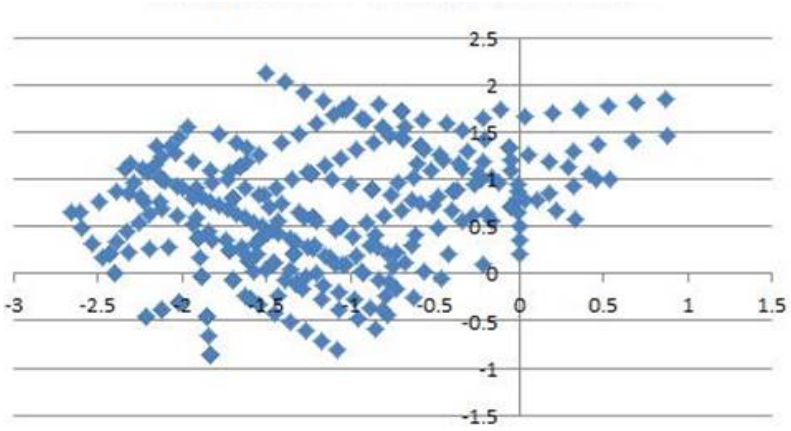

Figure 4.135 *Sensor positions for dense gas release from source 2 in the Paris case.*

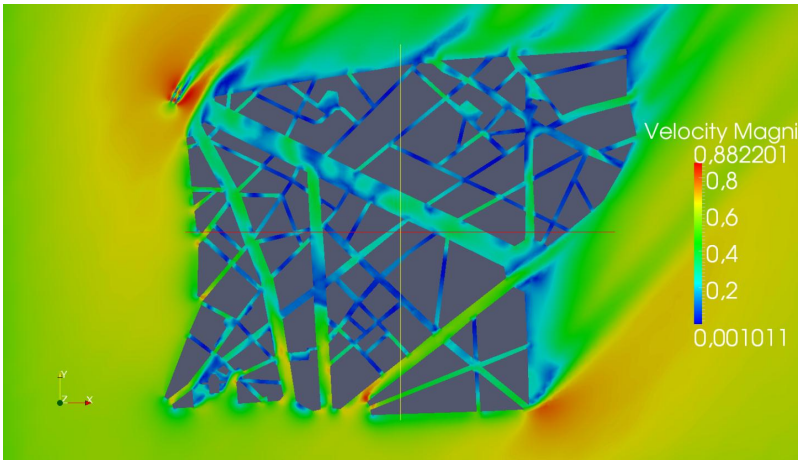

Figure 4.136 *Contours of mean velocity magnitude at z=0.01 m for the Paris case with dense gas release from source 2.*

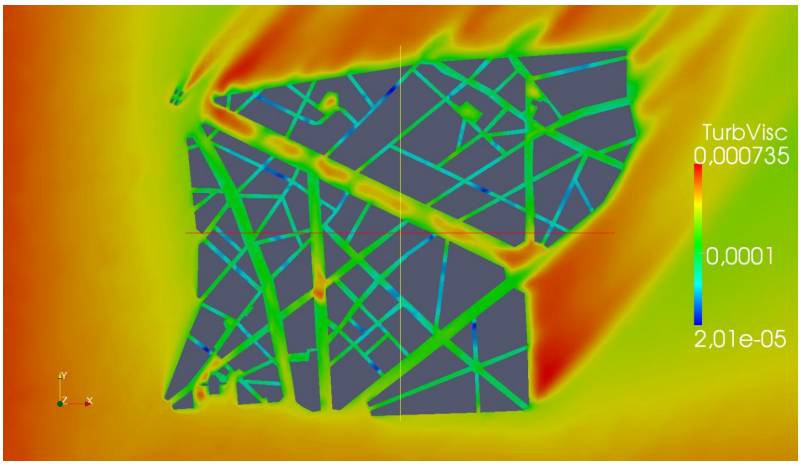

Figure 4.137 *Contours of turbulent viscosity at z=0.01 m for the Paris case with dense gas release from source 2.*

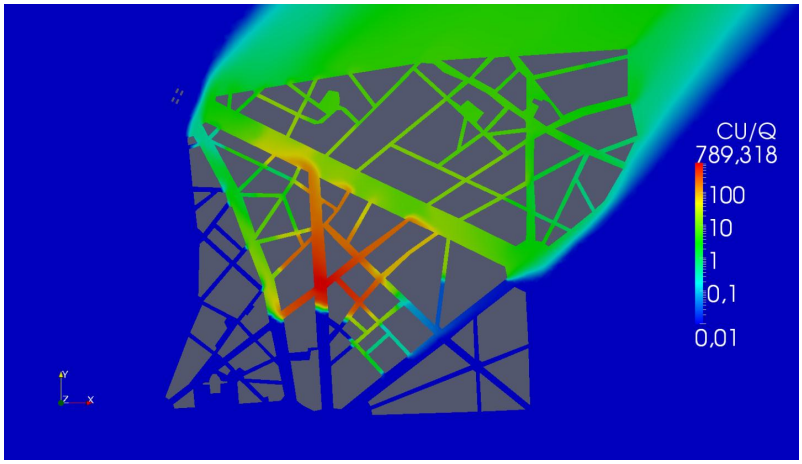

Figure 4.138 *Contours of normalized concentration of CO_2 at z=0.01 m for the Paris case with dense gas release from source 2.*

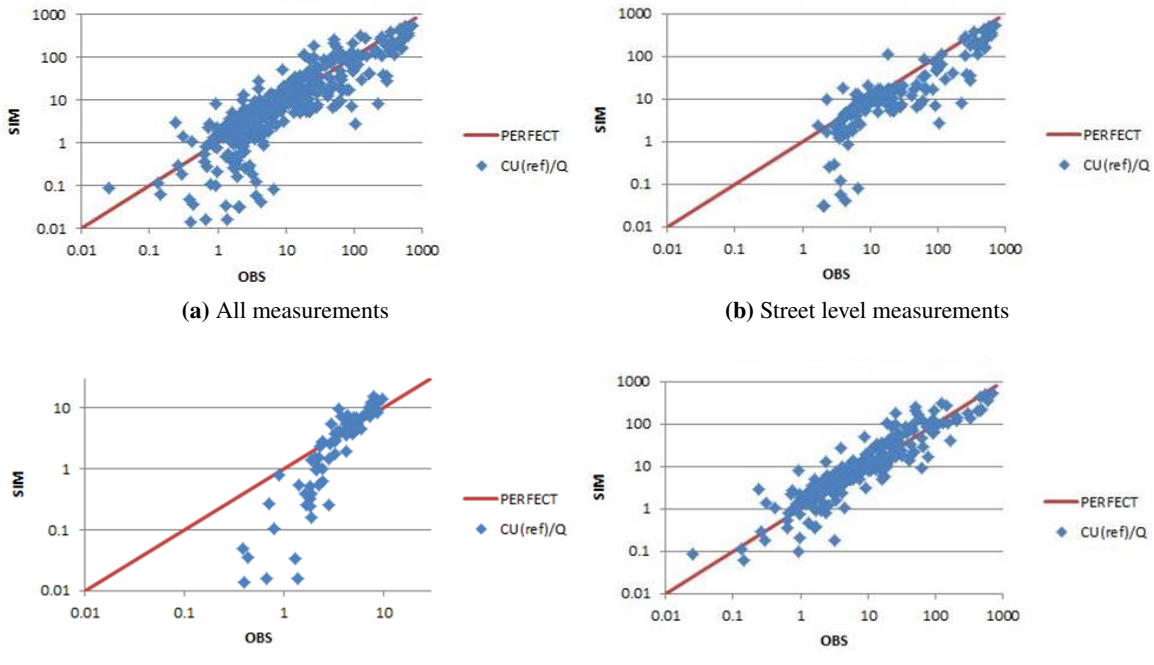

(a) All measurements

(b) Street level measurements

(c) Ropf top measurements

(d) Vertical profile measurements

Figure 4.139 *Simulated versus observed (experimental) values in the Paris case with dense gas release from source 2.*

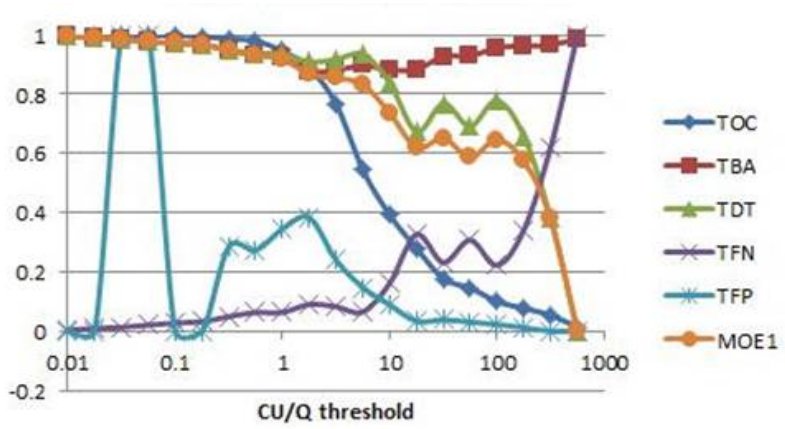

Figure 4.140 *Analyses Rates (among which MOE1 = overlapping) versus threshold normalized concentration for the Paris case with dense gas release from source 2.*

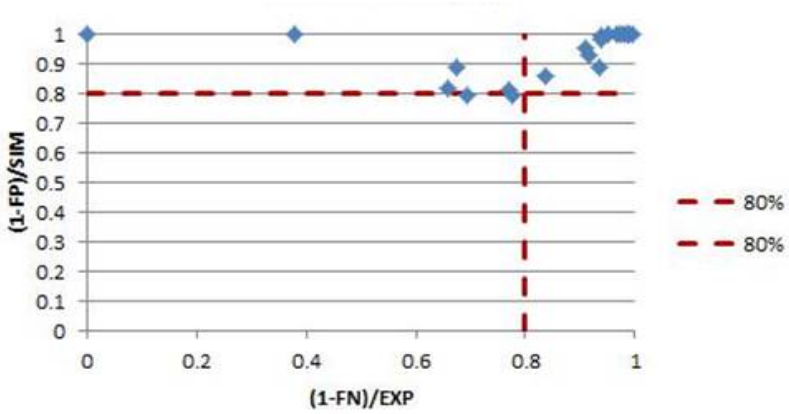

Figure 4.141 *MOE2s representation (False Positive versus False Negative) for the Paris case with dense gas release from source 2.*

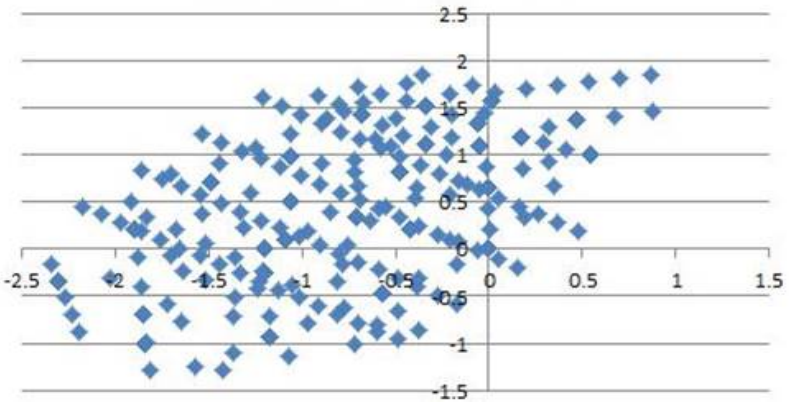

Figure 4.142 *Sensor positions for dense gas release from source 3 in the Paris case.*

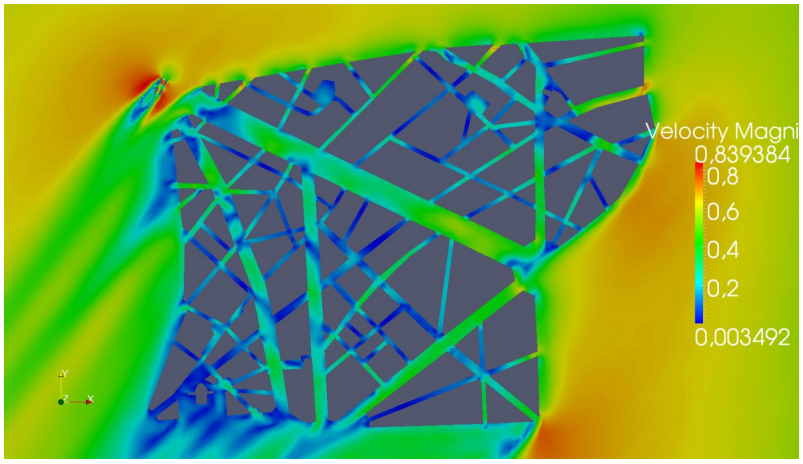

Figure 4.143 *Contours of mean velocity magnitude at z=0.01 m for the Paris case with dense gas release from source 3.*

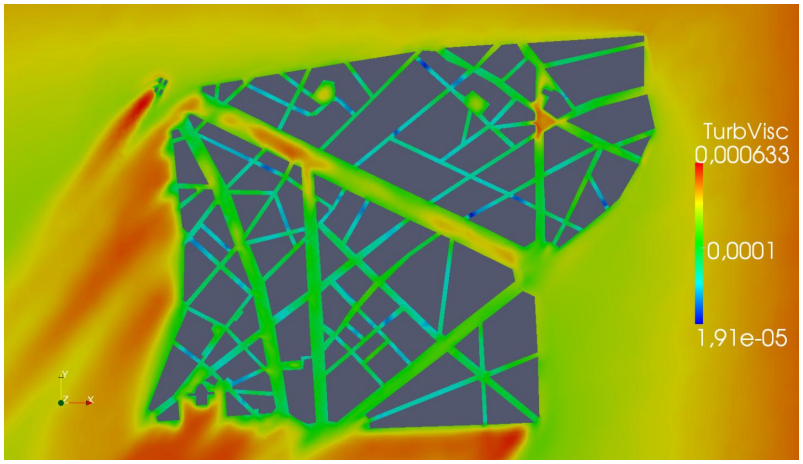

Figure 4.144 *Contours of turbulent viscosity at z=0.01 m for the Paris case with dense gas release from source 3.*

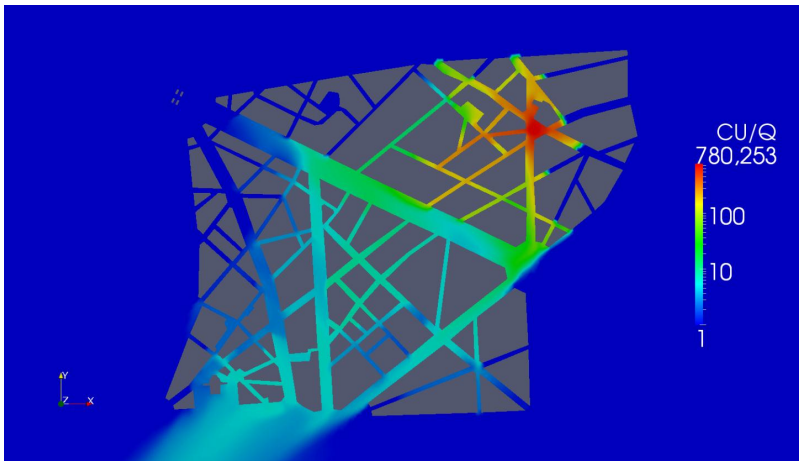

Figure 4.145 *Contours of normalized concentration of CO_2 at z=0.01 m for the Paris case with dense gas release from source 3.*

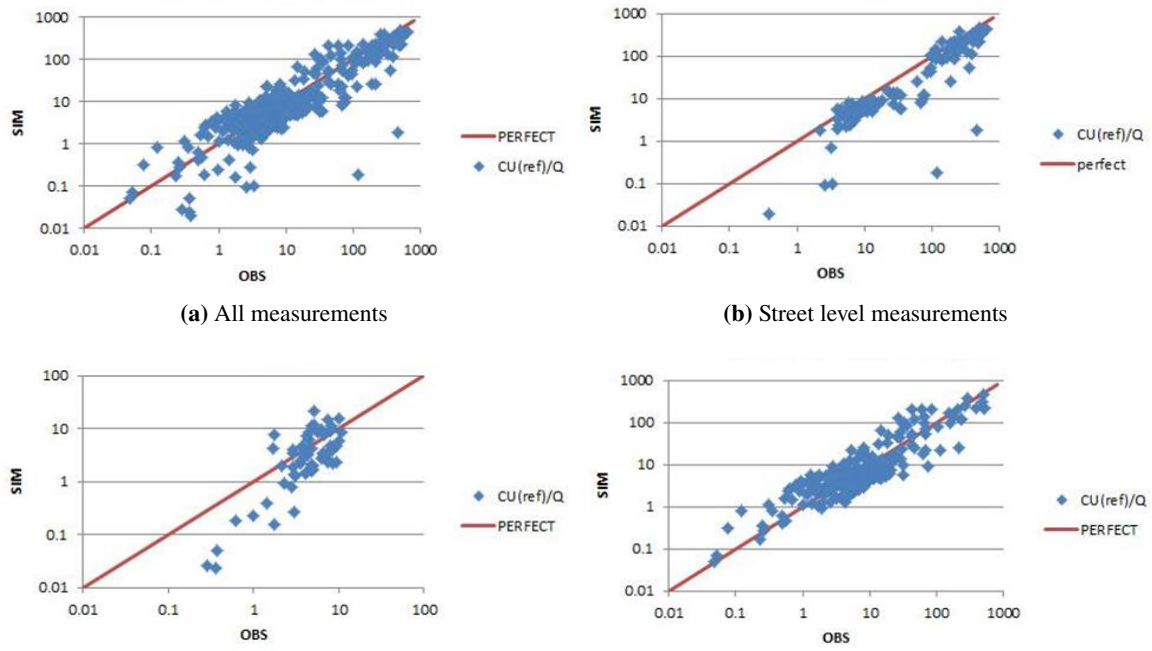

(a) All measurements

(b) Street level measurements

(c) Ropf top measurements

(d) Vertical profile measurements

Figure 4.146 *Simulated versus observed (experimental) values in the Paris case with dense gas release from source 3.*

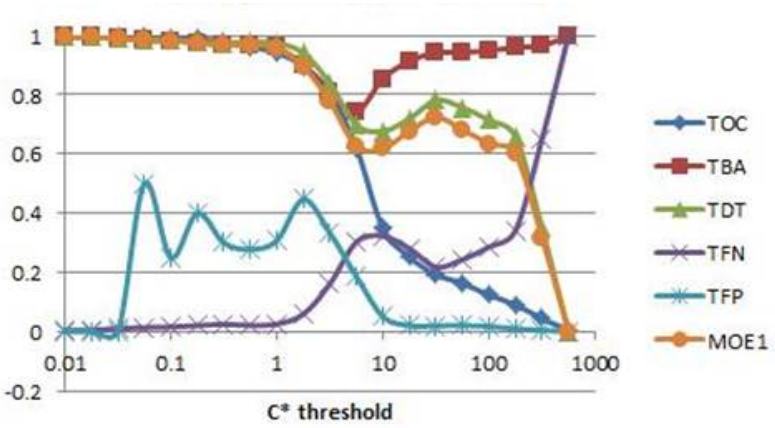

Figure 4.147 *Analyses Rates (among which MOE1 = overlapping) versus threshold normalized concentration for the Paris case with dense gas release from source 3.*

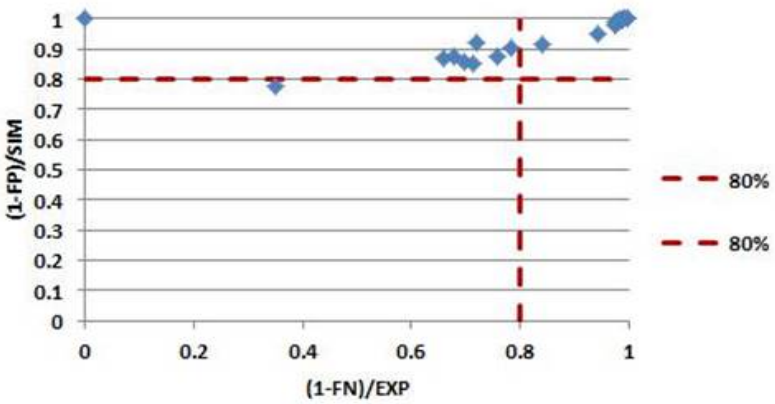

Figure 4.148 *MOE2s representation (False Positive versus False Negative) for the Paris case with dense gas release from source 3.*

4.7 Conclusions

A number of scenarios have been simulated and compared against experimental data obtained from the Environmental Wind Tunnel located at the University of Surrey. The scenarios handles passive (air) and dense gas (CO_2) releases at 50dm^3/min subjected to a neutral atmosphere. These cases were designed to increase the level of complexity. However, each of them brought their own issues.

The flat case is the more crucial for dense gas dispersion, as it is encountered in almost all scenarios (upstream of back-step, simple array, complex array, large avenues in the Paris case). The RANS high Reynolds turbulence model ($k-\varepsilon$ linear model) used by Saturn and coupled with an atmospheric module, is well suitable to reproduce experimental data for passive release, but shows insufficient correlation for dense gas release .It is not able to capture the 2 peaks occurring downstream, or the complete collapse of the gas under gravitational forces. The turbulence anisotropy is not well reproduced and this leads to an overestimation of the intensity by a factor of 2, and an underestimation of the plume width, also by a factor of 2. Although the stratified boundary layer is well resolved (fine mesh). Some slight improvement can be obtained using a low Reynolds model such as $k-\omega$, making the peaks appear and reducing the peak concentration levels, but still not sufficiently.

The hill scenario is adding a difficulty by forming a flow at the limit of separation. The air release results are better correlated with experimental data for the upstream source compared against the source on the leeward side of the hill. The CO_2 results exhibit the same drawbacks as the air release. Nevertheless, we capture part of the dense gas collapsing and broadening downstream of the hill.

The backward-facing step scenario was designed to test the ability of the model to address dense gas interaction with a quasi 2D recirculation zone behind the step, where the source is located. The RANS model captures the observed effect of lateral dispersion in the recirculation zone, enhanced by using dense gas emission instead of air, but not as much as the experimental data show. The CO_2 lateral profile is almost flat at different distance downwind, where the simulated one still keeps a slight peak.

The backward-facing step with cubes is similar to the last case with an array far from the step. With

the array close to the back-step, the dense gas is mixed faster by mechanical turbulence and the modelling performs better, although still underestimating the lateral dispersion and collapse of CO_2.

The simple array scenario simulation results are satisfying regarding air release, being at 0 degree or 45 degree orientation of the array to the main flow. Only an angle shift due to experimental uncertainty is preventing a perfect agreement. The CO_2 results are depending on the incoming dense plume, which we saw is not well captured in the flat scenario. Some complicated concentration patterns happen that are only partially captured.

The complex array scenario at 0 degree orientation to the main flow show an overestimation for the air concentration bellow roof level by at least a factor of 2, apparently due to underestimation of turbulent vertical fluxes (non-stationary effects not correctly taken care of in RANS). The CO_2 results have better agreement than the air results, at least for the source placed inside the array. The symmetric CO_2 source is affected negatively because the plume relies on the turbulent boundary layer before the geometry start to dictate the dispersion. Slightly improved for the non-symmetric source. Still the results have the right order of magnitude and geometric channeling and blocking effects are captured. The results for the central source and tilted array by 45 degree are good, less sensitive to orientation deviations of the incoming plume, due to an overestimation of the turbulence.

The Paris case finally has been addressed statistically owing to the large number of measurements. Three sources and associated wind orientations have been studied (placed respectively in the avenues, a crossroads and large places). The air results are acceptable (around 40-60% within a factor of 2, and around 70-80% in a factor of 5). The "Champ Elysees" avenue case (Source 1) has the best correlation because of channeling effect, with very good vertical profiles along the avenue. The MOE1 (plumes overlap) is close to 80% and MOE2s (False positives versus False negatives) within 80% also. The crossroad source (Source 2) has a rather good correlation against experimental results close to the source with an MOE1 between 60 and 80%, as do the MOE2s showing a few false negative values. Source 3 is worse for the air release. Some values of the MOE1 and MOE2 fall down to 40%. The statistics is influenced by a number of sensors with small concentrations which reduces the results. The simulated results versus the experimental are more scattered but evenly distributed from low to high values. This suggests that the concentration around the source field is more evenly distributed.

When looking at the CO_2 results, the worst case is the "Champs Elysees" avenue scenario (source 1) with only 25% of the values within a factor of 2 and 50% within a factor of 5. Some high concentration values are not seen, upstream of the source, which is missed by the model. For source 2, almost 70% are within a factor of 2 and 90% within a factor of 5. Some false negative values in MOE2s are close to 60%, but overall this case is well simulated. The last case with source 3 located close to many buildings the MOE1 and MOE2 are above 60% (some false negative values remain at high concentration levels close to the source).

For the use of the CFD software Saturn, with RANS model applied to simple to complex urban idealized environment we can conclude that air releases are most of the time correctly simulated at wind tunnel scale (except for the hill case).

A dense gas release of CO_2 is more problematic, already for the flat case that determines the other cases where the source is outside the urban area. The High Re turbulence model $k - \varepsilon$-linear overrates the turbulent viscosity and is unable to correctly compute anisotropic effects on turbulent

fluxes due to density stratification. Low Re model ($k - \omega$ sst) slightly improves this, but not sufficiently. Yet the stratified boundary layer is well resolved by the mesh.

A large scale domain like the Paris case is challenging in computational resources, but appears rather encouraging when looking at the results. The sources placed in dense urban areas seem to yield the best results (compared to sources far from buildings) for dense gas emissions.

It seems also permitted with some care to scale up the wind tunnel results from scale 1:350 to scale 1:1.

Bibliography

[1] P. Durbin and B. P. Reif, "The elliptic relaxation method," Closure Strategies for Turbulent and Transitional Flows, pp. 127–152, 2002.

[2] R. L. Lee, R. Calhoun, S. Chan, J. Leone, J. Shinn, and D. Stevens, "Urban dispersion CFD modeling, fact or fiction," in 3rd Symposium on the Urban Environment, pp. 14–18, 2000.

[3] W. Coirier, D. Fricker, M. Furmanczyk, and S. Kim, "A Computational Fluid Dynamics approach for urban area transport and dispersion modeling," Environmental Fluid Mechanics, vol. 5, no. 5, pp. 443–479, 2005.

[4] F.-S. Lien and E. Yee, "Numerical modelling of the turbulent flow developing within and over a 3D building array, Part I: A high-resolution Reynolds-Averaged Navier-Stokes approach," Boundary-Layer Meteorology, vol. 112, pp. 427–466, 2004.

[5] F.-S. Lien, E. Yee, H. Ji, A. Keats, and K. J. Hsieh, "Progress and challenges in the development of physically-based numerical models for prediction of flow and contaminant dispersion in the urban environment," Int. Journal of Computational Fluid Dynamics, vol. 20, pp. 323–337, 2006.

[6] J. L. Santiago, A. Martilli, and F. Martin, "CFD simulation of airflow over a regular array of cubes. Part I: Three-dimensional simulation of the flow and validation with wind-tunnel experiments," Boundary-Layer Meteorology, vol. 122, pp. 609–634, 2007.

[7] M. A. McBride, A. B. Reeves, M. D. Vanderheyden, C. J. Lea, and X. X. Zhou, "Use of advanced techniques to model the dispersion of chlorine in complex terrain," Process Safety Environment, vol. 79, pp. 89–102, 2001.

[8] G. A. Perdikaris and F. Mayinger, "Numerical simulation of heavy gas cloud dispersion within topographically complex terrain," Journal of Loss Prevention in the Process Industries, vol. 7, pp. 391–396, 1994.

[9] S. Sklavounos and F. Rigas, "Validation of turbulence models in heavy gas dispersion over obstacles," Journal of Hazardous Materials, vol. A108, pp. 9–20, 2004.

[10] S. Tauseef, D. Rashtchian, and S. Abbasi, "CFD-based simulation of dense gas dispersion in presence of obstacles," Journal of Loss Prevention in the Process Industries, vol. 24, no. 4, pp. 371–376, 2011.

[11] V. Boppana, Z.-T. Xie, and I. P. Castro, "Large-eddy simulation of dispersion from surface sources in arrays of obstacles," Boundary-Layer Meteorology, vol. 135, no. 3, pp. 433–454, 2010.

[12] H. E. Fossum, B. A. Pettersson-Reif, M. Tutkun, and T. Gjesdal, "On the Use of Computational Fluid Dynamics to Investigat Aerosol Dispersion in an Industrial Environment: A Case Study," Boundary-Layer Meteorology, vol. 144, pp. 21–40, 2012.

[13] Y. Liu, G. Cui, Z. Wang, and Z. Zhang, "Large eddy simulation of wind field and pollutant dispersion in downtown Macao," Atmospheric Environment, vol. 45, no. 17, pp. 2849–2859, 2011.

[14] Z.-T. Xie and I. P. Castro, "Large-eddy simulation for flow and dispersion in urban streets," Atmospheric Environment, vol. 43, no. 13, pp. 2174–2185, 2009.

[15] J. Burman, B. A. P. Reif, S. Burkhart, O. Parmhed, and A. Robins, "WP1000 - Scenario definition and dissemination strategy," Swedish Defence Research Agency, FOI Rapport, no. 2015/..., 2015.

[16] A. Robins, P. Hayden, and E. M. M. Wingstedt, "MODITIC wind tunnel experiments," Norwegian Defence Research Establishment, FFI Rapport, no. 2016/01483, 2016.

[17] L. Musson-Genon, E. Dupont, and D. Wendum, "Reconstruction of the surface-layer vertical structure from measurements of wind, temperature and humidity at two levels," Boundary-layer meteorology, vol. 124, no. 2, pp. 235–250, 2007.

[18] J.-F. GELEYN, "Interpolation of wind, temperature and humidity values from model levels to the height of measurement," Tellus A, vol. 40, no. 4, pp. 347–351, 1988.

[19] B. P. Reif, A. Ooi, and P. Durbin, "On stably stratified homogeneous shear flows subjected to rotation," in Proceedings of the 2000 Summer Program, Center for Turbulence Research, Stanford University, p. 241, Citeseer, 2000.

About FFI

The Norwegian Defence Research Establishment (FFI) was founded 11th of April 1946. It is organised as an administrative agency subordinate to the Ministry of Defence.

FFI's MISSION

FFI is the prime institution responsible for defence related research in Norway. Its principal mission is to carry out research and development to meet the requirements of the Armed Forces. FFI has the role of chief adviser to the political and military leadership. In particular, the institute shall focus on aspects of the development in science and technology that can influence our security policy or defence planning.

FFI's VISION

FFI turns knowledge and ideas into an efficient defence.

FFI's CHARACTERISTICS

Creative, daring, broad-minded and responsible.

Om FFI

Forsvarets forskningsinstitutt ble etablert 11. april 1946. Instituttet er organisert som et forvaltningsorgan med særskilte fullmakter underlagt Forsvarsdepartementet.

FFIs FORMÅL

Forsvarets forskningsinstitutt er Forsvarets sentrale forskningsinstitusjon og har som formål å drive forskning og utvikling for Forsvarets behov. Videre er FFI rådgiver overfor Forsvarets strategiske ledelse. Spesielt skal instituttet følge opp trekk ved vitenskapelig og militærteknisk utvikling som kan påvirke forutsetningene for sikkerhetspolitikken eller forsvarsplanleggingen.

FFIs VISJON

FFI gjør kunnskap og ideer til et effektivt forsvar.

FFIs VERDIER

Skapende, drivende, vidsynt og ansvarlig.

FFI's organisation

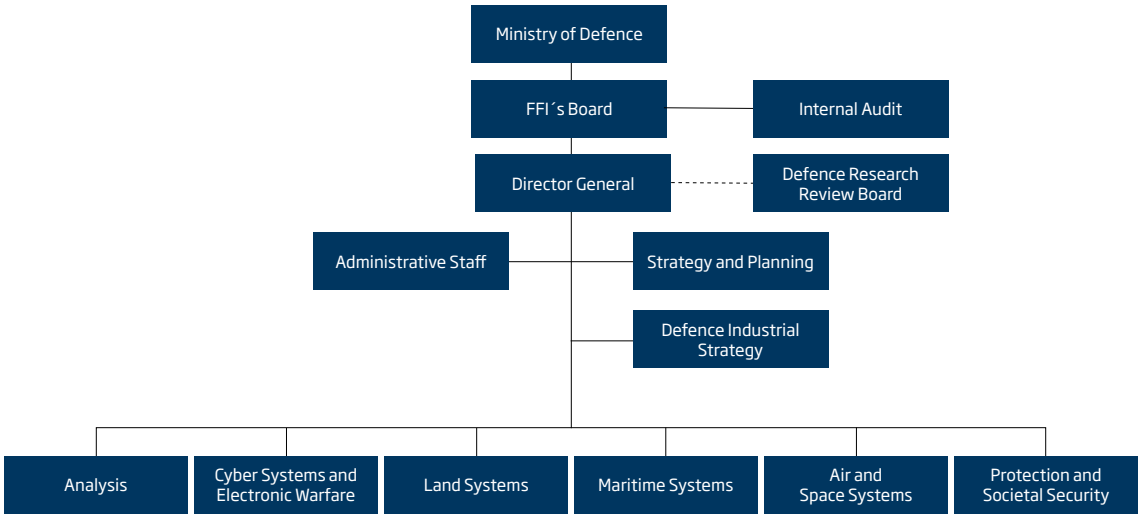

Forsvarets forskningsinstitutt
Postboks 25
2027 Kjeller

Besøksadresse:
Instituttveien 20
2007 Kjeller

Telefon: 63 80 70 00
Telefaks: 63 80 71 15
Epost: ffi@ffi.no

Norwegian Defence Research Establishment (FFI)
P.O. Box 25
NO-2027 Kjeller

Office address:
Instituttveien 20
N-2007 Kjeller

Telephone: +47 63 80 70 00
Telefax: +47 63 80 71 15
Email: ffi@ffi.no

FFI Forsvarets forskningsinstitutt
Norwegian Defence Research Establishment